Title

A TEMPERATURE-PROGRAMMED DESORPTION STUDY OF SUBSURFACE DIFFUSION IN HIGH SURFACE AREA CATALYSTS

Author

Leary, K.J.

Publication Date

1987-09-01

Center for Advanced Materials

CAM

A Temperature-Programmed Desorption Study of Subsurface Diffusion in High Surface Area Catalysts

K.J. Leary
(Ph.D. Thesis)

September 1987

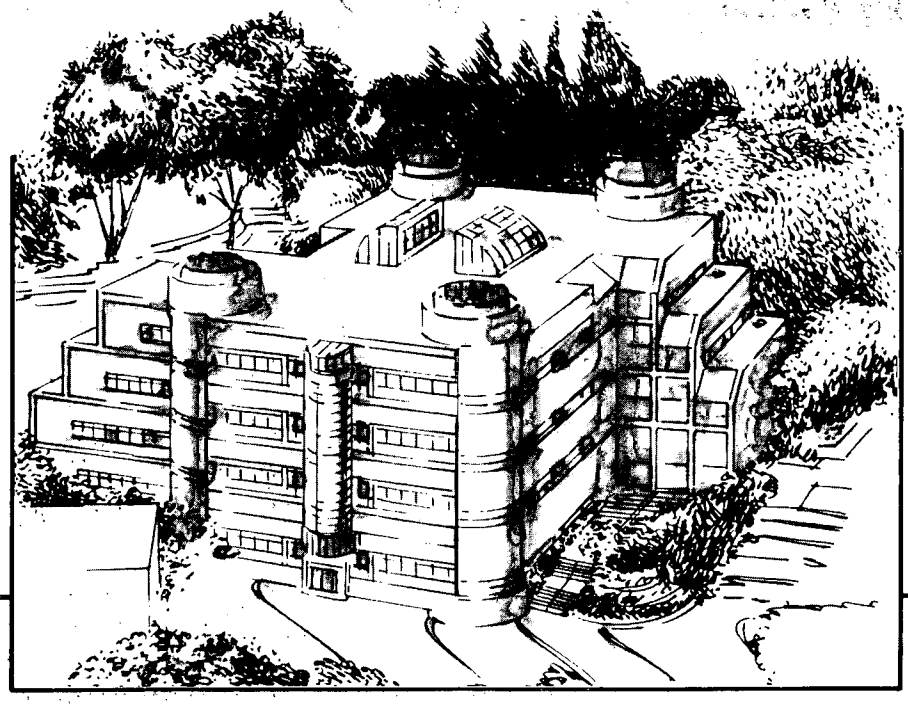

Materials and Chemical Sciences Division

Lawrence Berkeley Laboratory • University of California

ONE CYCLOTRON ROAD, BERKELEY, CA 94720 • (415) 486-4755

Prepared for the U.S. Department of Energy under Contract DE-AC03-76SF00098

DISCLAIMER

A Temperature-Programmed Desorption Study of Subsurface Diffusion in High Surface Area Catalysts

Kevin Joseph Leary

Center for Advanced Materials
Materials and Chemical Sciences Division
Lawrence Berkeley Laboratory
University of California
and
Department of Chemical Engineering
University of California, Berkeley
Berkeley, California 94720

September 1987

ABSTRACT

A Temperature-Programmed Desorption Study of
Subsurface Diffusion in High Surface Area Catalysts
by
Kevin Joseph Leary
Department of Chemical Engineering, University of California, and
Center for Advanced Materials, Lawrence Berkeley Laboratory
Berkeley, Ca. 94720

In heterogeneous catalysis it is generally assumed that molecules which adsorb and react on the solid surface do not penetrate into subsurface layers of the catalyst. In this work, temperature-programmed desorption (TPD) and reduction (TPR) are used to show that small atoms such as carbon and oxygen can move relatively easily between surface and subsurface layers of Mo_2C catalysts. Moreover, it is shown that hydrogen can penetrate into subsurface absorption sites of palladium. These results could have important implications in catalysis since the presence of these atoms in layers just below the surface could affect the way various adsorbates bind to and react on the surface.

The high mobility of carbon in Mo_2C allows the bulk Mo:C ratio, and therefore the catalytic properties, to be varied by proper choice of pretreatment conditions. One technique which is used to probe the changes in the catalyst surface as a function of the Mo:C ratio is TPR of chemisorbed oxygen. However, the high mobility of oxygen in Mo_2C complicates interpretation of the TPR spectra. During heating, oxygen moves between the surface and subsurface layers of the catalyst. This movement, which is referred to as subsurface diffusion, produces a high temperature peak in the TPR spectrum.

Since desorption in the high temperature peak is limited by diffusion from the subsurface to the surface, this peak is referred to as a diffusion peak.

It is also shown, with the aid of a numerical model, that subsurface diffusion produces a high temperature peak in the TPD spectrum of hydrogen on a Pd/SiO_2 catalyst. Since the solubility of hydrogen in bulk palladium is negligible under our experimental conditions, these results provide strong evidence for the presence of subsurface absorption sites for hydrogen in palladium. These results also suggest that hydrogen may be present in the palladium subsurface under typical catalytic reaction conditions.

This dissertation is dedicated
to my wife Joyce who has always
been there when I needed her.

ACKNOWLEDGMENTS

I would like to thank Dr. Angy Stacy and Dr. Jim Michaels for their contributions to this work. The opportunity to work on a joint project between the chemistry and chemical engineering departments has been an especially rewarding experience.

I also would like to express my appreciation to my dissertation committee members Dr. Birgitta Whaley and Dr. Alex Bell for their assistance.

I am also indebted to Mike Carolan for his numerous hours of assistance in disassembling and reassembling my laboratory equipment.

Finally, I would especially like to thank my parents for their constant support and encouragement throughout my life.

Funding for this work was provided in part by the Director, Office of Energy Research, Office of Basic Energy Sciences, Materials Science Division of the U.S. Department of Energy under Contract DE-AC03-76SF00098. Partial funding for equipment also was provided by the National Science Foundation under Contract numbers CBT-8552821 and CHE83-51881.

TABLE OF CONTENTS

Chapter 1: Introduction

Because of the widespread use of solid catalysts in a variety of industrial applications, there continues to be a great deal of time and effort devoted, both in academia and in industry, to the study of solid catalysts and reactions catalyzed by them. Reactions catalyzed by solids generally are thought to occur through a sequence of steps involving adsorption of reactants on the catalyst surface, reaction on the surface, and desorption of products from the surface. It is usually assumed that the adsorbates do not penetrate into the subsurface layers of the solid, but are restricted to the catalyst surface. This belief has been perpetuated by the recent advances in surface science which allow detailed investigation of solid surfaces. In this work, it is shown that in some cases, small atoms such as carbon, hydrogen, and oxygen can move relatively easily between the surface and subsurface layers of solid catalysts. This could have important implications in catalysis since the presence of these atoms in layers below the surface could affect the way various adsorbates bind to and react on the surface.

The study of subsurface mobility in solid catalysts was not the original goal of this research project. Initially, we were interested in studying the catalytic properties of transition metal carbides. The reason for this was that these materials had shown promise as substitutes for noble metal catalysts. When transition metals are carbided, they form interstitial compounds in which the carbon atoms are located in the voids between the close-packed, or nearly close-packed, layers of metal atoms. The presence of the interstitial carbon significantly alters the bonding in these metals, causing marked changes in their physical and electrical properties (1). Moreover, the carbon also changes their catalytic properties, in some cases, conferring to them properties more

typical of noble metals (2-8). These materials are particularly interesting because they tend to form nonstoichiometric phases with large variations in the metal-to-carbon ratio, and the catalytic properties depend very strongly on this ratio. Therefore, by adjusting this ratio we hoped to be able to optimize the catalytic properties.

The first catalyst we chose to study was Mo_2C since we knew we could synthesize this material with surface areas as high as 100 m^2/g using techniques described by Boudart and coworkers (7,9). However, first we had to determine how to properly activate this catalyst. When Mo_2C is exposed to air, it readily dissolves oxygen at room temperature (1,10). Since oxygen is often a poison, it is necessary to remove it from the surface by some pretreatment procedure before the catalyst will become active. The two most common pretreatment procedures which had been reported in the literature for activating these carbides involved either evacuation between 1050 and 1300 K (8,11,12), or reduction in flowing hydrogen between 600 and 1000 K (5-7). However, the little work that had been done suggested that the activation process involved more than just the simple removal of oxygen from the catalyst surface. Therefore, it was necessary to gain a better understanding of the activation process and the effect of different pretreatment procedures on the catalytic properties.

The activation process was studied using temperature-programmed desorption (TPD) and temperature-programmed reduction (TPR). These techniques, which are reviewed in Chapter 2, allowed us to study the changes which took place in the catalyst during heating in helium (TPD) and in hydrogen (TPR). To our surprise, we found that both carbon and oxygen are mobile in Mo_2C at relatively low temperatures. As a result of the high carbon mobility, it is not possible to remove oxygen from this material without also removing some

carbon. Moreover, as discussed in Chapter 4, it is possible to vary the amount of carbon removed, and therefore the Mo:C ratio of the catalyst, by proper choice of pretreatment conditions. This allowed us to study the effect of the Mo:C ratio on the catalytic properties, which was our original goal. Changes in the surface of the catalyst were probed using temperature-programmed reduction (TPR) of chemisorbed oxygen. We found that as the Mo:C ratio of the catalyst increased, the oxygen was bound more tightly to the surface, and the shape of the TPR spectrum changed.

The TPR spectrum of chemisorbed oxygen on nearly stoichiometric Mo_2C contains two water peaks, a relatively narrow low temperature peak and a second much broader high temperature peak. The presence of two peaks in the TPR spectrum suggested that the surface contains two distinct types of adsorption sites for oxygen with different binding energies. However, we found that as the Mo:C ratio increased, the low temperature peak shifted to higher temperature, and the high temperature peak shifted to lower temperature. Also, the size of the low temperature peak increased relative to the high temperature peak as the Mo:C ratio increased. These results were very difficult to explain assuming the two peaks were produced by two different types of adsorption sites for oxygen.

Instead, as discussed in Chapter 5, we were able to show experimentally that the high temperature peak is produced by oxygen which penetrates into the subsurface layers of the catalyst during heating. When the surface becomes depleted by the desorption process, the subsurface oxygen moves back to the surface where it reacts and desorbs as water. We referred to this movement of oxygen between the surface and subsurface regions as subsurface diffusion. To aid in interpreting the experimental results, we developed a numerical model which accounts for the effect of subsurface

diffusion on TPD and TPR spectra.

Although the discovery that subsurface diffusion could produce an extra peak in a TPD or TPR spectrum was an interesting one, we felt that it would be of much greater significance if we could show that this phenomenon is not confined to just oxygen in Mo_2C. Therefore, we decided to use this technique to study subsurface diffusion in systems of greater practical importance. We chose to study the hydrogen-palladium system because palladium is a very good hydrogenation catalyst and hydrogen is known to dissolve in palladium. Another reason for choosing palladium was that there was considerable evidence in the literature for the existence of subsurface absorption sites for hydrogen between the topmost and second atomic layers of palladium single crystals (13-19). However, it was not known whether such states were present in the small metal crystallites of supported palladium catalysts. Therefore, we postulated that if subsurface absorption sites are present in a supported palladium catalyst, then diffusion of hydrogen between the surface and subsurface sites might produce a high temperature peak in the TPD spectrum of hydrogen on this catalyst. However, since desorption from a high binding energy adsorption site on the catalyst surface also can produce a high temperature peak in a TPD spectrum, a method was needed to distinguish between a peak produced by desorption from a high binding energy adsorption site, and a peak produced by subsurface diffusion.

To devise a scheme by which one could distinguish between these two possibilities, we simulated TPD spectra with a multisite model and a subsurface diffusion model. We then investigated how the theoretical spectra changed as the carrier gas flow rate, heating rate and initial coverage were varied. As discussed in Chapter 6, we found that it is possible to distinguish between the two possibilities by measuring the effect of carrier gas flow rate and heating rate

on the TPD spectrum. These results are used in Chapter 7 to show that hydrogen penetrates into subsurface absorption sites of a Pd/SiO_2 catalyst during TPD at atmospheric pressure. The fact that hydrogen penetrates into subsurface sites during TPD strongly suggests that hydrogen also is present in the palladium subsurface under typical catalytic reaction conditions.

Chapter 2: Overview of TPD and TPR

Temperature-programmed desorption (TPD) and related techniques are very useful tools for characterizing solid materials. TPD has been used most commonly to study the binding of adsorbates to catalytic surfaces. A major advantage of this technique over other surface sensitive techniques is that ultra-high vacuum (UHV) conditions are not required to study the surface chemistry. Instead, the catalyst can be studied under conditions which more closely resemble catalytic reaction conditions. The application of TPD and related techniques to the study of practical catalysts has been reviewed by Cvetanovic and Amenomiya (20,21), and by Falconer and Schwarz (22).

In a typical TPD experiment, 10 - 100 mg of catalyst are placed in a reactor which is mounted inside a furnace. Following pretreatment to obtain a clean surface, the catalyst surface is covered with the adsorbate of interest. Adsorption is usually accomplished by pulsing known quantities of the adsorbate into an inert carrier gas stream (usually helium at atmospheric pressure) which flows over the catalyst. By monitoring the concentration of the adsorbate in the reactor effluent with a mass spectrometer, the amount of each pulse which adsorbs on the surface can be determined quantitatively. Following adsorption, the catalyst temperature is raised linearly. As the catalyst is heated, the adsorbate desorbs into the carrier gas stream from which it either readsorbs or is swept out of the reactor. The concentration of the adsorbate in the reactor effluent is monitored continuously with the mass spectrometer. In the absence of diffusion limitations, the adsorbate concentration in the reactor effluent is proportional to the net rate of desorption (R_d = desorption rate - readsorption rate) from the surface. Thus, a desorption spectrum is a record of the net desorption rate as a function of the catalyst temperature.

A schematic picture of a TPD experiment is shown in Figure 2.1. Initially the desorption occurs at an increasing rate since it is an activated process. Eventually, the surface becomes depleted of adsorbate, and the net desorption rate goes through a maximum and decreases again, producing a peak. The temperature of the desorption peak is indicative of the strength with which the adsorbate is bound to the surface. In general, the more strongly the adsorbate is bound to the surface, the higher the temperature of the desorption peak. As is discussed in Chapter 6, in the absence of mass transfer limitations, a quantitative determination of the heat of adsorption can be obtained from the shift in the peak temperature with heating rate. In many cases the surface contains more than one type of adsorption site. If the heat of adsorption on these sites differs significantly, the TPD spectrum will contain multiple peaks, one for each type of adsorption site. When this happens, the heat of adsorption on each type of site can be determined separately.

The detailed analysis of TPD spectra can be obscured by such factors as diffusion limitations, readsorption of the desorbing gas, and coverage-dependent kinetic parameters. The effects of diffusion limitations on TPD spectra have been considered by several investigators (23-26). It has been shown that intraparticle diffusion limitations can be made negligible by using very small particles, and that axial diffusion limitations can be minimized by using shallow catalyst beds (if possible, beds should be less than 1 mm deep). The effects of readsorption usually can not be eliminated when TPD is performed in a flow system, as described here. In most cases, equilibrium readsorption of the desorbing gas is usually approached, causing the peaks to be broadened substantially. Peak broadening due to readsorption can be minimized somewhat by working at higher carrier gas flow rates, or using smaller amounts of catalyst. However, this also results in a decrease in

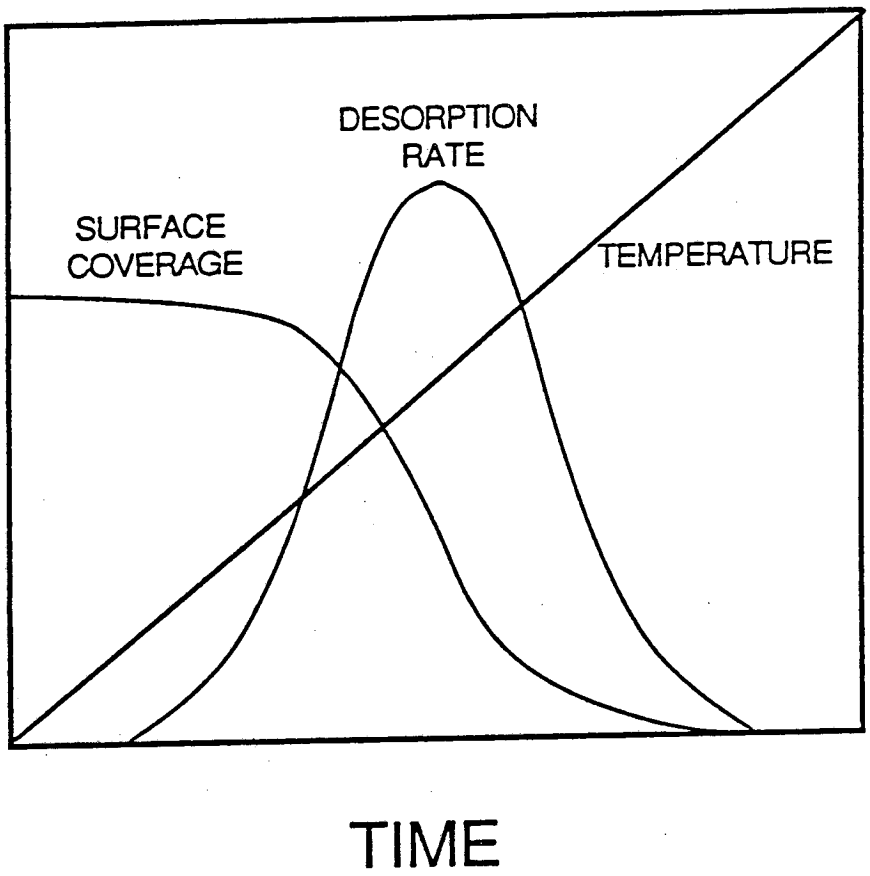

Figure 2.1: Schematic picture of a TPD experiment.

sensitivity. If the kinetic parameters for desorption are coverage-dependent, this also can complicate interpretation of TPD spectra. For example, in some cases, lateral interactions between adsorbate molecules (or atoms) cause the activation energy for desorption to vary with coverage. This is often referred to as induced heterogeneity. If the variation in the desorption activation energy with coverage is highly nonlinear, it is possible that this could produce an extra peak or peaks in the TPD spectrum (27,28). It is important to emphasize that all of these factors can alter TPD spectra significantly, making interpretation of the spectra difficult. Nevertheless, if proper care is taken in designing the experiment, and in critically analyzing the quantitative information derived, TPD can be a valuable tool for both fundamental and applied catalyst studies.

A technique which is closely related to TPD is temperature-programmed reduction (TPR). In this case, a reducing gas such as hydrogen is flowed over the sample instead of an inert gas. During heating, the hydrogen reacts with the adsorbate on the surface, and the desorption products are monitored downstream. This technique is very useful in cases where adsorbates such as oxygen do not desorb until temperatures above the range of a typical TPD experiment. By reacting the adsorbates with hydrogen, the desorption temperatures can be lowered substantially, and information can be obtained regarding the binding of these adsorbates to the surface.

The use of TPD and TPR in the study of catalysts is not restricted to just studying the desorption and reaction behavior of molecules adsorbed on the surface of a catalyst. TPR has been used extensively in studying the reduction of supported metal oxides to their metallic state prior to their use as catalysts (29). In this case, the reduction process often is limited by diffusion of oxygen through the crystallites. By measuring the amount of water produced during TPR, it is possible to measure the extent of reduction of the catalyst. In a similar

manner, TPD can be used to investigate the changes which take place in the catalyst during heating in helium or in vacuo. Thus, TPD and TPR can be used to guide the proper choice of pretreatment conditions for a particular catalyst. In addition, the same apparatus can be used as a differential reactor for steady-state and transient reaction studies.

A very important feature of both TPD and TPR is that these techniques are very sensitive to minor differences between samples. Thus, a TPD or TPR spectrum can be thought of as a "fingerprint" of a material. This property makes these techniques useful in quality control, and in studying changes which take place in a catalyst after use under reaction conditions. This property also makes these techniques powerful tools for studying solid materials in general, not just catalysts. For instance, we have found TPD and TPR to be extremely useful in characterizing the new oxide superconductors (30-32).

Chapter 3: Experimental

APPARATUS

A schematic flow diagram of the apparatus used to conduct the TPD and TPR experiments, and the reaction studies is shown in Figure 3.1. The apparatus is divided into four sections: gas purification, gas selection and flow control, the reactor, and gas analysis. Each of these four sections are discussed in detail in the sections below.

Gas Purification

Because of the large carrier gas flow rate relative to the quantity of adsorbed gas, extreme care needed to be taken to eliminate impurities from the carrier gas stream. In TPD experiments helium was primarily used as the carrier gas, except when it was desired to monitor deuterium desorption (mass = 4). In that case, argon was used. Traces of oxygen were removed from the helium (99.998%) by an "Oxisorb" cartridge (Alltech Associates), and water was removed by 5A molecular sieves cooled by a dry ice - ethanol bath. An "Oxisorb" cartridge also was used to remove oxygen from the argon (99.98 %) stream, and water was removed by molecular sieves.

During TPR experiments, hydrogen or deuterium were used as the carrier gas. Therefore, it was important that these gases also were very pure. Traces of oxygen in the hydrogen (99.995 %) stream were converted to water by passing the gas over a bed of 0.3 % Pd/SiO_2 heated to 150 C. This water was then trapped by cooled molecular sieves. When deuterium (98.5 % D_2) was used as the reducing gas, it had to be purified in the same manner.

The only other gases which required purification prior to use were

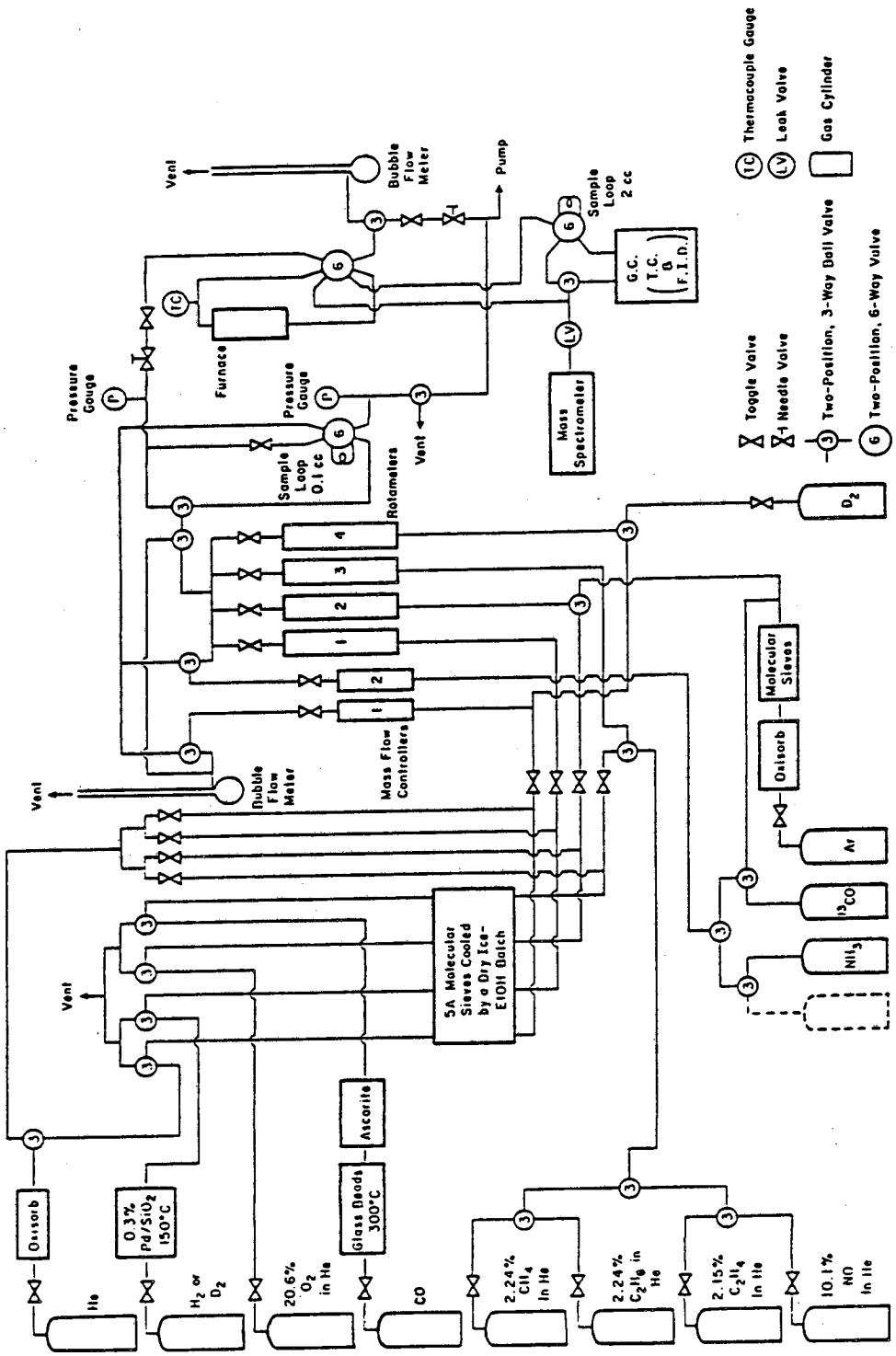

Figure 3.1: Flow diagram of the TPD apparatus.

oxygen and carbon monoxide. The major impurity in the oxygen (20.6 % O_2 in helium) stream was water which was removed by cooled molecular sieves. For CO, however, iron carbonyls could form in the tank. These were removed by passing the gas over glass beads heated to 300 C, and then over a bed of ascarite. Water was removed by cooled molecular sieves. It was important to remember that CO also was trapped by the molecular sieves. Therefore, time had to be allowed for the sieves to become saturated with CO before a constant CO concentration could be obtained. Moreover, when the sieves warmed up, the trapped CO was released and the pressure in the line built up. Therefore, it was necessary to vent the line when this occured.

Eventually, the molecular sieves used to remove water from the gas streams became saturated with continued use. The sieves were regenerated by heating to 300 C overnight while flowing helium over them. The "Oxisorb" cartridges also needed to be replaced every time a gas tank was replaced.

Gas Selection and Flow Control

Gas selection was accomplished with a network of three-way valves and toggle valves. The flow rates of the various gases were controlled either with one of two Tylan Model FC-260 mass flow controllers, or with one of four Matheson Series 601 rotameters equipped with high accuracy needle valves. The mass flow controllers operated at flow rates between 0 and 300 cc/min (STP). Calibration of the mass flow controllers was performed daily using a bubble flowmeter. A bubble flowmeter also was used to measure the flow rate through the four rotameters shown in Figure 3.1. The four rotameters allowed different gases to be mixed in a variety of combinations and compositions.

The gas used most commonly was helium which was used both as a carrier gas and as a diluent. When helium was used as a carrier gas, its flow

rate was precisely controlled by the mass flow controller labeled #1 in Figure 3.1. A great advantage of a mass flow controller is that the flow rate (STP) is unaffected by the downstream pressure. This is not the case for rotameters. When helium was used as a diluent, it flowed through the rotameter lableled # 4 in Figure 3.1. Argon also was used both as a carrier gas and as a diluent. When it was used as a carrier gas, the flow rate was controlled with the mass flow controller labeled # 2 in Figure 3.1. When it was used as a diluent, the flow rate was adjusted with the rotameter labeled # 2. In TPR experiments, hydrogen (or deuterium) was used as the carrier gas. Although a mass flow controller was preferable, in this system, a rotameter was used to adjust the hydrogen flow rate.

Reactor

The reactor used in the TPD system was made of quartz and is drawn to 3/8 scale in Figure 3.2. It consisted of two 6-mm-o.d. sections at the inlet and exit, and a 9-mm-o.d. section in the middle. A quartz frit was used to support the catalyst, and quartz wool was placed on top to hold the catalyst in place. The reactor was mounted inside a furnace which consisted of 6 feet of nichrome wire (2 Ω/ft) wrapped around a 13-mm-o.d. quartz tube. The wire was held firmly in place by coating it with a layer of Sauereisen electrotemp cement (J.A. Crawford Co., No. 8 powder).

Power to the furnace was controlled by a programmable temperature controller (built in-house) capable of ramping the temperature linearly in time up to 1200 K at rates ranging from 0.01 to 5 K/s. The catalyst temperature was monitored with an exposed-junction thermocouple placed in the catalyst bed. Feedback to the controller was provided by a sheathed chromel-alumel thermocouple placed outside between the reactor and the inside wall of the

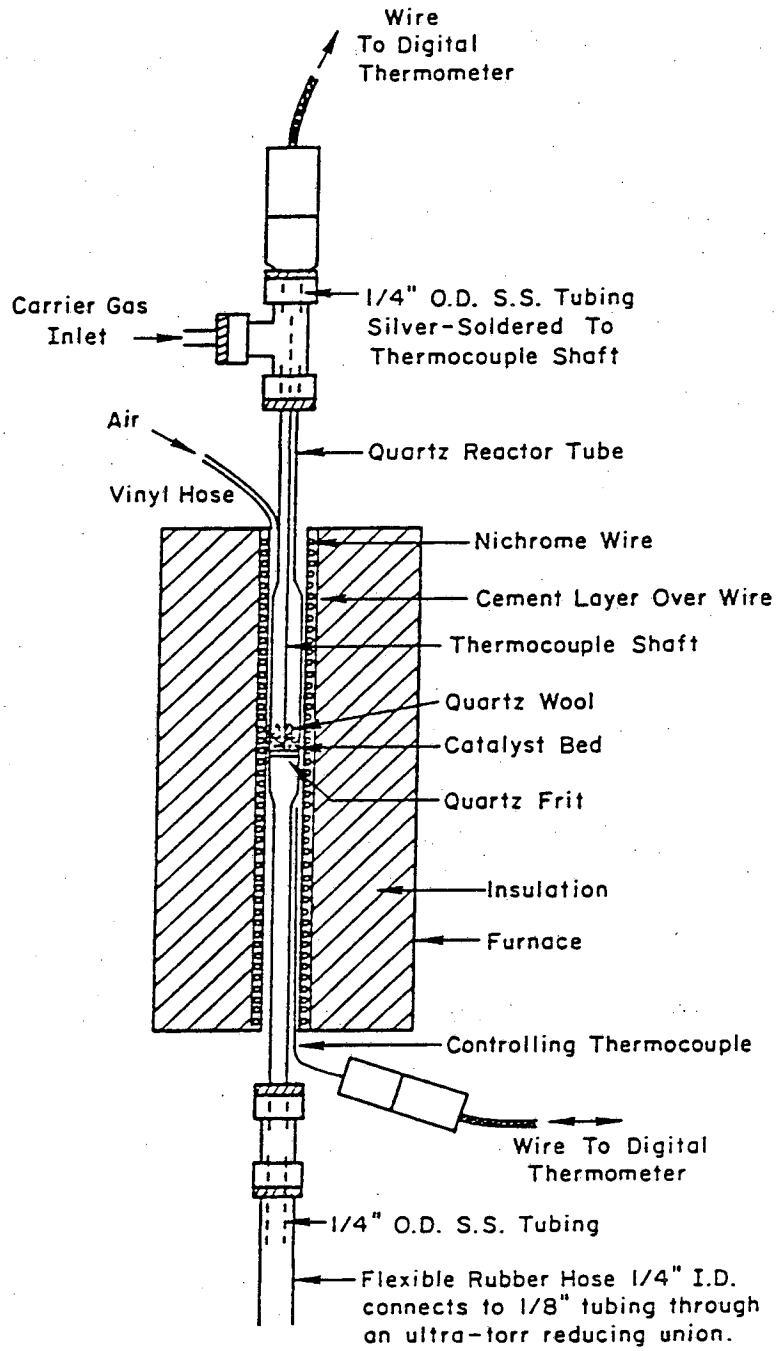

Figure 3.2: Schematic picture of the reactor mounted inside the furnace, drawn to 3/8 scale.

furnace. The reason why the outside thermocouple was used for feedback was that the temperature at the furnace wall responded much faster to changes in the furnace power than the temperature in the catalyst bed. This served to damp out oscillations in the heating rate rate of the catalyst bed.

Gas Analysis

The composition of the effluent gas from the reactor was monitored primarily with a UTI Model 100 C quadrupole mass spectrometer. This was accomplished by continuously leaking a small portion of the effluent through a Granville-Phillips Series 203 variable leak valve into the vacuum system housing the mass spectrometer. The mass spectrometer was interfaced to an IBM PC through a Metrabyte Model Dash-16 interface board. Up to 10 different masses could be monitored and signal averaged (over 100 points) every 0.5 seconds. A listing of the computer program used for data acquisition and control during TPD experiments is given in Appendix A. Since the temperature of the catalyst bed also was monitored by the computer, the mass spectrometer signal for each mass could be plotted as a function of either time or temperature. The integrated area under the desorption spectrum also was calculated so that the total amount of desorption products could be determined.

During reaction studies, the products from the reactor also were analyzed with a Varian Model 3760 gas chromatograph, equipped with thermal conductivity and flame ionization detectors. For the ethylene hydrogenation studies discussed in Chapter 4, a 78" X 1/8 " activated alumina 60/80 column was used to separate the reaction products. By switching the position of the six-way valve prior to the reactor, the reactant stream could be analyzed instead of the product stream. This allowed determination of the reaction conversion.

MATERIALS

Mo_2C

All but one of the Mo_2C samples used in this study were taken from a single batch of catalyst prepared in a manner similar to that described by Boudart and coworkers (7); the details are given elsewhere (33). The synthesis involved first heating MoO_3 from 573 to 973 K in flowing hydrogen over a period of 5 hours according to a programmed temperature schedule (33). Then the MoO_3 was reduced an additional 15 hours at 973 K. The Mo product was removed from the reactor, crushed, and reduced an additional 2 hours at 573 K prior to carburization. To carburize the sample, it was heated in a flowing 3:1 mixture of methane:hydrogen from 573 to 773 K over a period of 3 hours, and then held at 773 K for 72 hours. It was determined by powder X-ray diffraction that the sample was predominantly hcp Mo_2C, but also contained approximately 13 % Mo by weight. This Mo presumably was confined to the inner core of the catalyst since the core is expected to be carburized last. There was no evidence of any molybdenum oxides in the diffraction patterns. The BET surface area of the hcp Mo_2C was measured to be approximately 6 m^2/g, although it varied slightly depending on the pretreatment conditions. The BET experiments were performed at 77 K using nitrogen as the adsorbate. The area occupied by a nitrogen molecule was assumed to be 0.162 m^2/g (34).

A sample of fcc Mo_2C also was used for one experiment. This sample was prepared by a method outlined by Volpe and Boudart (9). The synthesis involved conversion of MoO_3 to Mo_2N by reaction with ammonia, and then carburization to Mo_2C using a methane/hydrogen mixture. The powder X-ray diffraction results on this sample showed only fcc Mo_2C. The BET area of the sample was 87 m^2/g.

Pd/SiO_2

A 9 wt % Pd/SiO_2 catalyst was prepared according to the method described by Hicks, et.al. (35). Cab-O-Sil HS5 silica (BET area = 300 m^2/g) was impregnated with a solution of H_2PdCl_4 dissolved in 1 N HCl. Then the sample was dried in vacuum at 338 K, calcined in a 21 % O_2/He mixture at 623 K for 2 hours, and reduced in H_2 at 573 K for 3 hours. The catalyst dispersion was determined from the irreversible uptake of H_2, D_2, and CO at 290 K. Adsorption of these gases was performed using the pulse adsorption technique described later. The results of all three agreed to within 5 % assuming an adsorption stoichiometry of one hydrogen or deuterium atom, and one CO molecule per surface Pd atom (35). The catalyst used in the deuterium desorption experiments had a 15 % dispersion. The same catalyst was used for the hydrogen TPD experiments, except that it had been sintered somewhat by a 30 min evacuation at 873 K. This lowered the dispersion to 9 %.

EXPERIMENTAL PROCEDURE

Before the catalyst was placed in the reactor, it was sieved to obtain 30/60 mesh granules. These small particle sizes assured that intraparticle mass transfer limitations were negligible in all measurements (26). After placing the catalyst in the reactor, the system was flushed with helium and evacuated for 1 hour. Then, prior to performing adsorption, TPD, TPR, or reaction studies, the catalyst was pretreated in some manner to obtain a clean surface. The pretreatment conditions used for each catalyst are described later.

Adsorption

Adsorption of probe molecules was performed by pulsing known quantities of the adsorbate into a carrier gas stream which flowed over the catalyst. By monitoring the reactor effluent with a mass spectrometer, the amount of adsorbate in each pulse which did not adsorb was determined quantitatively. This amount was subtracted from the amount of adsorbate in each pulse to determine the amount which adsorbed. The amount of adsorbate in each pulse was determined from the size of the sample loop on the six-way pulse valve (0.1cc), and the composition of the adsorbate containing stream used to charge the sample loop. Typically, the amount of adsorbate in each pulse was adjusted so that between 5 and 10 pulses were sufficient to saturate the catalyst surface. Although the adsorption methods used to achieve partial coverages may result in intraparticle gradients in coverage, modeling studies have shown this to have a negligible effect on the TPD spectrum (26).

Mass Spectrometer Calibration

Calibration of the mass spectrometer for H_2, D_2, O_2, CO, CO_2, CH_4, C_2H_4, and C_2H_6 was performed in the following manner. Known quantities of each gas were injected into a 100 cc/min (STP) helium stream using the six-way pulse valve, and the concentration of the gas in the helium stream was monitored with the mass spectrometer. The integrated area of the mass spectrometer signal as a function of time for each pulse was found to vary linearly with the amount of gas pulsed in each case. This allowed a calibration factor to be determined for each gas. Once the calibration procedure was performed for each gas, the relative sensitivity of the mass spectrometer to each gas could be determined. The relative sensitivity of the mass spectrometer to different gases did not vary significantly over the course of these experiments.

Therefore, following a TPD or TPR experiment, it was necessary only to calibrate the mass spectrometer for one of the gases, and the relative sensitivities were used to determine the calibration factors for the other gases.

The mass spectrometer was calibrated for water by performing a series of TPR experiments on the hcp Mo_2C catalyst. A known quantity of oxygen was adsorbed onto the catalyst surface, and then the temperature was raised linearly in time while hydrogen was flowed over the sample. During heating, the oxygen on the surface reacted with the hydrogen to form water which desorbed. By integrating the area under the TPR spectrum, the sensitivity of the mass spectrometer to water relative to oxygen was determined. This relative sensitivity remained constant as the amount of oxygen adsorbed was varied.

TPD and TPR Experiments

Following adsorption of the probe molecule, the reactor was flushed with helium (or argon). In a TPD experiment, the temperature was then raised linearly in time while helium (or argon) flowed over the sample. During heating, the desorption products were monitored continuously with the mass spectrometer. In a TPR experiment, hydrogen or deuterium was used as the carrier gas. During heating, the hydrogen or deuterium reacted with the adsorbate on the surface, and the desorption products were monitored downstream.

In all cases the bed depth was kept as shallow as possible to minimize the effects of axial diffusion limitations. Assuming the reactor was well-mixed (23), the adsorbate concentration in the carrier gas was proportional to the net rate of desorption from the surface (R_d = desorption rate - readsorption rate). Since the mass spectrometer signal varied linearly with the adsorbate concentration in the carrier gas, the mass spectrometer signal was proportional

to R_d, and the integrated area under the desorption spectrum was proportional to the initial coverage. As a result, R_d could be determined quantitatively by dividing the mass spectrometer signal at each temperature by the integrated area under the desorption spectrum for an initially saturated surface ($\theta_0 = 1$).

Ethylene Hydrogenation Studies

In Chapter 4, the effect of Mo:C ratio on the activity of Mo_2C for ethylene hydrogenation is discussed. For these experiments, 2.15 % C_2H_4 in helium (Matheson certified standard) was mixed with hydrogen, and flowed over the catalyst. The C_2H_4 flow rate was set at 187 cc/min (STP), and the hydrogen flow rate was 12 cc/min (STP), giving an H_2/C_2H_4 ratio of 3/1. The total pressure in the reactor remained constant at 830 torr. The reaction products were monitored continuously with the mass spectrometer, and periodically with the thermal conductivity detector of the gas chromatograph.

Chapter 4: Carbon and Oxygen Mobility During Activation of Mo_2C Catalysts

As discussed in Chapter 1, the original goal of this research project was to study the catalytic properties of transition metal carbides. The reason for this was the growing interest in the catalytic properties of transition metal carbides generated by the reports of several workers (2-8) that alloying carbon to these metals changes their catalytic properties. Most of the previous catalytic studies which had been performed on these carbides had focussed on determining the activity of TaC, TiC, WC, and Mo_2C toward such reactions as ethylene hydrogenation, ethane hydrogenolysis, and CO hydrogenation. Prior to reaction, the catalysts were activated by evacuation between 1050 and 1300 K (8,11,12), or by reduction in flowing hydrogen between 600 and 1000 K (5-7). The purpose of the pretreatments was to remove oxygen which often is a poison and which readily dissolves in these materials at room temperature (1,10). Following activation, the carbides exhibited activities for these reactions that were much higher than those of the parent metals and comparable to those of some noble metals (4,6,7,12). However, the activities were still about an order of magnitude lower than the activity of the most active noble metal for each particular reaction (36).

While a number of studies have focussed on the catalytic activity of transition metal carbides after activation, there has been very little work directed at studying the nature of the activation process. Kojima and coworkers (11) found that the activities of WC, TaC, and TiC for ethylene hydrogenation varied strongly with evacuation temperature. Up to some critical evacuation temperature the catalysts were inactive. Then as the evacuation temperature was raised, the activity rose sharply, went through a maximum, and then

decreased sharply. XPS studies revealed that the evacuation temperature at which the carbides became active, corresponded to the temperature at which oxygen was removed from the surface. However, they were unable to explain the sharp decrease in activity caused by higher evacuation temperatures since their data showed that the loss of activity was not due to sintering. Also, they were unable to explain why the activity of TaC for ethylene hydrogenation was lower after reduction at 1270 K than after evacuation (12).

Thus, before we could study the catalytic properties of these materials, it was necessary first to gain a better understanding of the activation process, and the effect that different pretreatment procedures have on the catalytic properties of the transition metal carbides, in particular, unsupported Mo_2C. The activation process was studied using temperature-programmed-desorption (TPD) and reduction (TPR). By integrating the TPD and TPR spectra, the amount of carbon and oxygen removed from Mo_2C was determined as a function of the evacuation or reduction temperature. The effects of different pretreatment procedures on the catalytic properties of Mo_2C were studied using ethylene hydrogenation as a probe reaction. Also, TPR of chemisorbed oxygen was used to probe changes in the catalyst surface resulting from different activation procedures.

RESULTS

TPD and TPR of Mo_2C

To gain insight into the nature of the activation process, samples of Mo_2C that had been exposed to air were heated in either flowing helium (TPD) or hydrogen (TPR) to 1173 K. In both cases, H_2O, CO, CO_2, and CH_4 were observed desorbing from the sample; in addition, C_2H_6 was observed in the

TPR spectrum. The TPD and TPR spectra of each product were integrated to determine the amounts of carbon and oxygen removed from the catalyst so that changes in the bulk composition of the catalyst due to the activation process could be monitored.

Figures 4.1a and b present the results of a 1 K/s ramp in helium for a 100 mg of sample of Mo_2C, which was previously evacuated at 298 K for 1 hour. In this experiment, the helium flow rate was 100 cc/min (STP). An important feature of the TPD spectrum is that oxygen is not removed from the sample as molecular O_2. Instead, it combines with carbon in the sample and desorbs as CO and CO_2 in four distinct peaks at approximately 583, 658, 918, and 1068 K, with a fifth CO peak starting to rise at 1150 K. Water and methane peaks also appear both at 583 and 658 K; the origin of these peaks is not clear at this time. It is possible that these peaks might be produced by reaction of oxygen and carbon with either residual hydrogen that might have dissolved in the sample during synthesis, or with hydrogen produced from the dissociation of strongly bound water. The water peak at 393 K is assigned to water that is either strongly bound to the surface or trapped in the pores of the catalyst. It must be pointed out that the exact position and shape of each of the peaks in Figure 4.1 (and in Figure 4.3) vary slightly from sample to sample. This variation most likely is caused by a minor degree of inhomogeneity in the batch of catalyst from which they were taken. However, the general nature of the desorption spectrum does not change.

The spectra in Figure 4.1 were integrated to determine the quantity of each product which desorbed as a function of temperature; the results are shown in Figure 4.2. The horizontal dashed line in Figure 4.2 represents the number of surface Mo atoms per gram, based on the BET area of 6 m^2/g and assuming 1.1 X 10^{15} sites/cm^2 (9). It is evident that the samples contained the

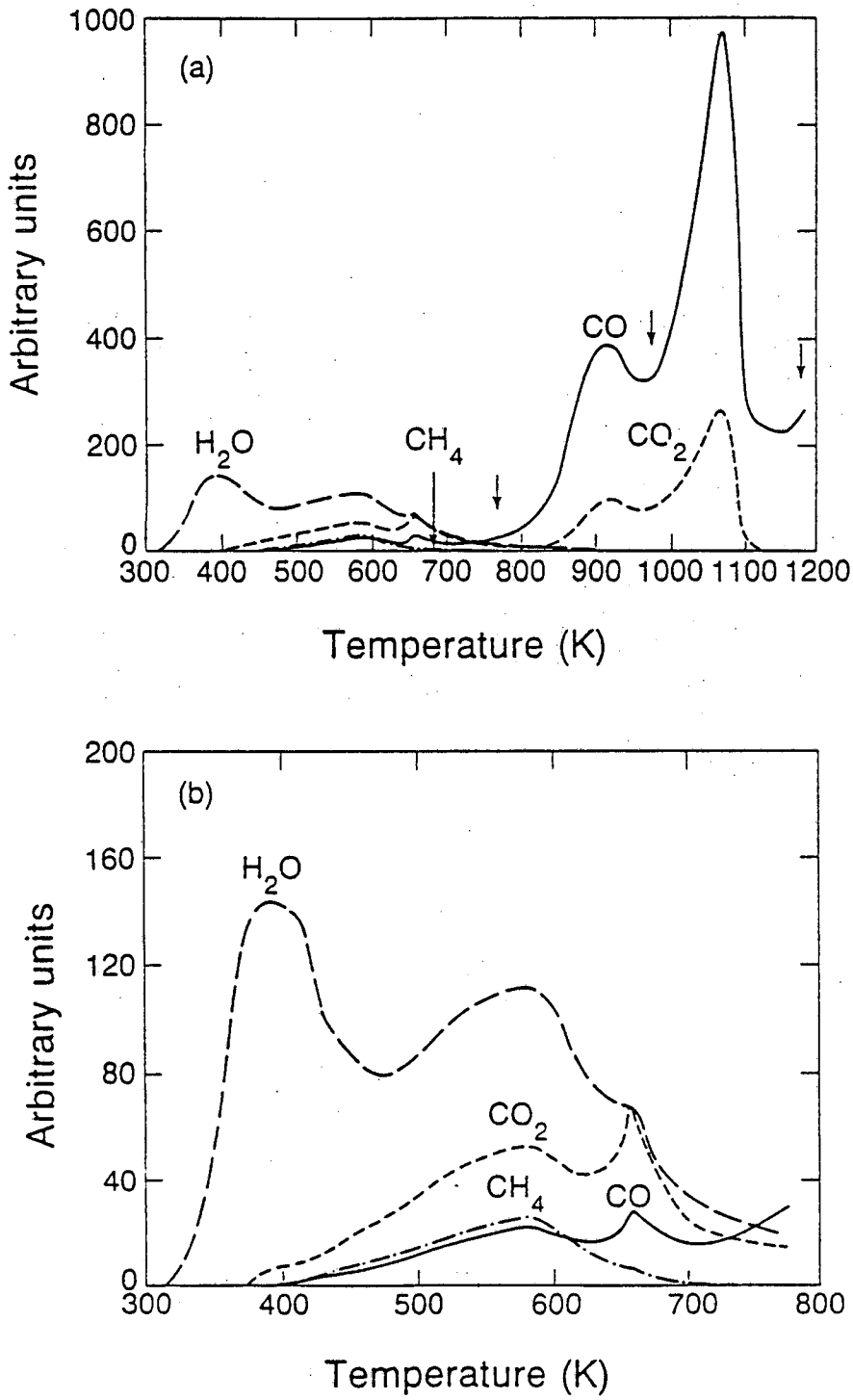

Figure 4.1: (a) Desorption spectrum for a 1 K/s ramp in He to 1173 K for 100 mg of Mo_2C after evacuation for one hour at 298 K. (b) First part of ramp expanded by a factor of five.

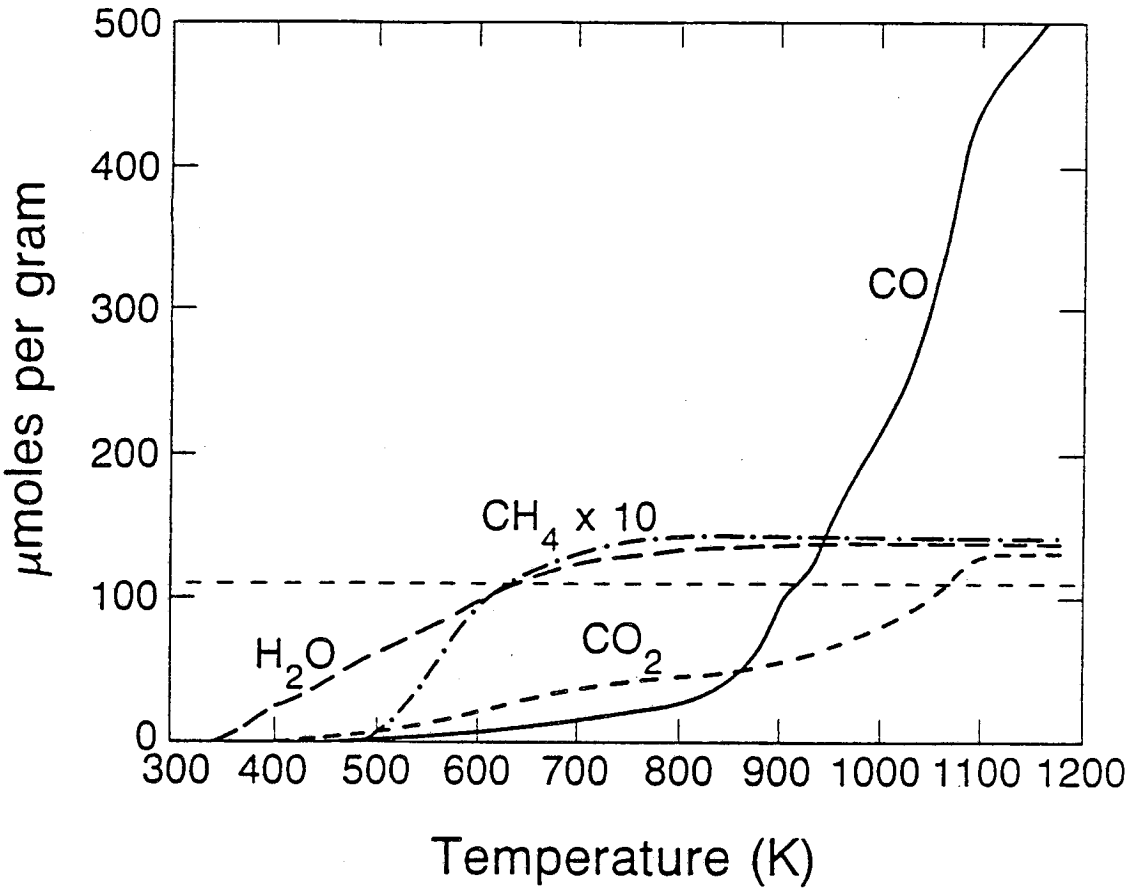

Figure 4.2: Integrated area under desorption curves in Figure 4.1 converted to μmoles of each gas desorbed per gram of catalyst as a function of temperature. The dashed horizontal line represents the number of surface sites per gram, assuming 1.1 X 10^{15} sites/cm^2 and a BET area of 6 m^2/g.

equivalent of more than 7 monolayers of oxygen (assuming one monolayer corresponds to one oxygen atom per surface Mo atom). In removing this oxygen, more than 650 μmoles/g of carbon were removed simultaneously. This corresponds to 13 % of the carbon originally contained in the sample. Even more carbon was removed for higher surface area samples. In fact, when the 87 m^2/g sample was subjected to the same temperature ramp, carbon was removed quantitatively. This was verified by powder X-ray diffraction which showed that the carbide had been converted completely to molybdenum metal. This proves that the carbon being removed as CO and CO_2 is predominantly coming from the carbide, and not from any carbonaceous surface species.

Figures 4.3a and b show the results of a 1 K/s ramp in 100 cc/min (STP) of hydrogen for another 100 mg sample of Mo_2C taken from the same catalyst batch. Prior to taking this TPR spectrum, the sample was evacuated at 298 K for 1 hour. The major difference between the TPD spectrum in Figure 4.1 and the TPR spectrum in Figure 4.3, is the mechanism by which the oxygen is removed from the catalyst. During heating in helium, the oxygen is removed by reaction with bulk carbon, whereas during heating in hydrogen, the oxygen reacts with hydrogen and desorbs as water. This results in as many as 5 water peaks in the TPR spectrum: a sharp peak at 518 K denoted α, two peaks at 598 and 658 K designated β and γ, respectively, which nearly merge into one very broad peak, and two smaller peaks at 818 and 878 K. The water peak at 388 K is assigned to water that is either tightly bound to the surface or trapped in the pores of the catalyst.

Although most of the oxygen is removed as water during heating in hydrogen, approximately 15 % of it still reacts with carbon in the sample, desorbing in two small CO and CO_2 peaks at approximately 500 and 630 K. Furthermore, the carbon in the sample also reacts with the hydrogen to form

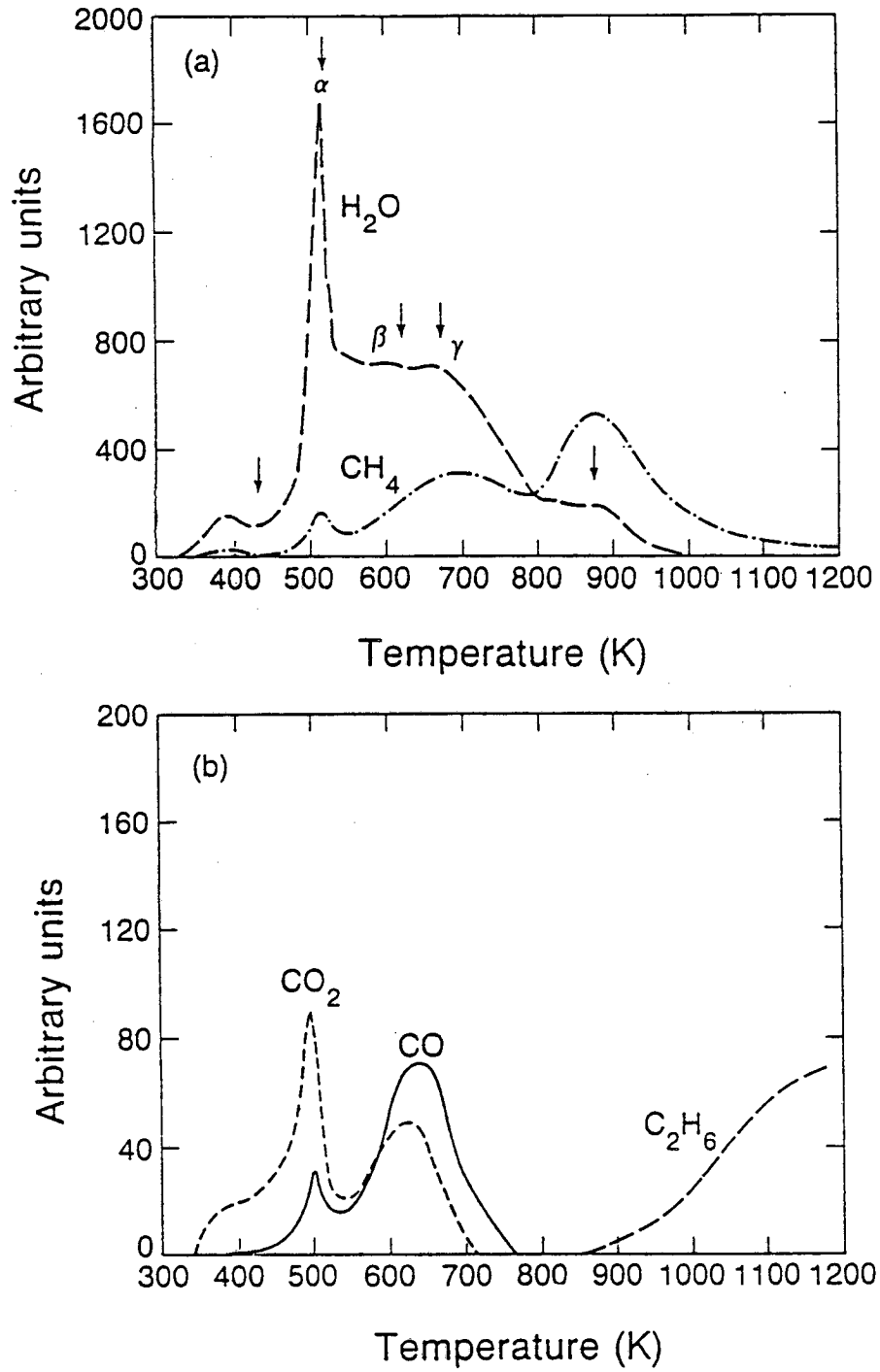

Figure 4.3: (a) Desorption spectrum of water and methane for a 1 K/s ramp in H_2 to 1200 K for 100 mg of Mo_2C after evacuation for one hour at 298 K. (b) CO and CO_2 desorption during the same ramp in H_2, magnified by a factor of 10.

CH_4, and at higher temperatures C_2H_6. As shown in Figure 4.4, close to 750 μmoles/g of carbon (approximately 15 % of the carbon originally in the sample) were removed during the ramp in hydrogen, and still more could be removed during heating at 1200 K. Powder X-ray diffraction analysis of samples heated to 1200 K in either He or H_2 showed that the removal of carbon results in an increase in the fraction of molybdenum metal in the sample.

To investigate how quickly Mo_2C incorporates oxygen during exposure to air at room temperature, reduced samples were removed from the reactor and exposed to air for various lengths of time ranging from a few minutes to several weeks. Then the exposed samples were placed back in the reactor, evacuated for one hour, and heated in H_2. It was found that after a few minutes of exposure, the catalyst contained between one and two monolayers of oxygen, as verified by TPR. Following this initial rapid uptake of oxygen, the samples continued to incorporate oxygen at a slower rate for several weeks as evidenced by increasing amounts of oxygen removed in the TPR experiments as a function of exposure time. The TPR spectrum of a sample which had been exposed to the air for one day is shown in Figure 4.5. The amount of oxygen removed as water in Figure 4.5 is equivalent to more than 3 monolayers, whereas over 9 monolayers of oxygen were removed from a sample that had been exposed to the air for over a month (Figure 4.3a). This indicates that the rate of oxygen incorporation by Mo_2C is significant even at room temperature, and that the incorporation of oxygen into the bulk is not the result of a rapid autothermal oxidation of the sample. It also should be noted that no bulk oxides could be detected in any of the samples by powder X-ray diffraction. The spectrum in Figure 4.5 also shows the clear distinction between the β and γ peaks that was not as obvious in Figure 4.3.

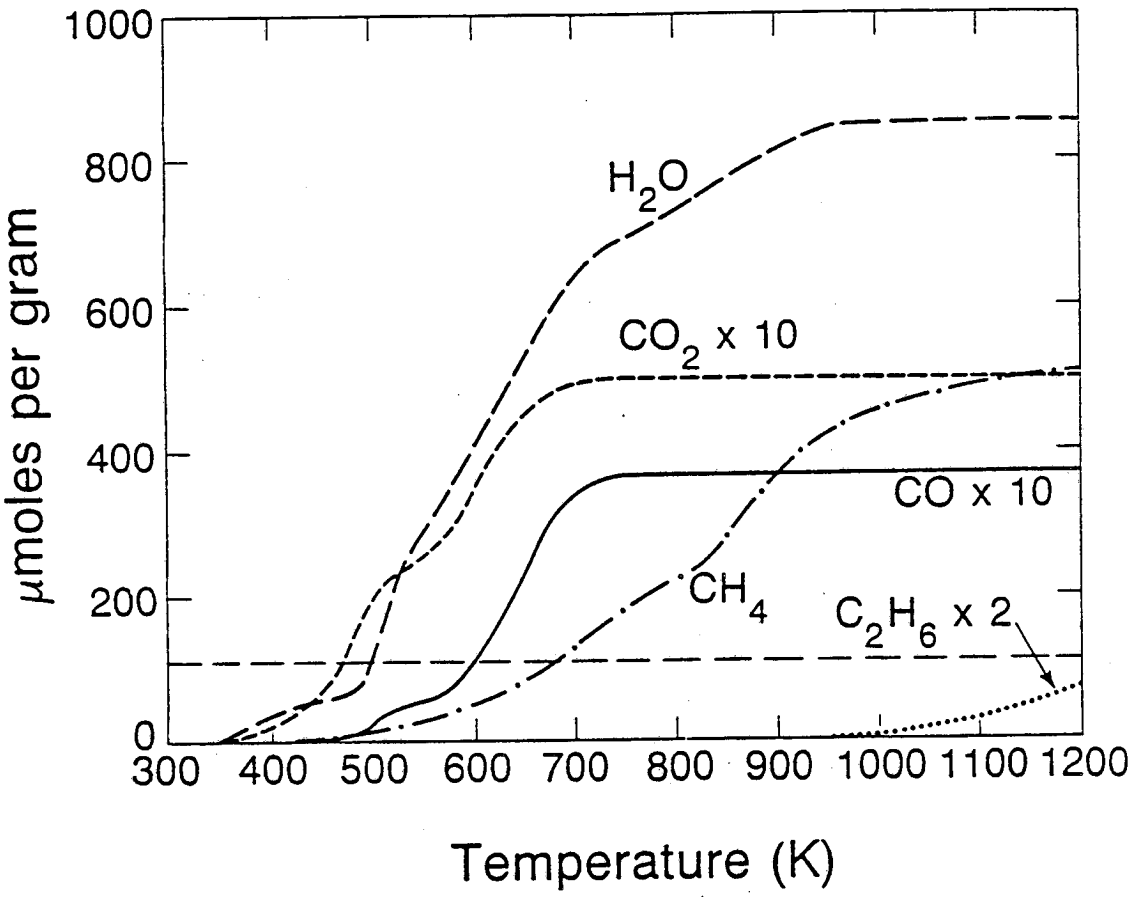

Figure 4.4: Integrated area under desorption curves in Figure 4.3 converted to μmoles of each gas removed per gram of catalyst as a function of temperature. The dashed horizontal line represents the number of surface sites per gram.

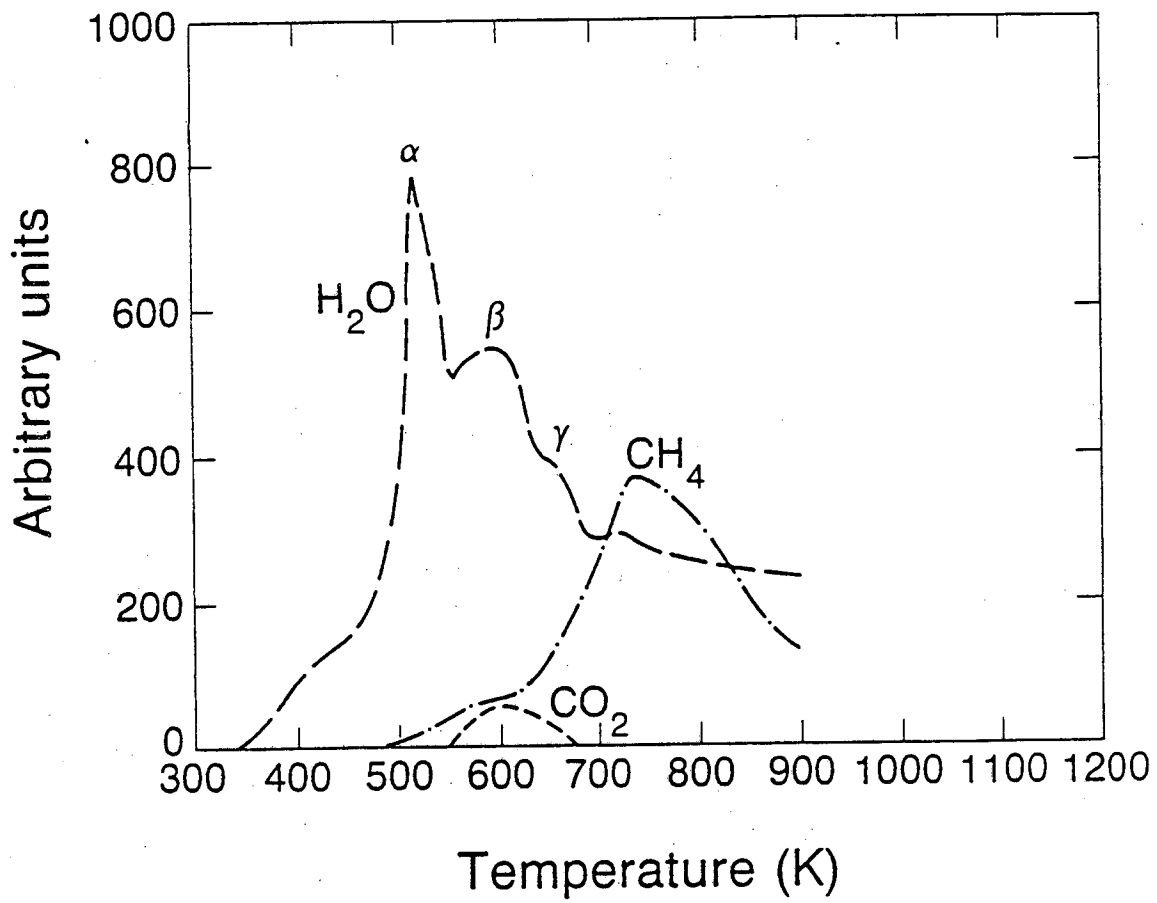

Figure 4.5: TPR of an Mo_2C sample that was reduced at 1200 K, and subsequently exposed to the air for 24 hours.

The results presented above show that oxygen is readily incorporated into Mo_2C during exposure to air at room temperature, and that it is not possible to remove all the oxygen from the catalyst by evacuation or reduction without also removing a significant amount of bulk carbon. Moreover, the mechanism and rate of removal of the oxygen and carbon are not the same for evacuation and reduction, as evidenced by the differences between the TPD and TPR spectra.

Activation of Mo_2C for Ethylene Hydrogenation

It was suggested by Kojima, et.al. (11), and verified in this laboratory, that surface oxygen poisons Mo_2C for ethylene hydrogenation at 298 K. Therefore, it was known that the pretreatment conditions required to fully activate the Mo_2C for this reaction would have to be sufficent to remove oxygen from the surface. However, the TPD and TPR results suggested that oxygen removed from the surface was replenished by oxygen from the bulk. As a result, it was not known whether all the oxygen in the sample would have to be removed to fully activate the catalyst for ethylene hydrogenation. Therefore, the activity of the catalyst for ethylene hydrogenation was compared after pretreatment conditions which removed different amounts of oxygen from the sample.

The TPD and TPR results also showed that the pretreatment conditions required to remove oxygen, simultaneously removed carbon from the sample. Since carbiding the Mo is known to change its catalytic properties, it was expected that removing carbon from Mo_2C would affect its catalytic properties. Moreover, since the amount of carbon removed during heating in helium was not the same as in hydrogen, the catalytic properties were expected to change for different pretreatment methods. Therefore, the activity of Mo_2C for ethylene

hydrogenation was measured after evacuation or reduction at several different temperatures.

The evacuation and reduction temperatures used were chosen based on the TPD and TPR spectra presented in Figures 4.1 and 4.3. During heating in either helium or hydrogen, oxygen is removed in several peaks. To determine the effect of removing the oxygen corresponding to each peak, the carbides were pretreated at temperatures slightly above each of the various peak temperatures in the TPD and TPR spectra. These temperatures are indicated by the arrows in Figures 4.1 and 4.3.

The effect of the evacuation or reduction temperature on the activity of the catalyst for ethylene hydrogenation, the amount of carbon and oxygen removed from the sample, and the BET area is shown in Table 4.1. In each case, 14.7 mg of catalyst were heated to the designated activation temperature at 1 K/s in the gas listed, and held at that temperature for the time listed in the table. The activities were normalized such that the maximum observed integral rate of 1.96×10^{-4} moles/g·s (97% conversion) corresponded to an activity of 100%. This initial rate corresponds to a turnover number of 1.79 s^{-1}, assuming 1.1×10^{15} sites/cm^2. This rate is slightly higher than the turnover number of 0.9 s^{-1} that can be calculated from the results of Kojima, et. al. (11) on WC at 273 K, for an ethylene partial pressure of 10 torr and a hydrogen pressure of 20 torr.

As shown in Table 4.1, if changes in the surface area are accounted for, a 5 minute reduction at 673 K gives the same initial activity as a 30 minute reduction at 873 K. However, the 30 minute reduction at 873 K removes all the oxygen from the sample, and the 5 minute reduction at 673 K only removes 86% of the oxygen. Thus, it is not necessary to remove all the oxygen to fully activate the catalyst. However, it is necessary to remove more than the

TABLE 4.1

Effect of Pretreatment Conditions on the Activity of Mo_2C for Ethylene Hydrogenation

Gas	Activation Temperature (K)	Time (min)	H_2O[a,b] (μmole/g)	CO[a] (μmole/g)	CO_2[a] (μmole/g)	CH_4[a] (μmole/g)	% Carbon Removed	Initial Activity %	Deactivation Curve Shape[c]	BET Area (m^2/g)
He	773	10	135	50	50	14	2.3	0.3	-	5.0
He	973	10	135	350	80	14	9.0	93	3	-
He	1173	10	135	550	130	14	14.0	100	2	-
H_2	433	5	90	1	7	5	0.3	0	-	-
H_2	523	5	525	7	25	30	1.3	40	1	-
H_2	623	15	725	30	50	90	3.4	95	1	6.0
H_2	673	5	735	37	50	200	5.8	100	3	-
H_2	873	30	850	37	50	900	20.0	90	2	5.4

[a] Quantity desorbed during pretreatment.

[b] Includes contributions of adsorbed water plus water from reaction of oxygen and hydrogen

[c] Shapes corresponding to each number are shown in Figure 4.6.

equivalent of one monolayer. After a 10 minute evacuation at 773 K, the initial activity is only 0.3 % of the maximum observed activity, despite removing the equivalent of more than one monolayer of oxygen as CO and CO_2. Furthermore, a 5 minute reduction at 523 K results in only a 40 % initial activity, despite having removed the equivalent of almost 4 monolayers of oxygen. This suggests that as oxygen is removed from the surface, oxygen from the bulk replenishes it, leaving the surface partially covered with oxygen. This is supported by the fact that oxygen continued to react with the hydrogen and desorb as water even after 5 minutes at 523 K.

The results presented above demonstrate that it is not necessary to remove all the oxygen from Mo_2C to activate it fully for ethylene hydrogenation. However, it is necessary to remove the equivalent of several monolayers since oxygen removed from the surface can be replenished by oxygen from the bulk. Furthermore, the initial activity does not depend on the amount of carbon removed by the activation process for the conditions considered. However, as shown below, the rate at which the catalyst deactivates depends strongly on the amount of carbon removed.

Deactivation of Mo_2C

Along with the initial activity of the catalyst, Table 4.1 also indicates the general shape of the activity vs. time curve (deactivation curve) after each pretreatment. The three different shapes corresponding to the numbers 1 through 3 in Table 4.1 are shown in Figure 4.6. Each curve is normalized to give an initial activity of 100 %. As shown in Table 4.1 and Figure 4.6, the shape of the deactivation curve varies significantly depending on the amount of carbon removed by the pretreatment.

When the catalyst was activated by reduction below 623 K, less than

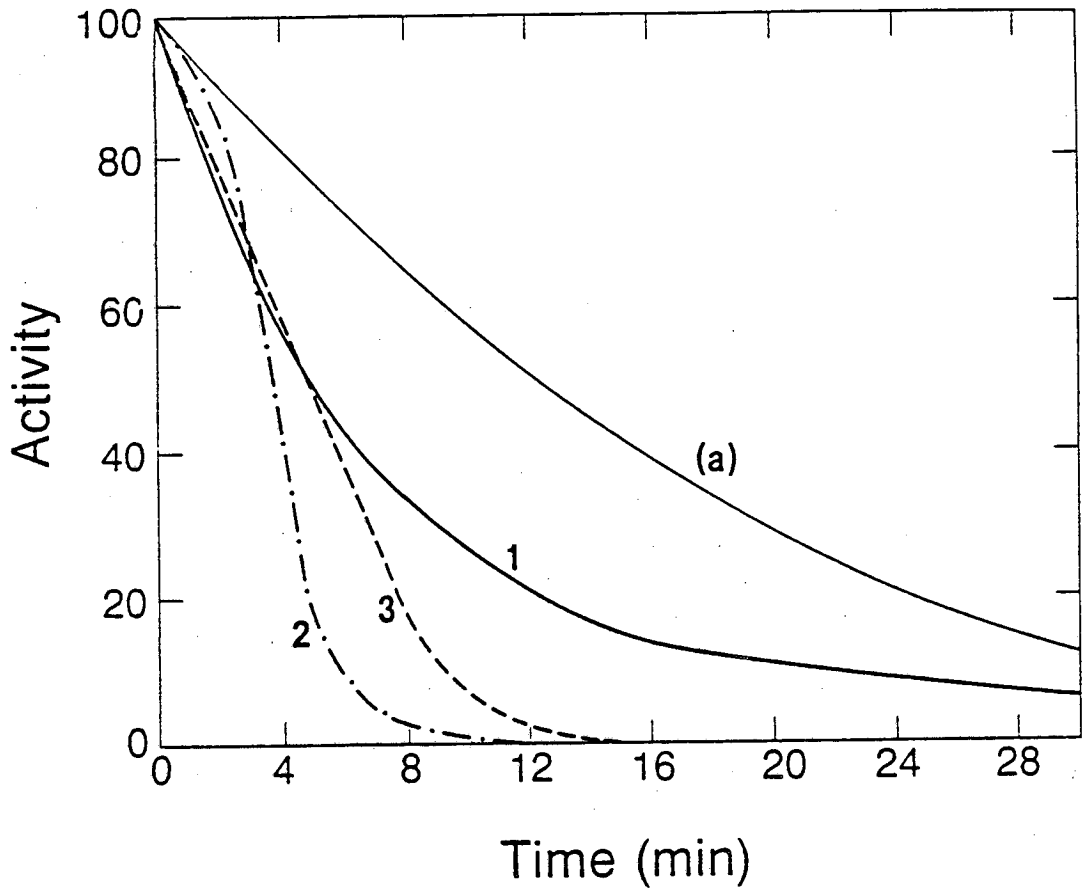

Figure 4.6: Shapes of the three different deactivation curves for ethylene hydrogenation at 298 K after different activation treatments. All curves are normalized for an initial activity of 100%. Also shown is the deactivation curve expected for deactivation solely due to oxygen poisoning (curve a).

3.5% of the carbon in the sample was removed, and the activity appeared to decay exponentially with time, dropping 3 orders of magnitude after one hour. However, if the pretreatment procedure removed between 6 and 9 % of the carbon, as was the case for the 973 K evacuation and the 673 K reduction, the activity decreased almost linearly with time initially, before decaying exponentially at longer times. In this case, the activity decreased by three orders of magnitude in just 15 minutes. Finally, if the pretreatment procedure removed between 14 and 20 % of the carbon as in the 1173 K evacuation and 873 K reduction, the deactivation curve had a sigmoidal shape, and the activity decreased three orders of magnitude in just 12 minutes. Molybdenum metal that was reduced in H_2 at 1073 K for 30 minutes also followed a type 2 deactivation curve, although it deactivated slightly faster than Mo_2C that had been reduced at 873 K. Thus, the rate at which the catalyst deactivates during ethylene hydrogenation at room temperature increases as the Mo:C ratio increases.

As shown above, the slowest deactivation rates were obtained for reductions below 623 K, but a 15 minute reduction at 623 K was not sufficient to activate the catalyst fully. If instead, the catalyst was reduced at 673 K for 5 minutes, an extra 1.4% of oxygen was removed and the catalyst was fully activated. However, as shown in Table 4.1, this pretreatment removed 70% more carbon than the 15 minute reduction at 623 K. As a result, the catalyst deactivated almost four times faster after the 673 K reduction (type 3 deactivation curve) than after the 623 K reduction (type 1 deactivation curve). Therefore, a pretreatment method was devised which removed the extra 1.4 % of oxygen while only removing 10% more carbon. This required reducing the catalyst in hydrogen according to the temperature schedule shown in Figure 4.7. This "low-temperature reduction" resulted in an initial activity of 100% and

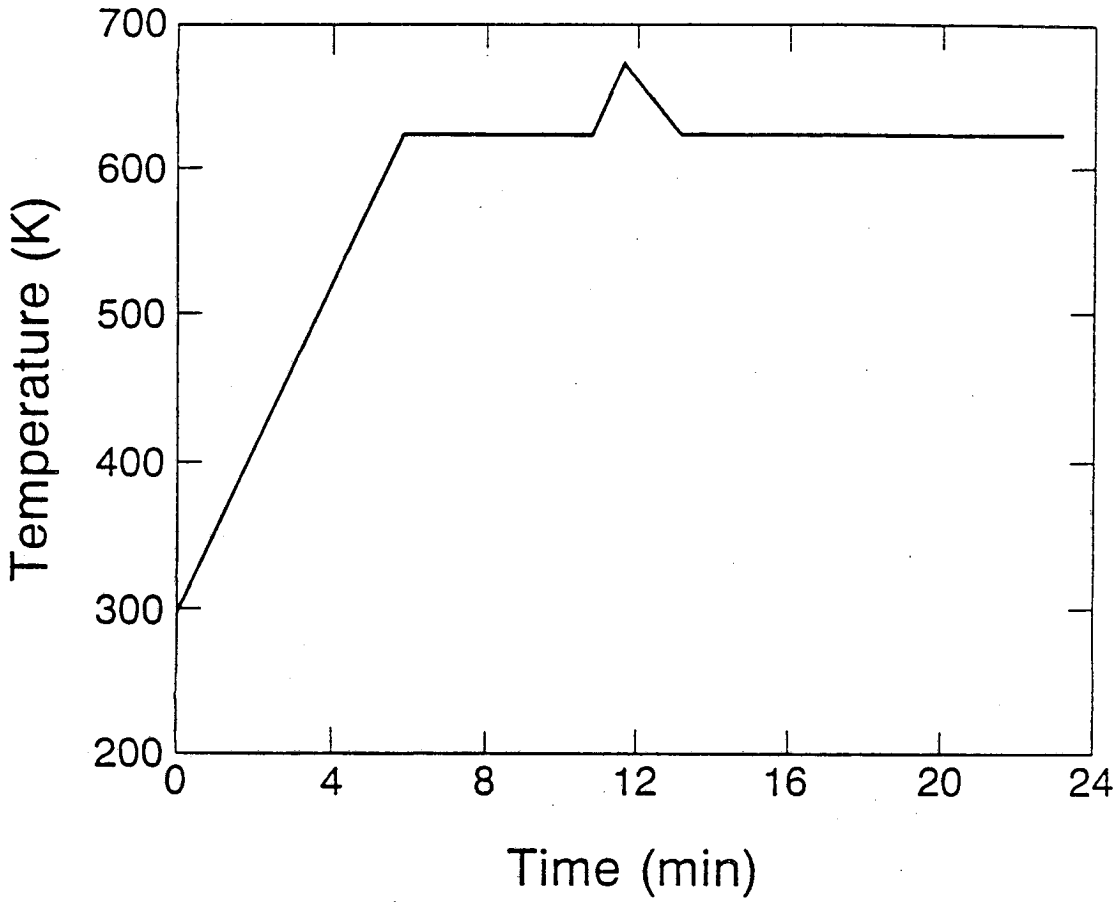

Figure 4.7: Temperature schedule used during "low-temperature reduction". H_2 flow rate = 100 cc/min (STP).

a type 1 deactivation curve.

It must be emphasized that the only difference between activating the catalyst by a 5 minute reduction at 673 K and activating it by the low-temperature reduction procedure, was the amount of carbon removed from the sample; both pretreatments removed the same amount of oxygen. Therefore, the changes in the shape of the deactivation curve after different pretreatments only could have been caused by differences in the amount of carbon removed from the sample.

An interesting property of these catalysts is that even though they deactivated rather quickly, they could be reactivated completely by either a 10 minute evacuation at 973 K or a 10 minute reduction at 523 K. During either reactivation procedure no carbon species were observed to desorb from the catalyst surface. However, a small amount of water was detected when the catalyst was reactivated by reduction at 523 K. We believe that the source of this water was residual oxygen in the system which slowly accumulated on the surface during ethylene hydrogenation. In separate experiments, the rate of oxygen accumulation on the surface due to residual oxygen was measured to be approximately 5×10^{-10} moles of O atoms/s, which corresponds to an oxygen concentration in the gas stream of 1.68 ppm.

To account for the deactivation due to poisoning by residual oxygen, experiments were performed in which varying amounts of oxygen were pulsed onto the surface, and the initial reaction rate was measured. It was found that inhibition of the hydrogenation rate by oxygen is third order in oxygen coverage ($r = r_0 (1 - \theta_O)^3$), assuming dissociative adsorption of the oxygen. This is consistent with the work of Kojima and coworkers (8) who found that poisoning of TaC for ethylene hydrogenation by CO was third order in CO coverage. From these data, the deactivation curve due solely to poisoning by residual

oxygen was calculated for the sample sizes used, and is shown as curve (a) in Figure 4.6. It is clear from Figure 4.6 that the rate of deactivation due to residual oxygen is significantly smaller than the observed deactivation rates. Therefore, another mechanism must be responsible for the higher deactivation rates observed experimentally. This is discussed in more detail later.

Another interesting property of these catalysts is that with each subsequent reactivation, the rate of deactivation decreased slightly. If the sample originally had a type 1 deactivation curve, three or more reactivations were sufficient to slow the deactivation to the point where the deactivation curve approached curve (a) in Figure 4.6 (deactivation solely due to oxygen poisoning). Additional reactivations had no effect on subsequent deactivation curves.

The results presented above show that although the initial activity of the catalyst does not depend strongly on the amount of carbon removed during the activation process, the rate of deactivation does. Moreover, the shape of the deactivation curve also varies with the amount of carbon removed.

TPR of Oxygen on Activated Mo_2C

The changes in the shapes of the deactivation curves after different activation treatments suggested that the pretreatment conditions in some way changed the surface of the catalyst. To explore this further, a sample of Mo_2C was activated in two ways: first by low-temperature reduction (LTR); and second, by a 15 minute reduction at 873 K (high-temperature reduction, HTR). Following each activation procedure, oxygen was adsorbed on the surface and the catalyst was heated in H_2. The differences in the resulting TPR spectra verified that the surface was not the same after the two different activation procedures.

As shown earlier, oxygen is readily incorporated into Mo_2C when it is exposed to air at room temperature. However, it was found that if the oxygen was pulsed onto the catalyst by injecting known quantities into a carrier gas (i.e. He), the catalyst became saturated after adsorbing the equivalent of one monolayer, suggesting that all of the adsorbed oxygen was on the surface. Monolayer coverage was taken as one oxygen atom per surface Mo atom, assuming dissociative adsorption (110 μmoles O atoms/gram, for a catalyst with a BET area of 6 m^2/g).

After activating a 15.3 mg sample by low-temperature reduction (LTR), it was evacuated for 5 minutes at 623 K to remove any hydrogen that might be adsorbed on the surface and then cooled under He to 298 K. Then a monolayer of oxygen was pulsed onto the surface and the catalyst was heated in 100 cc/min (STP) of hydrogen to 623 K at 1 K/s. The results of this TPR are shown in Figure 4.8. The same sample was reduced subsequently at 873 K for 15 minutes (HTR) to remove the bulk oxygen that was not removed by the low-temperature reduction. This also removed an additional 550 μmoles/g of carbon so that after the HTR, a total of 14.5 % of the carbon originally contained in the sample had been removed. Then after evacuation at 623 K for 5 minutes, the sample was cooled to 298 K under He and a monolayer of oxygen was pulsed onto the surface. Finally, the temperature was raised at 1 K/s in 100 cc/min (STP) of hydrogen to 873 K. The resulting TPR spectrum is presented in Figure 4.8.

As shown in Figure 4.8, the TPR spectra are quite different for the two different reduction temperatures. In both cases, two peaks are observed, corresponding to the α and β peaks in Figure 4.3. However, the position of the α peak shifts from 483 K after LTR up to 513 K after HTR, while the β peak shifts from 586 K after LTR down to 573 K after HTR. The relative intensities of the

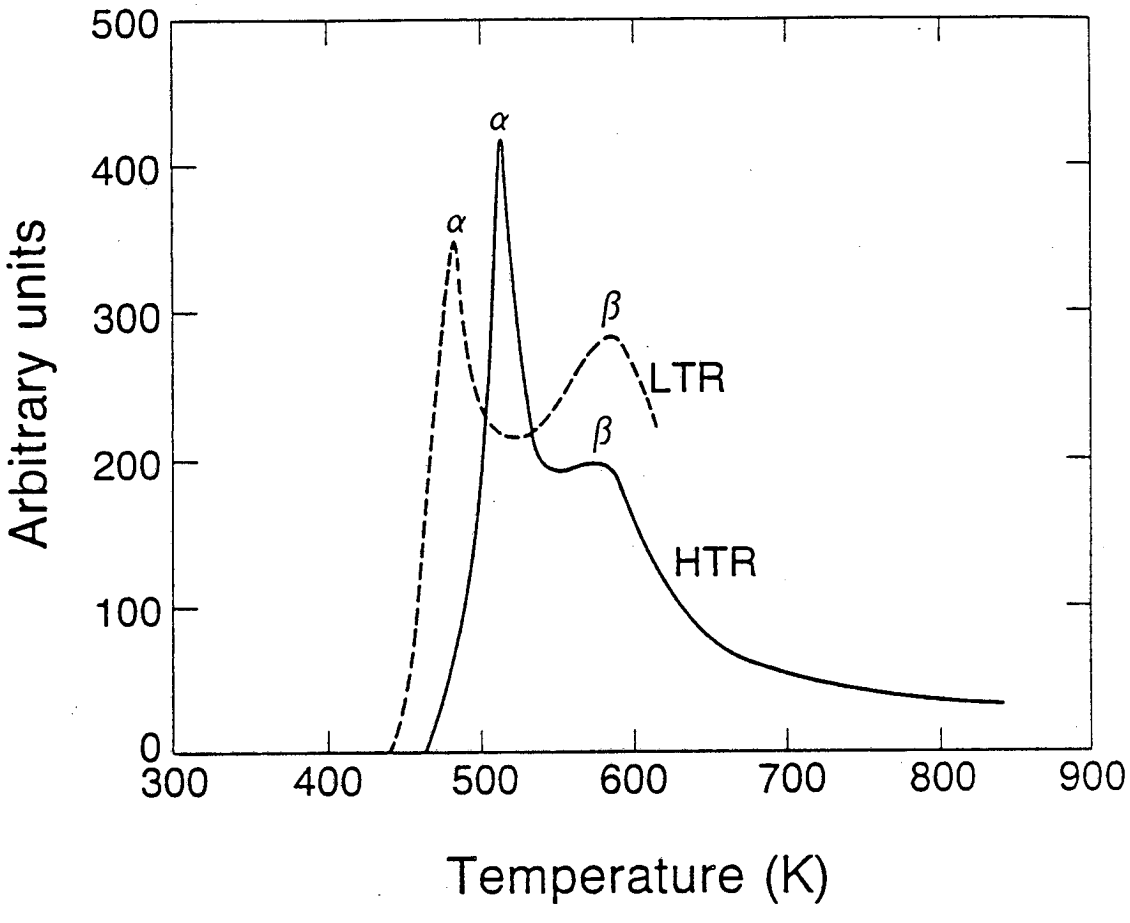

Figure 4.8: TPR of oxygen chemisorbed on 15.3 mg. of Mo_2C after activation by low-temperature reduction (LTR) compared to after high-temperature reduction (HTR).

two peaks also changes after different pretreatments. These results clearly show that the surface is very different after HTR than after LTR.

DISCUSSION

The results presented above show that carbon and oxygen are quite mobile in Mo_2C. In fact, oxygen is readily incorporated into this carbide even at room temperature. Since oxygen is a poison, it must be removed from the surface to activate Mo_2C for ethylene hydrogenation. However, the oxygen cannot be removed by evacuation or reduction without removing a significant amount of bulk carbon from the catalyst. When heated in vacuo, oxygen does not desorb molecularly, but instead reacts with carbidic carbon in the catalyst and desorbs as CO and CO_2. When the catalyst is reduced in hydrogen, on the other hand, oxygen is removed by reaction with the hydrogen to form water, and bulk carbon is removed by reaction with the hydrogen to form methane. By varying the pretreatment conditions, different amounts of carbon and oxygen can be removed. This allows investigation of the effects of bulk composition on surface chemistry and catalytic activity.

One of the more surprising results of this study was that the initial activity of the Mo_2C for ethylene hydrogenation did not depend on the amount of carbon removed by the activation process. Sinfelt and Yates (4) found that the activity of Mo for ethane hydrogenolysis increased by several orders of magnitude as it was carbided. Thus, it was expected that the activity of Mo_2C for ethylene hydrogenation would change as carbon was removed, but this was not the case. However, the rate of deactivation and the shape of the deactivation curve strongly depended on the extent of carbon removal.

The increase in the deactivation rate as more carbon was removed

indicates that the bulk Mo:C ratio influences the surface chemistry. While the details of the deactivation mechanism are not understood, we believe that the deactivation is caused by an accumulation of carbon on the surface which blocks the active sites. This carbon is produced by the slow cracking of ethylene which presumably occurs faster on a surface that binds ethylene more tightly. Therefore, the higher rate of deactivation of the carbon-deficient sample suggests that ethylene is bound more strongly to the surface as the Mo:C ratio increases. Unfortunately, no direct measurement of the heat of adsorption of ethylene to the surface could be made using TPD or TPR because no desorption products were observed. However, the assumption that ethylene adsorbs more strongly on the carbon-deficient catalyst is supported by the TPR spectra shown in Figure 4.8. The shift in the position of the α peak from 483 to 513 K as more carbon was removed by the pretreatment procedure indicates that oxygen is bound more tightly to the surface as the Mo:C ratio increases. Thus, it seems reasonable that ethylene also would be bound more tightly to the carbon-deficient surface. This is consistent with the work of Ko and Madix (37) who showed that ethylene adsorbs more strongly on a Mo(100) surface than on a carbided Mo(100)-C surface.

The change in shape of the deactivation curve may indicate that the deactivation mechanism changes as more carbon is removed, or it simply may indicate a change in the ability of carbon to diffuse into the bulk. The sigmoidal shape of the deactivation curve for the carbon-deficient sample suggests that as carbon is deposited on a surface which is not fully carbided, it can diffuse into the first few layers of the bulk. As a result, carbon does not build up on the surface and the rate of deactivation is slow initially. Eventually, the first few layers become saturated with carbon, and the rate of diffusion into the bulk decreases considerably; the deactivation then follows the exponential-type

decay expected in the absence of diffusion into the bulk. This model of competition between diffusion into the bulk and deposition of surface carbon is similar to the competition model invoked in the Fischer-Tropsch literature (38, 39) to explain the time dependence of the activity of iron catalysts.

If the explanation given above for the change in shape of the deactivation curve is correct, one might have expected that once the first few layers were filled with carbon, the surface composition of the catalysts would be identical, and therefore the rate of deactivation would be the same regardless of the amount of bulk carbon removed. However, this was not the case. After a short induction period in which the first few layers were filled, the catalyst activated by HTR deactivated more than 5 times faster than the catalyst activated by LTR. Thus, it appears that although the composition of the first few layers might have been the same, something about the surface was still different.

Another interesting finding in this study was that even though Mo_2C deactivates quickly, it can be reactivated completely by either a 10 minute evacuation at 973 K or a 10 minute reduction at 523 K. Moreover, during reactivation no carbon species were observed desorbing from the surface. This suggests that during reactivation, the surface carbon simply diffuses into the bulk, unblocking the active sites. This is consistent with the TPD and TPR results which showed that carbon is mobile in Mo_2C under the conditions used for reactivation, and with the deactivation model discussed above. It is interesting to note that the catalyst can be reactivated in H_2 at only 523 K, whereas a temperature of 973 K is necessary for reactivation in vacuo. This suggests that hydrogen facilitates carbon transport in Mo_2C, perhaps by producing a mobile CH_x species.

The suggestion that surface carbon diffuses into the bulk of the catalyst

during reactivation is consistent with the observation that following reactivation of the catalyst, the subsequent deactivation is slightly slower than before. During the reactivation, any carbon deposited on the surface diffuses into the subsurface of the catalyst, which results in a lower Mo:C ratio near the surface. After multiple reactivations, the Mo:C ratio of the near surface region is sufficiently low that the deactivation can be attributed solely to oxygen poisoning. Thus, within the error of the experiment, it appears that ethylene does not crack on a fully carbided surface.

We also have shown that because of the relative ease with which oxygen diffuses through Mo_2C, it is necessary to remove the equivalent of several monolayers of oxygen to obtain an oxygen-free surface and completely activate the catalyst. It is not sufficient to remove only one monolayer because as oxygen is removed from the surface during the pretreatment procedure (evacuation or reduction), it can be replenished by oxygen from the bulk. The high mobility of oxygen also complicates interpretation of the TPD and TPR spectra, as evidenced by comparing Figures 4.3, 4.5, and 4.8 (after HTR). In Figure 4.8, oxygen initially was present only on the surface of the catalyst and two peaks (α and β) were observed in the TPR spectrum. As oxygen was added to the bulk in Figures 4.5 (the catalyst contained the equivalent of 3 monolayers of oxygen) and 4.3 (the equivalent of more than 7 monolayers of oxygen) the size of both the α and β peaks increased. Moreover, a third peak denoted γ appeared near 658 K, and two smaller peaks appeared at higher temperatures. Thus, when bulk oxygen is present, the peak sizes increase and new peaks appear in the spectra.

Another possible explanation should be mentioned for the increase in the number of peaks in the TPR spectra when the catalyst is exposed to air as in Figure 4.3a, compared to when oxygen is just pulsed onto the surface as in

Figure 4.5. As mentioned previously, when exposed to air, the samples rapidly incorporated between one and two monolayers of oxygen. If this oxygen uptake corresponded to a surface oxidation, it is possible that the surface was not oxidized homogeneously. This could result in multiple surface states which would produce extra peaks in the TPR spectra. However, if the extra peaks in the spectra were produced by multiple surface states, then a greater number of surface sites should have been exposed following activation by HTR than after LTR since the HTR procedure removes the higher temperature peaks while the LTR procedure does not. Therefore, both the initial activity of the catalyst for ethylene hydrogenation, and the capacity of the surface for oxygen chemisorption (by pulsing) should be greater following HTR than after LTR. Since this was not the case, these additional peaks must not be the result of inhomogeneous surface oxidation, but are produced by oxygen in the bulk of the catalyst.

From the discussion above, it is evident that the γ peak, and the other higher temperature peaks in the TPR spectra result from the presence of bulk oxygen. Furthermore, the sharpness and symmetry of the α peak suggests that this peak is produced by surface oxygen. At first glance, the presence of the β peak in the TPR spectra of Figure 4.8 in which oxygen initially was present only on the surface of the Mo_2C, might suggest that this peak is produced by another surface state of adsorbed oxygen. However, the anomalous shift in the peak temperatures of the α and β peaks as the Mo:C ratio increases, and the change in the relative sizes of the peaks as the Mo:C ratio increases, is very difficult to explain if the two peaks are assumed to be produced by desorption from two different types of adsorption sites on the catalyst surface. Another possible explanation for the β peak is that it is produced by oxygen which penetrates into the subsurface of the catalyst during heating. This may be explained as

follows. During the temperature ramp, oxygen is removed from the surface by two processes: reaction with hydrogen to desorb as water in the α peak; and diffusion into the subsurface region of the catalyst. When the surface becomes depleted of oxygen by the desorption process, the subsurface oxygen diffuses back to the surface where it reacts with hydrogen and desorbs in the β peak. This assignment of the β peak is proven in Chapter 5.

Chapter 5: Oxygen Diffusion in Mo_2C

In our opinion, the most important finding in the work described in Chapter 4 was that both carbon and oxygen are mobile in Mo_2C at relatively low temperatures. The high carbon mobility allowed us to vary the Mo:C ratio of the catalyst by varying the pretreatment conditions, which allowed us to study the effect of this ratio on the catalytic properties. Because of the high mobility of oxygen in Mo_2C a large amount of oxygen is incorporated into this material during exposure to air at room temperature. This oxygen is very difficult to remove from the surface since it can be replenished by diffusion of oxygen from the layers below the surface. At the end of Chapter 4, we suggested that diffusion of oxygen between surface and subsurface layers of Mo_2C during heating is responsible for the high temperature peak in the TPR spectrum of chemisorbed oxygen. In this chapter, we present definitive data which show that subsurface diffusion of oxygen does indeed produce the high temperature peak. To aid in interpreting the experimental results, a numerical model is developed which accounts for the effects of subsurface diffusion on the TPR spectrum. These results illustrate how TPD and TPR can be used to study subsurface diffusion in high surface area catalysts. This system is particularly interesting because the oxygen mobility depends on the Mo:C ratio of the catalyst.

EXPERIMENTAL

The hcp Mo_2C catalyst used in this study was not taken from the same batch of catalyst as the samples used in the work described in Chapter 4, although the catalyst preparation was similar. The catalyst used in this study

contained less than 5 wt % Mo as determined by powder X-ray diffraction, compared to almost 13 % Mo in the catalyst used in the previous study. No evidence of oxide formation was found in the XRD patterns. The BET area of the Mo_2C catalyst used in this study was approximately 4 m^2/g.

Before each TPR spectrum was measured, the catalyst was pretreated in one of three ways. By varying the pretreatment conditions, the Mo:C ratio of the catalyst could be varied, and thus it was possible to study the effect of this ratio on the oxygen mobility. In each case, 100 mg of catalyst were placed in the reactor and evacuated at 0.1 torr or less for at least one hour. Then the catalyst was reduced by heating in 100 cm^3 (STP)/min of flowing deuterium according to one of three temperature schedules which will be described later. Deuterium was used instead of hydrogen because of a relatively high water background in the mass spectrometer at the time of the experiments. After reduction, the catalyst was evacuated for 5 minutes at the final temperature and then cooled under helium to 298 K.

Oxygen was adsorbed on the freshly pretreated catalyst by injecting known quantities into a helium carrier gas which flowed over the sample. Following a 5 minute evacuation at 298 K, deuterium was flowed over the catalyst and the temperature was raised linearly while monitoring the products with the mass spectrometer. Then the catalyst was reduced for 5 minutes at the final ramp temperature to completely remove all of the adsorbed oxygen. After a 5 minute evacuation, the catalyst was cooled to room temperature and was ready for subsequent TPR experiments.

EXPERIMENTAL RESULTS

TPR Spectra of Oxygen After Low-Temperature Reduction

Figure 5.1 shows the effect of initial coverage on the TPR spectrum of oxygen adsorbed on the Mo_2C catalyst after activation by the low-temperature reduction (LTR) procedure described in Chapter 4. Before each spectrum was measured, the sample was dosed with differing amounts of oxygen corresponding to initial coverages between 0.45 and 1.0. In each case, the heating rate used was 1 K/s. At saturation (θ_0 = 1), one oxygen atom was adsorbed per surface Mo atom, assuming there are 1.1 X 10^{19} Mo atoms/m^2 (9). This suggests that the oxygen is adsorbed dissociatively on the surface, and that no surface oxide is formed. If a surface oxide were formed, we would expect the oxygen saturation coverage to exceed one oxygen atom per surface Mo atom.

As shown in Figure 5.1, the TPR spectrum contains two peaks when θ_0 = 1; a relatively narrow peak at 479 K, and a second much broader peak at 570 K. These peak temperatures agree quite well with those obtained in the previous study (Chapter 4) with a different Mo_2C catalyst, but the peaks are not as well resolved. As mentioned in Chapter 4, the presence of two peaks in a TPD or TPR spectrum often indicates the presence of one or more adsorption states on the catalyst surface (22). Therefore, the results shown in Figure 5.1 might suggest that there are two distinct types of sites present for oxygen chemisorption with different binding energies on the Mo_2C catalyst. However, as discussed below, it is difficult to explain the coverage-dependence of these spectra in the context of a 2-site model.

The broadness of the high temperature peak could be explained either by assuming that readsorption of water on this site is important, or by assuming

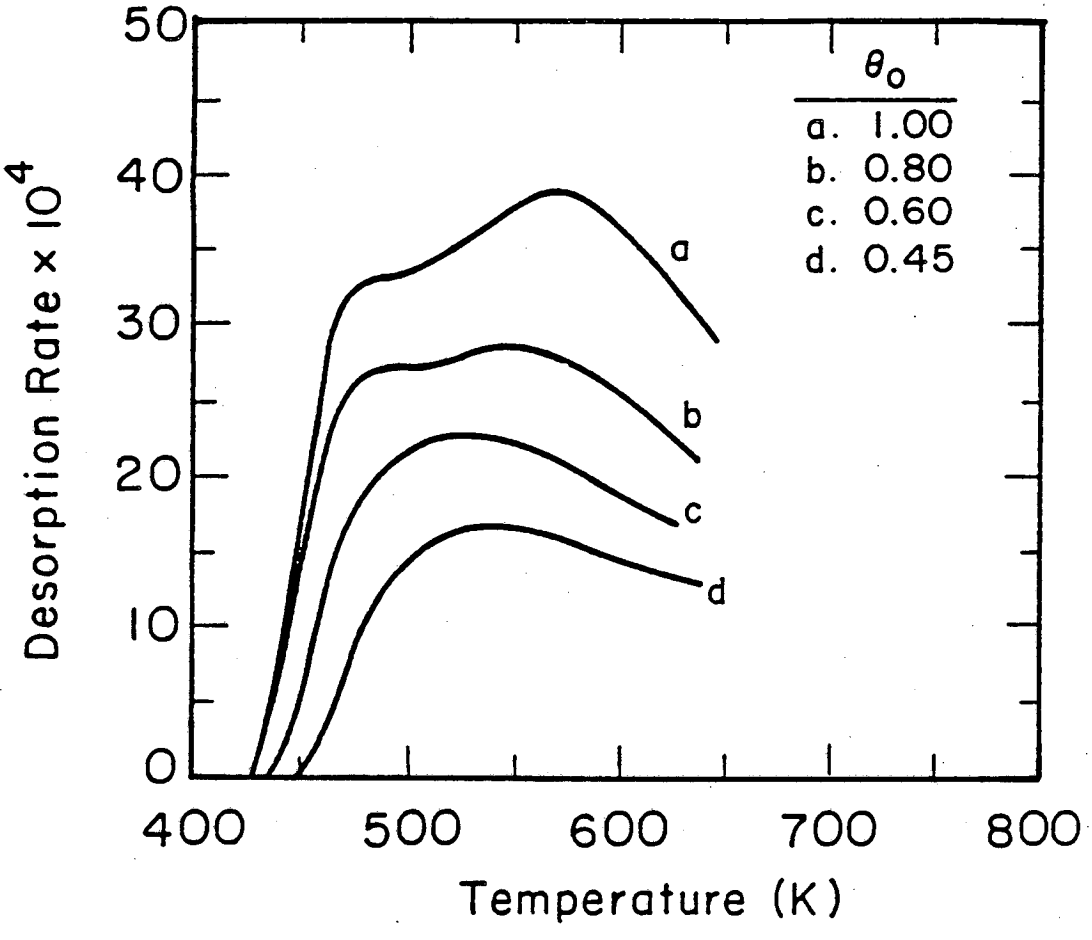

Figure 5.1: TPR spectra of oxygen adsorbed on LTR-activated Mo_2C as a function of the initial surface coverage.

that the activation energy is coverage-dependent for this site. However, in either case, the peak should shift to higher temperatures as the initial coverage decreases (22). As shown in Figure 5.1, the high temperature peak shifts to lower temperature with decreasing oxygen coverage. This apparently anomalous shift in peak temperature could be explained by assuming that the rate of reaction of hydrogen with oxygen, R, follows a rate expression of the form

$$R = k\theta(1-\theta)^n \qquad (5.1)$$

where k is an Arrhenius-type rate constant, and θ is the oxygen coverage. However, this type of rate expression should produce a very narrow peak, whereas the high temperature peak is very broad. Furthermore, if the two peaks result from adsorption on two sites, then as the initial coverage decreases, the low temperature peak should disappear before the high-temperature peak since the highest binding energy sites are expected to fill first (40). This type of behavior was not observed. Comparison of the spectra for $\theta_0 = 1.0$ and $\theta_0 = 0.8$ reveals that the size of both peaks decrease as the initial coverage decreases, and the second peak shrinks more than the first. Thus, we conclude that the two peaks are not the manifestation of two distinct adsorption sites on the surface of the catalyst. Instead, we believe that the high temperature peak is produced by oxygen which penetrates into subsurface layers of the sample during heating and then diffuses back to the surface when it becomes depleted by the desorption process.

To test whether oxygen penetrates into the subsurface during the temperature ramp, we conducted the following experiment. The surface of the catalyst was saturated with oxygen at 298 K. Then the catalyst was heated to

403 K at 1 K/s in flowing deuterium and annealed at this temperature for one minute. Subsequently, the catalyst was evacuated for 5 minutes at 403 K and cooled to 298 K. During the anneal period less than 1 % of the oxygen reacted with the deuterium and desorbed. However, upon cooling to 298 K, 16% more oxygen adsorbed on the catalyst surface. This strongly suggests that oxygen diffused into the subsurface during the anneal, and this has a significant effect on the TPR spectrum as shown in Figure 5.2.

The upper curve in Figure 5.2 shows the TPR spectrum obtained following saturation with oxygen at 298 K, a 1 minute anneal in deuterium at 403 K, and subsequent resaturation with oxygen at 298 K. Also shown in the figure is the TPR spectrum for the case in which the catalyst was not resaturated with oxygen following the anneal in deuterium. The desorption rate from the resaturated sample is higher at all temperatures. Also the relative height of the low temperature peak to the high temperature peak is larger when the catalyst surface is resaturated compared to when it is not.

We also observed that shorter evacuation times at 403 K had a negligible effect on the amount of oxygen that could be readsorbed. Thus oxygen diffusion is apparently much faster in the presence of deuterium than in vacuo. This is consistent with a further observation that it was necessary to heat the catalyst in helium for 10 minutes at 573 K to allow the same amount of oxygen to penetrate into the subsurface as had penetrated during the 1 minute anneal in deuterium at 403 K.

The results presented above show that the two peaks in the TPR spectrum of the catalyst activated by LTR are not produced by two distinct surface sites. Moreover, the results strongly suggest that the high temperature peak is produced by subsurface diffusion. In Chapter 4, we showed that the relative height of the high temperature peak decreased compared to the low

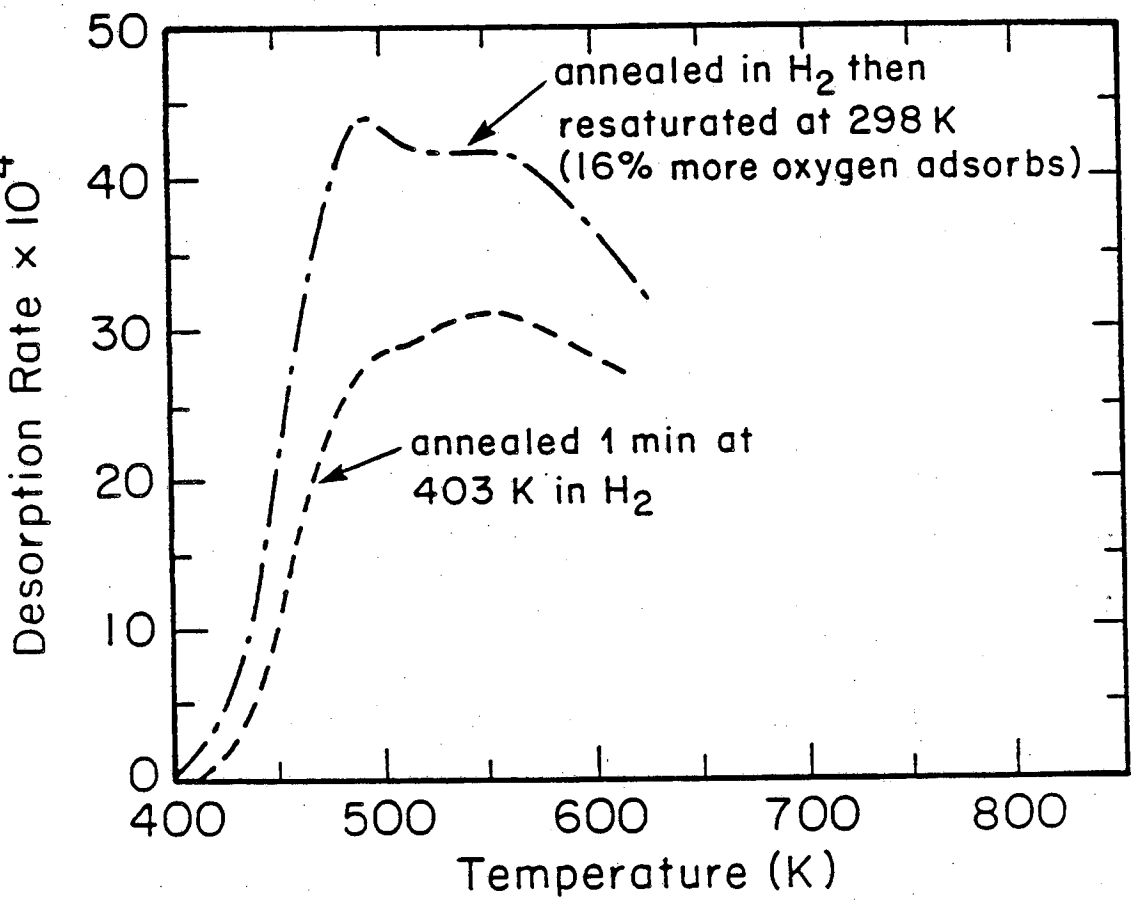

Figure 5.2: TPR spectrum of oxygen on LTR-activated Mo_2C after saturating the surface at 298 K, annealing in deuterium for 1 minute at 403 K (lower curve), and resaturating with oxygen at 298 K (upper curve).

temperature peak as the catalyst became more carbon-deficient. If the high temperature peak is produced by subsurface diffusion as suggested, then this would indicate that less oxygen penetrates into the subsurface when the Mo:C ratio is increased. Therefore, we need to check whether this is indeed the case.

TPR Spectra of Oxygen After High-Temperature Reduction

Figure 5.3 shows TPR spectra of oxygen on an Mo_2C sample that was activated by high-temperature reduction (HTR) and subsequently dosed with oxygen. The initial surface coverage was varied from 0.53 to 1.0. The spectra contain one narrow peak at 510 K with a long tail at higher temperatures. This peak temperature is consistent with the results reported in Chapter 4 for a different Mo_2C catalyst. Unlike the previous results, however, a second high temperature peak is not resolved. Since the location of the sharp peak is independent of the initial oxygen coverage, we conclude that the reaction rate (or desorption rate) is first order in oxygen coverage. Also, water readsorption must be negligible since this would cause the peak temperature to increase with decreasing coverage (22). Moreover, the activation energy must not be coverage-dependent on the carbon-deficient surface since this would also cause a shift in the peak temperature with initial coverage.

The fact that the high temperature peak is unresolved in the TPR spectrum of the carbon-deficient catalyst suggests that less oxygen penetrated into subsurface layers during the temperature ramp. To test this hypothesis, we repeated the annealing experiment described above. During this annealing procedure, less than 0.5 % of the oxygen reacted with the deuterium and desorbed, yet after cooling to 298 K, we were able to readsorb an additional 3 % of oxygen. Therefore, penetration of oxygen into the subsurface does take place during the 1 minute anneal in deuterium, however the rate of diffusion is

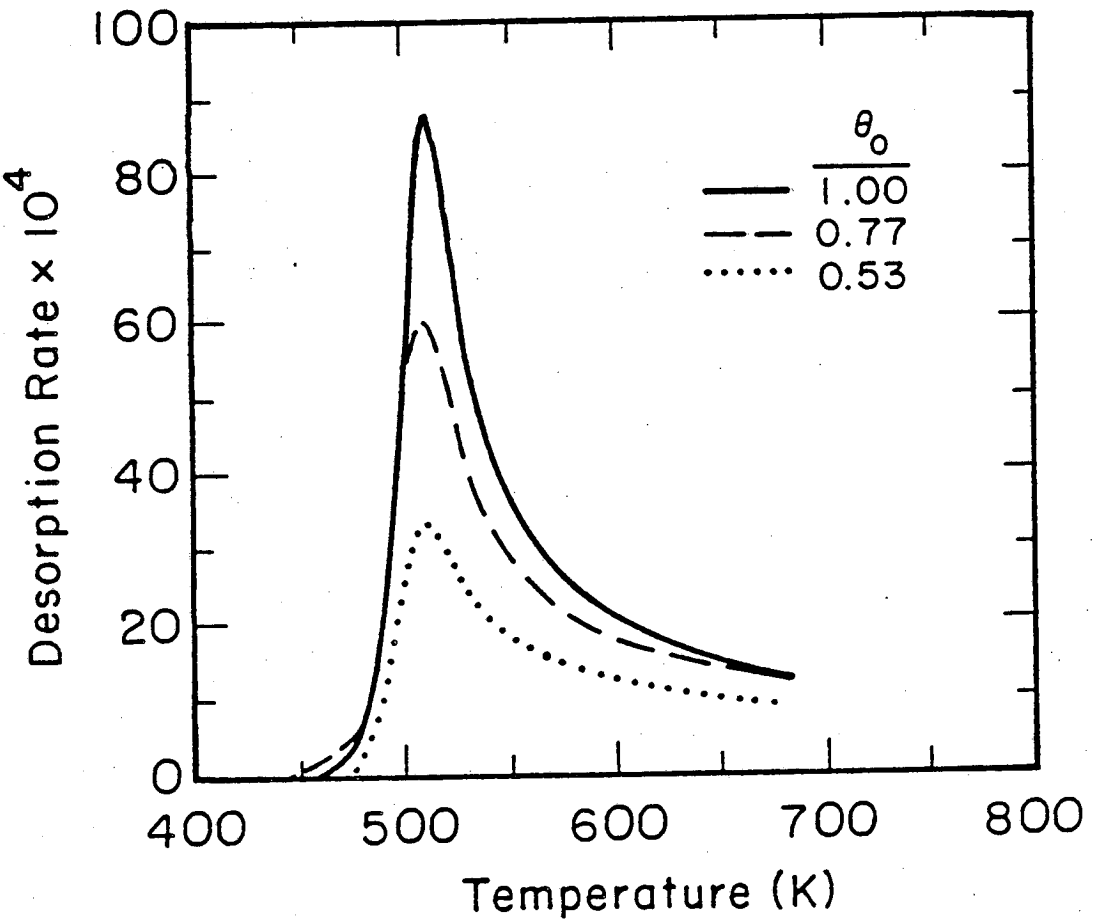

Figure 5.3: TPR spectra of oxygen adsorbed on HTR-activated Mo_2C as a funtion of the initial surface coverage.

measureably lower for the highly carbon-deficient surface than for the relatively carbon-rich catalyst. If we replaced the 1 minute anneal in deuterium at 403 K with a 15 minute anneal in helium at 773 K, we found that a significant amount of oxygen could penetrate into the subsurface of the carbon-deficient catalyst. In this experiment, the catalyst was saturated with oxygen at 298 K, and subsequently heated at 1 K/s to 773 K in flowing helium and held there for 15 minutes. During this anneal in helium, nothing desorbed from the catalyst, yet after cooling to 298 K, 33 % more oxygen could be readsorbed on the surface. This has a marked effect on the TPR spectrum as shown in Figure 5.4.

Figure 5.4 shows three different TPR spectra of oxygen on the HTR-activated Mo_2C catalyst. The bold curve is the TPR spectrum shown in Figure 5.3 for a saturated surface. The dashed curve is the TPR spectrum obtained after saturating the surface with oxygen at 298 K, and then annealing for 15 minutes in helium at 773 K. As seen in the figure, the narrow peak at 510 K is removed by the annealing process and is replaced by a second much broader peak at 690 K. If after annealing in helium, the catalyst is cooled to 298 K and resaturated with oxygen, the narrow peak reappears in the spectrum along with the second broader peak, as shown by the dot-dashed curve. The broadness of the peak produced by annealing the sample indicates that diffusion of oxygen into the subsurface produces a broad peak in the TPR spectrum. This is further evidence that the second peak in the TPR spectum after LTR is produced by subsurface diffusion.

TPR Spectra of Oxygen as a Function of Mo:C Ratio

The results presented above suggest that as the catalyst becomes more carbon deficient, the amount of oxygen that diffuses into the subsurface region decreases. As a result, the relative size of the high temperature peak

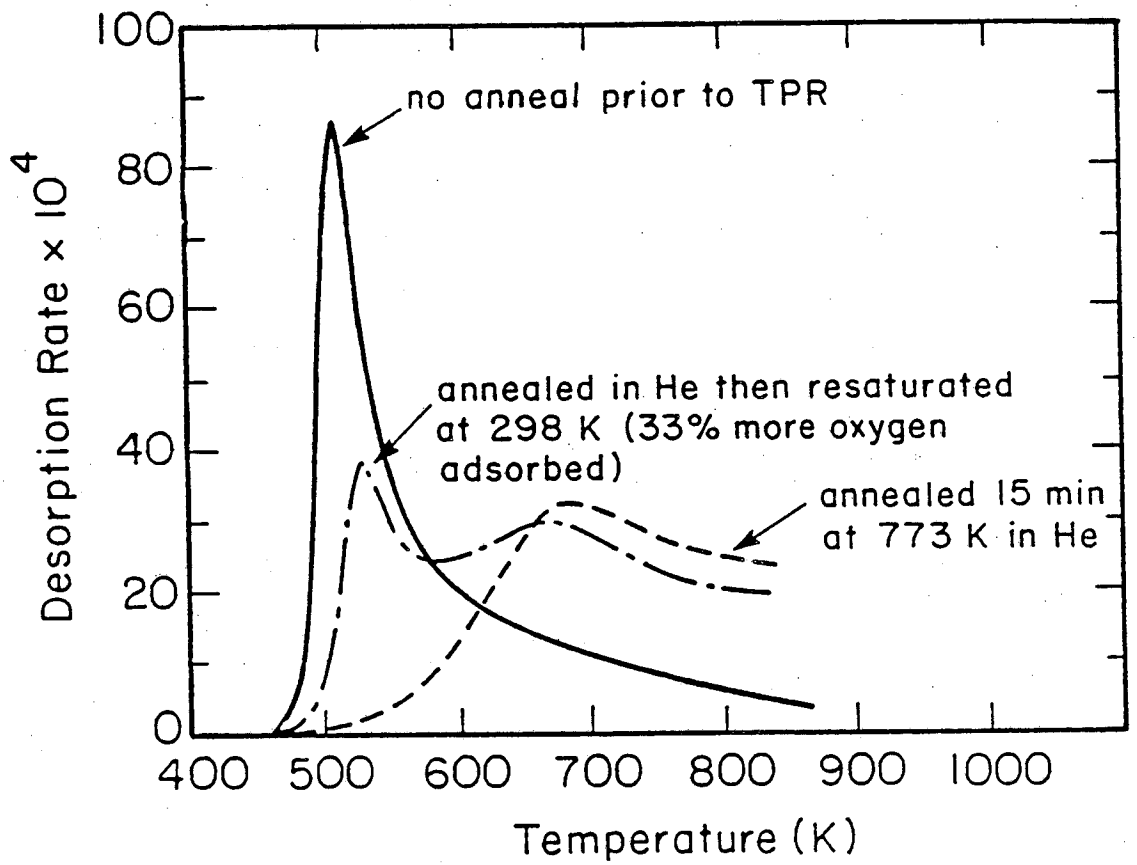

Figure 5.4: TPR spectrum of oxygen on HTR-activated Mo_2C after saturing the surface at 298 K (bold curve), annealing in helium for 15 minutes at 773 K (dashed curve), and resaturating the surface at 298 K (dot-dashed curve).

compared to the low temperature peak decreases. This trend is shown more clearly in Figure 5.5a. This figure shows the TPR spectra from oxygen-saturated surfaces of Mo_2C samples which were activated by low- (dotted curve) and high- (solid curve) temperature reduction. Also shown are two additional spectra at intermediate levels of carbon deficiency. The dashed curve is the spectrum obtained after a 15 minute reduction at 823 K. This does not remove quite as much carbon as the high-temperature reduction process. The other curve is the spectrum obtained on a catalyst that was activated by low-temperature reduction and then subjected to several TPRs up to 650 K. During each TPR, a small amount of carbon was removed so that this catalyst became slightly more carbon-deficient than the one activated by LTR.

It is clear from Figure 5.5a that the relative size of the high temperature peak decreases as the sample becomes more carbon deficient. Also, the temperature difference between the two peaks decreases. Eventually the two peaks merge as shown by the spectrum of the HTR-activated sample. The activation energies for desorption (or reaction) were measured for the low temperature peak in each of the spectra shown in Figure 5.5a using the heating rate variation method (22), which is described in Chapter 6. For these measurements, a heating rate range of 0.3 to 3.0 K/s was used. The results are shown in Table 5.1. The uncertainties in the measured activation energies reflect the uncertainties in measuring the peak temperatures. As seen in Table 5.1, the desorption activation energy for the low temperature peak increased from 9.3 ± 0.5 to 15 ± 1 kcal/mole as the sample became more carbon deficient. Thus it appears that as the Mo:C ratio increases, oxygen is held more strongly, and the rate of diffusion into the subsurface decreases. The desorption activation energy for the high temperature peak in the spectrum of the catalyst activated by LTR also was measured and found to be 18 ± 2 kcal/mole.

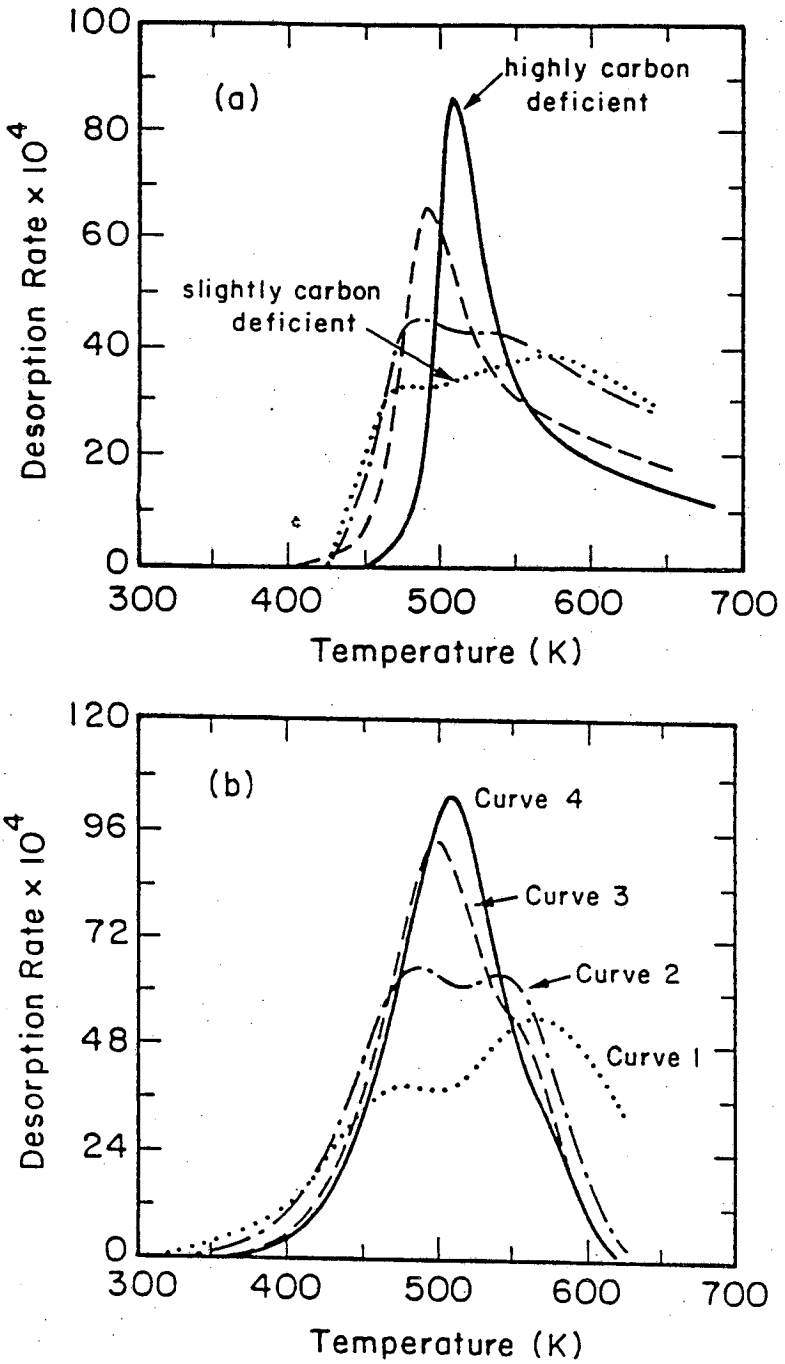

Figure 5.5: (a) TPR spectra of oxygen adsorbed on Mo_2C as a function of the Mo:C ratio. After LTR, the catalyst is only slightly C-deficient; after HTR, it is highly C-deficient. Also shown are two intermediate cases described in the text. (b) Simulated TPR spectra for the four cases considered in Table 5.2.

TABLE 5.1

Desorption Activation Energies Measured

for the Low Temperature Peaks in Figure 5.5a

Desorption Spectrum	Activation Energy (kcal/mole)
After LTR (dotted curve in Figure 5.5a)	9.3 ± 0.5
Dot-dashed curve in Figure 5.5a	12 ± 1
Dashed curve in Figure 5.5a	15 ± 1
After HTR (solid curve in Figure 5.5a)	15 ± 1

Effect of Deuterium Flow Rate on the TPR Spectra

Before attempting to model the TPR spectra, we wanted to verify that the spectra were not affected either by readsorption of water or by slow diffusion in the pores of the catalyst. To do this, we examined how the TPR spectrum varied with deuterium flow rate. If flow rate has no effect on the TPR spectrum, then it can be concluded that readsorption is not important and that pore diffusion-limitations do not affect the spectra. Figure 5.6 shows the effect of deuterium flow rate on the TPR spectrum of a moderately carbon-deficient Mo_2C sample. From this figure, we conclude that readsorption and pore diffusion limitations are not significant.

The small changes observed in the TPR spectrum when the deuterium flow rate is varied are inconsistent with a model which assumes that the two peaks are the result of two distinct adsorption sites with different binding energies on the catalyst surface. In such a model, the broadness normally would be attributed to readsorption, and the resolution between the peaks

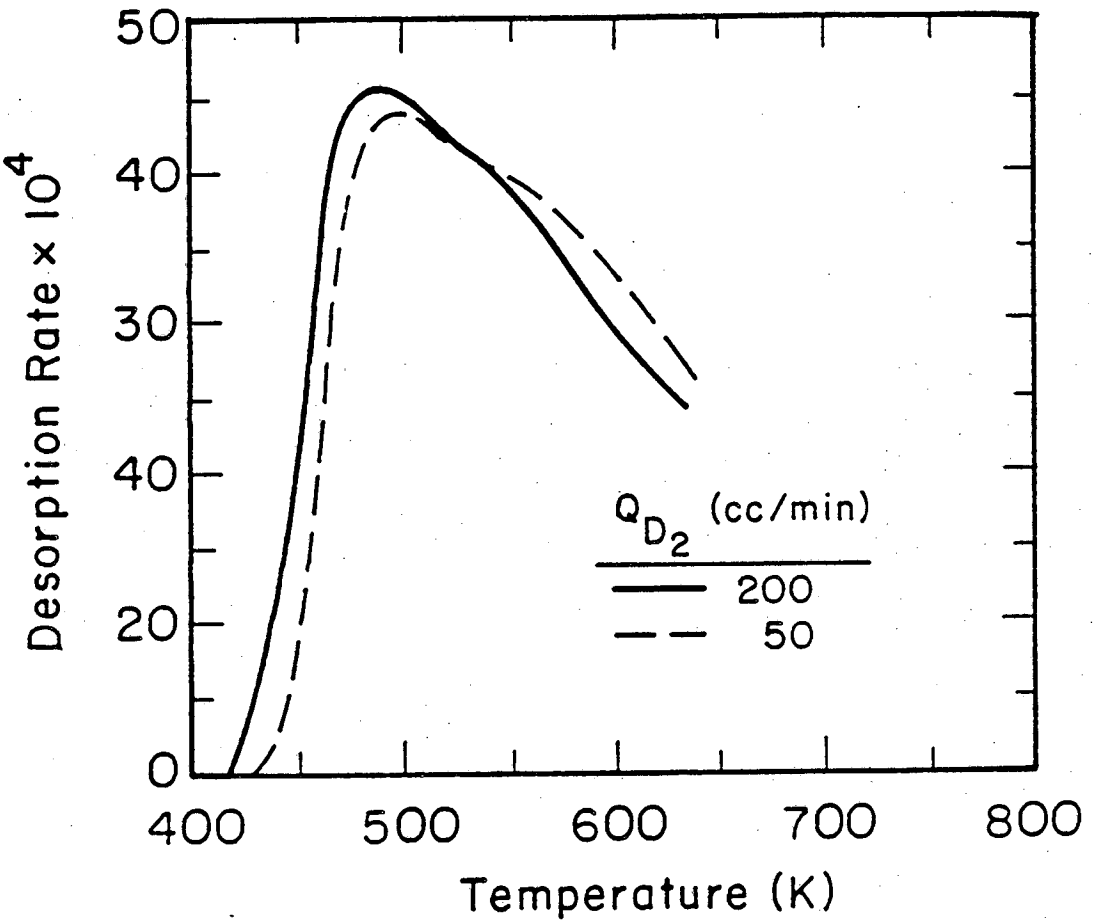

Figure 5.6: Effect of D_2 flow rate on the TPR spectrum of oxygen on a moderately C-deficient Mo_2C catalyst.

should increase with increasing flow rate. However, the opposite behavior is observed. The decrease in peak resolution is consistent with the subsurface diffusion model described below. Since a slightly higher deuterium pressure is required for the higher flow rate, the rate of reaction (water desorption) is larger at the higher flow rate. The higher deuterium pressure does not affect the rate of diffusion into the subsurface, therefore, the rate of surface reaction increases relative to the rate of subsurface diffusion as the flow rate increases. As a result, less oxygen diffuses into the subsurface during the temperature ramp, and the relative size of the high temperature peak decreases compared to the low temperature peak as shown in Figure 5.6.

The results presented above provide strong evidence that the high temperature peak in the TPR spectrum of oxygen adsorbed on Mo_2C is produced by oxygen that penetrates into subsurface layers of the catalyst during the temperature ramp. To aid in interpreting these results we now present a numerical model which accounts for the effect of subsurface diffusion on TPD and TPR spectra.

MODEL

Any quantitative model to desribe TPD or TPR spectra in which subsurface diffusion of adsorbates is significant would involve a large number of parameters. Since the values of many of the parameters can not be measured independently, they would become adjustable parameters, and this would make discrimination between models difficult. Therefore, in the model presented below, we have not included many of the complexities required to model the system quantitatively. The purpose of this model is to demonstrate that subsurface diffusion of adsorbates can produce extra peaks in a TPD or

TPR spectrum. We also hope to gain a semi-quantitative understanding of how subsurface diffusion affects the TPD or TPR spectrum. Although the model is developed to describe TPR spectra of oxygen on Mo_2C, it can easily be adapted to any system in which subsurface diffusion is important. This is demonstrated in Chapters 6 and 7.

The model is shown schematically in Figure 5.7. The surface is assumed to be energetically homogeneous. A fraction of the surface sites, θ, is covered by pre-adsorbed oxygen. As the sample temperature is raised, this oxygen can either react with the gas-phase hydrogen and desorb as water with rate r_d, or it can penetrate into the subsurface layers of the catalyst with rate r_p. It is expected that the oxygen will penetrate only a small number of atomic layers during the temperature ramp; therefore, it is inappropriate to use a distributed model for diffusion such as Fick's Law. For simplicity, we have chosen a lumped formulation for subsurface diffusion. Oxygen penetrates into a subsurface region of N atomic layers and distributes itself evenly in this region, filling a fraction, ξ, of the available subsurface sites. At higher temperatures, when the surface becomes depleted, the oxygen diffuses out of the subsurface back to the surface at a rate r_D.

Since the location of the first, narrow peak in the TPR spectrum of carbon-deficient Mo_2C showed no dependence on the initial oxygen coverage, we conclude that the reaction of adsorbed oxygen with hydrogen is first order in oxygen coverage. We also conclude that readsorption is not significant, and that the activation energy for desorption is not a strong function of coverage. These conclusions may not be valid for the relatively carbon-rich catalyst for which the location of the first peak did vary with the initial coverage. Nevertheless, to keep from adding additional parameters to the model, we make these assumptions for the carbon-rich catalyst as well. We also neglect

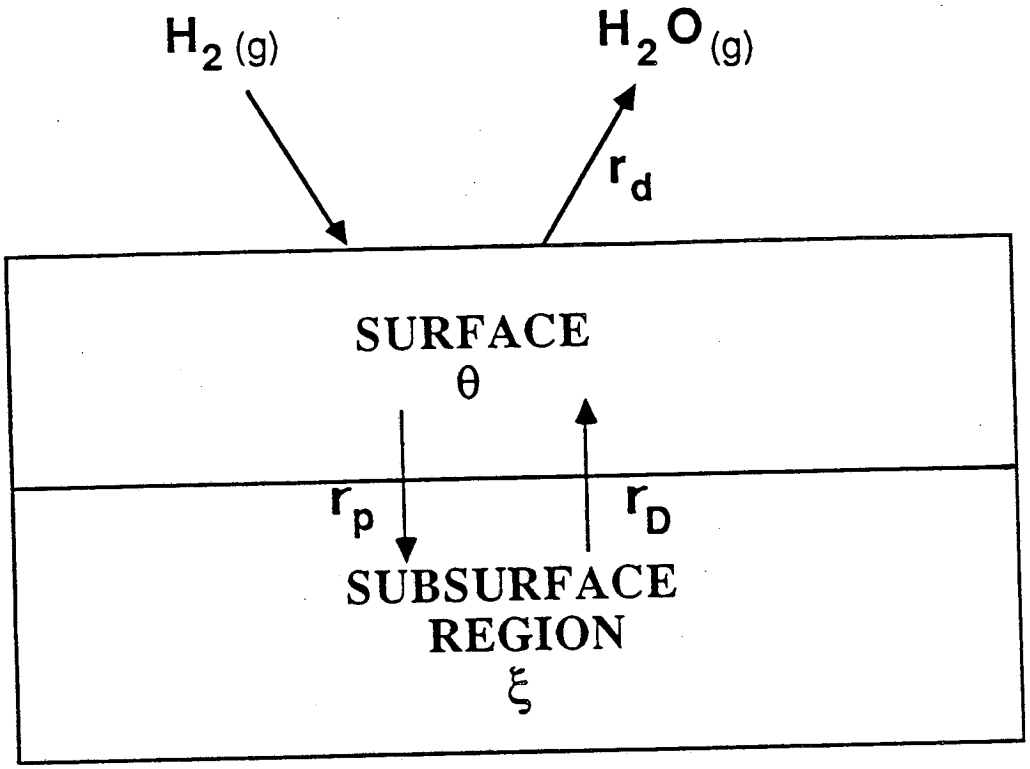

$$r_d = k_d\theta$$

$$r_p = k_p\theta\,(1 - \xi)$$

$$r_D = k_D\,(1 - \theta)\xi$$

Figure 5.7: Schematic of the subsurface diffusion model used to explain the TPR spectra of oxygen on Mo_2C. Surface oxygen can react with gas phase hydrogen and desorb as water, or penetrate into the subsurface during the temperature ramp.

diffusion limitations in the pores of the catalyst. With these assumptions, we can express the desorption rate simply as

$$r_d = \upsilon_d \exp\left[-\frac{E_d}{RT}\right]\theta \qquad (5.2)$$

where r_d is the desorption rate (s^{-1}), E_d is the desorption activation energy (kcal/mole), υ_d is the desorption preexponential factor (s^{-1}) which is assumed to be independent of temperature and coverage, and θ is the surface coverage.

The rate of penetration of oxygen into the subsurface is assumed to be first order in the surface oxygen coverage, and first order in the fraction of subsurface sites available. Since this is an activated process, it is assumed to follow the Arrhenius expression given in equation (5.3).

$$r_p = \upsilon_p \exp\left[-\frac{E_p}{RT}\right]\theta\,(1-\xi) \qquad (5.3)$$

where r_p is the penetration rate (s^{-1}), E_p is the activation energy for penetration, υ_p is the preexponential factor for penetration, and ξ is the fraction of filled subsurface sites. It is assumed that the preexponential factor and activation energy for diffusion are independent of coverage. In a similar manner, the rate of diffusion of oxygen from the subsurface back to the surface is assumed to be first order in the fraction of filled subsurface sites and available surface sites. This is expressed as

$$r_D = \upsilon_D \exp\left[-\frac{E_D}{RT}\right](1-\theta)\,\xi \qquad (5.4)$$

where r_D is the rate of diffusion, and υ_D and E_D are the preexponential factor and activation energy for diffusion, respectively.

These reaction and diffusion rate expressions can be combined with unsteady-state material balances on the surface and subsurface regions to describe the time evolution of the system:

$$\frac{d\theta}{dt} = -k_d\,\theta - k_p\,\theta(1-\xi) + k_D\,(1-\theta)\,\xi \qquad (5.5)$$

$$\frac{d\xi}{dt} = \left[\frac{1}{M}\right]\left[k_p\,\theta\,(1-\xi) - k_D\,(1-\theta)\,\xi\right] \qquad (5.6)$$

where

$$k_i = \upsilon_i \exp\left[-\frac{E_i}{RT}\right] \qquad (5.7)$$

and M is the ratio of the total number of subsurface sites to the total number of surface sites. For TPD or TPR experiments, the temperature is varied in a linear fashion, so we can write

$$\frac{dT}{dt} = \beta \qquad (5.8)$$

We now have the equations which describe the system. Examination of equations 5.5 - 5.7 reveals that there are seven parameters that must be set in the model: three preexponential factors (υ_d, υ_p, υ_D), three activation energies (E_d, E_p, E_D), and the relative capacity of the subsurface for oxygen (M). For

each of the TPR spectra shown in Figure 5.5a, the desorption activation energy, E_d, was measured by the heating rate variation method (22). As mentioned earlier, for LTR-activated samples, it also was possible to measure the activation energy for the high temperature peak in a similar manner. If desorption in this peak is diffusion-limited, we would expect this activation energy to correspond to E_D. This was verified by simulating a heating rate variation experiment and comparing the calculated value of E_D to the actual value input to the model. The value of E_D was not measureable for the three spectra at higher levels of carbon deficiency because of the poor resolution of the high temperature peak, and must therefore be left as an adjustable parameter. The remaining parameters also are unknown. However, we can estimate values for each of the parameters as a first guess, and then iterate on those estimates to obtain a best fit of the spectra.

It seems reasonable that the activation energy for penetration into the subsurface should not be very different from the activation energy for diffusion from the subsurface to the surface. Therefore, as a first guess, E_p was set equal to E_D. Then in the iteration procedure used to fit the spectra, the value of E_p was not allowed to vary from that of E_D by more than 1 kcal/mole. Since the system being modeled is TPR of adsorbed oxygen, we do not expect the preexponential factor for "desorption" (or reaction) to be the same as it would be for a simple first order desorption process (10^{15} s^{-1}). In this case, the preexponential factor must incorporate the adsorption/desorption kinetics of hydrogen. However, it is possible to obtain a good estimate of υ_d from the desorption data. This is done by simulating a first order desorption process with the measured value of E_d and determining the value of υ_d which yields the correct peak temperature. As seen in Table 5.2, the values of υ_d which best fit the data are many orders of magnitude different from the values expected for a

simple first order desorption process.

TABLE 5.2

Parameter Values Used to Simulate the TPR Spectra

	Curve 1	Curve 2	Curve 3	Curve 4
υ_d (s^{-1})	130	3800	75,000	75,000
E_d (kcal/mole)	9.3	12.1	15.0	15.2
υ_p (s^{-1})	1.9×10^6	1.9×10^6	1.9×10^6	1.9×10^6
E_p (kcal/mole)	17.5	18.0	19.2	20.0
υ_D (s^{-1})	1.9×10^6	1.9×10^6	1.9×10^6	1.9×10^6
E_D (kcal/mole)	18.0	18.2	19.0	19.5
M	1.0	1.0	1.0	1.0

For the LTR-activated sample, since E_D was measureable we used the same approach to obtain an estimate of υ_D. By assuming that υ_D is unaffected by the Mo:C ratio, this estimate of υ_D could be used for each spectrum in Figure 5.5a. Furthermore, we assume that the preexponential factor for diffusion between the surface and subsurface is the same ($\upsilon_p = \upsilon_D$). Thus we have estimates for all three of the preexponential factors for each Mo:C ratio. The most difficult parameter to estimate is the value of M. Since we believe that the oxygen only penetrates a few layers into the subsurface during the ramp, we arbitrarily set the value of M = 1 (the subsurface capacity is the same as the surface oxygen capacity).

MODEL RESULTS

Equations 5.5 to 5.8 were solved numerically using a fourth order Runge-Kutta method. A listing of the computer program used is given in Appendix B. Figure 5.8 presents a simulation of the TPR spectrum for an Mo_2C catalyst activated by low-temperature reduction. For this simulation, the initial surface oxygen coverage was set equal to unity. This simulation can be compared to the experimental spectrum shown in Figure 5.1 for $\theta_0 = 1$. The values of the parameters used in this simulation are listed in the first column of Table 5.2. Also shown in Figure 5.8 are the surface and subsurface oxygen concentrations as a function of temperature. From this figure we see that at lower temperatures, oxygen is removed from the surface by both desorption and penetration into the subsurface. As the surface becomes depleted of oxygen, the desorption rate goes through a maximum and then decreases, producing the low temperature peak. As the surface coverage approaches zero, there is a net diffusion of oxygen from the subsurface back to the surface, and the TPR spectrum becomes diffusion-limited. As the temperature increases, the rate of diffusion increases since diffusion is an activated process, and therefore, the desorption rate also increases. Eventually, the subsurface also becomes depleted, and the desorption goes through another maximum and decreases again, producing the high temperature peak. Thus, it is clear from Figure 5.8 that subsurface diffusion can produce an extra peak in a TPD or TPR spectrum.

In a similar manner, simulations were made of each of the TPR spectra shown in Figure 5.5a for various levels of carbon deficiency; the results are shown in Figure 5.5b. The values of the parameters used to simulate each spectrum are listed in Table 5.2. As seen in Figure 5.5b, the model reproduces

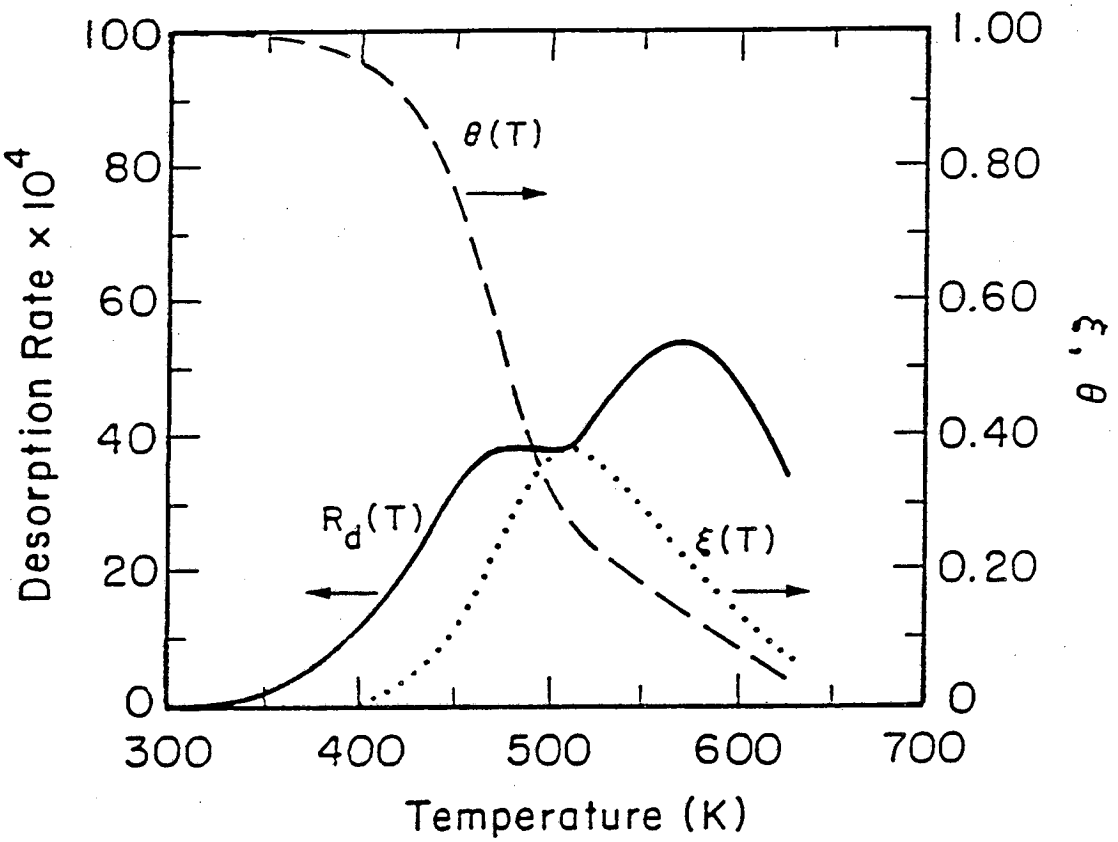

Figure 5.8: Simulated TPR spectrum of oxygen adsorbed on LTR-activated Mo_2C. Changes in the surface and subsurface oxygen coverage as a function of temperature also are shown.

the changes in the relative heights of the two peaks as the sample becomes more carbon deficient. This variation is caused by a decrease in the rate of penetration of oxygen into the subsurface relative to the rate of desorption, although both rates decreased with increasing carbon-deficiency. This is consistent with the observation that less oxygen penetrated into the subsurface region of HTR-activated Mo_2C than into LTR-activated Mo_2C during a 1 minute anneal in deuterium at 403 K. The model also suggests an explanation for why the peaks move closer together as the catalyst becomes more carbon deficient. This can be explained by a larger increase in E_p than in E_D as the sample becomes more carbon deficient. A possible reason for this might be that as carbon is removed from the material, the surface becomes depleted before the layers deep below the surface. Therefore, there could be a significant gradient in the carbon content as a function of distance into the material. If there is a larger increase in the Mo:C ratio at the surface than in the layers just below the surface, we might expect a larger increase in the activation energy for moving from the surface into the subsurface (E_p) than for moving from the subsurface to the surface (E_D).

Comparison of the simulated spectra in Figure 5.5b with the experimental spectra in Figure 5.5a reveals some interesting differences. The simulated values for the desorption rate at each temperature are slightly higher than the experimentally measured values. This suggests that a significant amount of the oxygen that penetrates into the subsurface does not desorb completely during the temperature ramp. This is consistent with the experimental results; examination of Figure 5.5a reveals that a large amount of oxygen continues to desorb as water at the end of the temperature ramp. In fact, it was necessary to reduce the catalyst an additional 5 minutes at the final ramp temperature to remove all of the oxygen that was adsorbed originally.

This was confirmed by integrating the area under the TPR spectrum. The probable reason why the model overestimates the desorption rate is that it does not account for the fact that the oxygen is inhomogeneously distributed over several subsurface layers.

The low temperature peak in the simulated spectrum for each case is significantly broader than what is experimentally observed, and the high temperature peak is slightly narrower. We believe that the reason the model predicts a broader low temperature peak is because it oversimplifies the kinetics and the mechanism of the reaction of hydrogen with surface oxygen and the subsequent desorption of water. The probable reason why the high temperature peak in the simulated spectrum is slightly narrower than the experimental peak is because we have not accounted for the gradient in the subsurface oxygen concentration.

Despite the discrepancies between the simulated and experimental TPR spectra, we have been able to show with a simple model that subsurface diffusion can produce an extra peak in a TPD or TPR spectrum.

DISCUSSION

The results presented above have shown that the two peaks in the TPR spectrum of oxygen on Mo_2C are not produced by two distinct adsorption sites for oxygen with different binding energies on the surface of the catalyst. Such a model cannot explain the broadness of the high temperature peak and its shift to lower temperatures with decreasing initial coverage. It also cannot explain the observation that after saturating the surface of Mo_2C with oxygen at 298 K, annealing in deuterium at 403 K frees surface sites for the adsorption of additional oxygen despite the fact that nothing desorbs.

Instead, we have shown that the high temperature peak is produced by initially-adsorbed oxygen which penetrates into the subsurface region during the temperature ramp. Such a diffusion-limited peak is expected to be very broad if the oxygen in the subsurface is distributed over several layers. As shown by the annealing experiments, the rate at which surface oxygen penetrates into the subsurface decreases as the catalyst becomes more carbon deficient. This change in oxygen mobility causes the observed change in the relative heights of the two peaks in the TPR spectrum. Furthermore, if the activation energy for penetration, E_p, increases more than the activation energy for diffusion from the subsurface to the surface, E_D, then the two peaks in the TPR spectrum should move closer together as the Mo:C ratio increases. This was observed experimentally.

Another possible explanation for the data presented above, is that a second state of more strongly bound surface oxygen is created during the temperature ramp. However, this explanation is inconsistent with our previous observation that more than nine monolayers of oxygen could be removed from an air-exposed Mo_2C sample during activation. For this to occur, oxygen must be able to diffuse from the subsurface to the surface of the catalyst. Therefore, we conclude that the high temperature peak is produced by subsurface diffusion.

An interesting observation in this study is that a 10 minute anneal in helium at 773 K is necessary to allow the same amount of oxygen to penetrate into the subsurface region as penetrates during a 1 minute anneal in deuterium at 403 K. This suggests that hydrogen (or deuterium) facilitates oxygen transport in Mo_2C, perhaps by producing a mobile OH species. This is consistent with an observation in Chapter 4 that carbon mobility in Mo_2C was higher in the presence of hydrogen than in helium.

It is important to note that the competition between desorption and diffusion of adsorbates into the subsurface layers of catalysts during TPD or TPR is not confined to oxygen on Mo_2C. This competition exists in any system in which adsorbed atoms or molecules are small enough to penetrate into the subsurface region. For example, we also have found that subsurface diffusion of hydrogen in Pd produces an extra peak in the TPD spectrum of hydrogen on Pd/SiO_2. This is shown in Chapter 7. Whether or not a diffusion-limited peak is seen in a TPD or TPR spectrum and how far it is separated from the surface desorption peaks depends on the relative rates of desorption and subsurface diffusion. As a result, care should be taken when assigning TPD peaks to different sites on a catalyst surface.

An important result of this work is that when a peak produced by subsurface diffusion is resolved, it may be possible to estimate the activation energy for diffusion from the subsurface to the surface by the same technique used to measure desorption activation energies; namely, the heating rate variation method (22). This is discussed in more detail in Chapter 6. Also, it is important to note that this activation energy is not necessarily the same as the bulk diffusion activation energy which can be measured by other methods.

The observation that subsurface mobility has a pronounced effect on a TPD or TPR spectrum, suggests that this technique might be useful in studying the role of carbon, oxygen, and hydrogen mobility in catalysis. It is interesting to note that one very good hydrogenation catalyst is palladium which absorbs hydrogen. One might speculate that subsurface mobility of hydrogen is important to the catalysis over this metal.

Chapter 6: A Comparative Study of a Multisite Model and a Subsurface Diffusion Model for TPD

In Chapter 5, we were able to show experimentally that subsurface diffusion produces a high temperature peak in the TPR spectrum of oxygen adsorbed on Mo_2C. These results illustrated how TPD and TPR can be used to study subsurface diffusion in high surface area catalysts. However, before one can use TPD to study subsurface diffusion in other systems, it is necessary to be able to distinguish between a high temperature peak produced by subsurface diffusion, and one produced by a high binding energy adsorption site on the catalyst surface. In this chapter, we show how to distinguish between these two possibilities experimentally by measuring the effect of carrier gas flow rate and heating rate on the spectrum. This is shown by simulating TPD spectra with a multisite model and a subsurface diffusion model, and comparing how the spectra change as these parameters are varied. For simplicity, only spectra containing two distinct peaks are considered.

The multisite model presented is similar to the one described by Chin and Bell (41). The model assumes the two peaks are produced by desorption from two distinct adsorption sites with different binding energies on the catalyst surface. This might be the case if the surface is composed of two different crystal planes. The subsurface diffusion model assumes that only one type of adsorption site exists on the surface, and that desorption from this site produces a low temperature peak in the TPD spectrum referred to as a desorption peak. The high temperature peak is produced by adsorbate which penetrates into the subsurface region of the material during heating, and then diffuses back to the surface when it becomes depleted by the desorption process. Since desorption in the high temperature peak is limited by diffusion of the adsorbate

from the subsurface to the surface, this peak is called a diffusion peak. Once it is determined that a diffusion peak is present in the spectrum, we show that one can estimate the activation energy for diffusion of the adsorbate from the subsurface to the surface from the shift in the diffusion peak temperature with heating rate.

THEORY

In both of the models presented here, desorption is taken to occur from a fixed bed of catalyst into a carrier gas stream which flows through the bed. It is assumed that the TPD experiment is performed under conditions for which the Peclet number is small enough that the catalyst bed can be modeled as a continuous-stirred-tank reactor (CSTR). Since the measured adsorbate concentration is proportional to the net desorption rate only for a CSTR, it is very important that this requirement be met (23). For reasonable carrier gas flow rates, we also can neglect accumulation of the adsorbate in the reactor (20-22). This assumption was not made by Chin and Bell (41) in their multisite model. It also is assumed that the catalyst particles are small enough that intraparticle diffusion limitations can be neglected. The conditions under which this assumption is valid, and the effects of intraparticle diffusion limitations on TPD spectra have been considered previously (23-26).

Multisite Model

In modeling the desorption from a heterogeneous surface, we consider the case where the surface contains two distinct adsorption sites of different binding energies. As the catalyst is heated, the adsorbate desorbs at different rates from each site. This is shown schematically in Figure 6.1. Since the

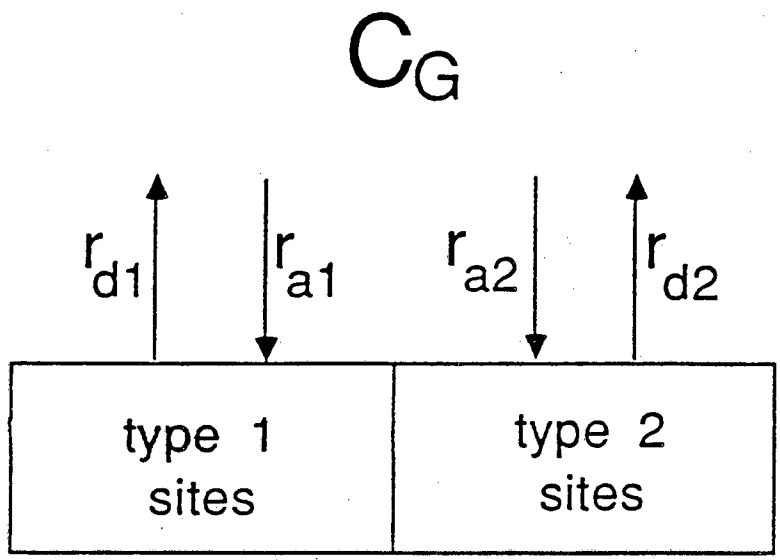

$$r_{d1} = n\, k_{d1}\theta_1^{\,n}$$

$$r_{a1} = n\, k_a\, (1 - \theta_1)^n C_G$$

$$r_{d2} = n\, k_{d2}\theta_2^{\,n}$$

$$r_{a2} = n\, k_a\, (1 - \theta_2)^n C_G$$

Figure 6.1: Schematic picture of TPD from a catalyst containing two distinct adsorption sites of differing binding energies. r_{di} is the desorption rate from type i sites, and r_{ai} is the readsorption rate on type i sites.

reactor is well-stirred, the adsorbate also can readsorb on either site before it is swept from the reactor by the carrier gas.

In this model, we do not explicitly consider surface diffusion of the adsorbate from one site to another. This process occurs in parallel with readsorption, and both processes provide a path for transfer of adsorbate between the two sites. Typically, the adsorption and desorption rates in an atmospheric pressure TPD system are several orders of magnitude larger than the net desorption rate. This high rate of exchange of adsorbate between the surface and the gas phase allows for rapid equilibration of the adsorbate between the two sites. For this reason it is not necessary to include surface diffusion in this model. It is important to note that this assumption may not be valid under ultra-high vacuum conditions.

Mass balances on the adsorbate on each site yield the following expressions.

$$\frac{d\theta_1}{dt} = n k_a (1 - \theta_1)^n C_G - n k_{d1} \theta_1^n \qquad (6.1)$$

$$\frac{d\theta_2}{dt} = n k_a (1 - \theta_2)^n C_G - n k_{d2} \theta_2^n \qquad (6.2)$$

The first term on the right side of Equations 6.1 and 6.2 describes the rate of adsorption from the gas phase, and the second term expresses the rate of desorption of the adsorbate from the surface. It is assumed that adsorption and desorption can be modeled as n'th order processes, with n typically being 1 or 2. In cases where precursor adsorption kinetics are observed, these equations may have to be modified. The fractional coverage of type 1 and type 2 sites are

given by θ_1 and θ_2, respectively.

A mass balance on the reactor yields the following expression for the gas phase concentration of the adsorbate

$$C_G = -\frac{N_S}{nQ}\left[X_1\frac{d\theta_1}{dt} + X_2\frac{d\theta_2}{dt}\right] \qquad (6.3)$$

where N_S is the total number of surface sites, and Q is the carrier gas flow rate. The fraction of sites that are type 1 and 2 are given by X_1 and X_2, respectively. It is important to note that Equations 6.1 and 6.2 are coupled through Equation 6.3. Therefore, one cannot model desorption from a surface containing two sites by simulating the desorption from each site independently and then simply adding the results.

During a TPD experiment, the carrier gas molar flow rate is held constant, and since the reactor operates isobarically, the volumetric flow is temperature-dependent. Assuming the gas behaves ideally, the volumetric flow rate varies as

$$Q = Q_0\left[\frac{T}{273}\right] \qquad (6.4)$$

where T is the temperature and Q_0 is the flow rate at 1 atmosphere and 273 K (STP).

The rate constants in Equations 6.1 and 6.2 also are temperature-dependent according to Equations 6.5 and 6.6 below.

$$k_a = S_0 \left[\frac{RT}{2\pi m} \right]^{\frac{1}{2}} \sigma \qquad (6.5)$$

$$k_{di} = \upsilon_{di} \exp \left[- \frac{E_{di}}{RT} \right] \qquad (6.6)$$

The expression for the adsorption rate constant in Equation 6.5 is derived from kinetic theory. In Equation 6.5, m is the molecular weight of the adsorbate and σ is the area occupied by one mole of adsorption sites. It is assumed that the sticking coefficient, $S_{0,}$ is equal for both sites and independent of temperature and coverage. We also assume that the adsorption is not activated (26). In Equation 6.6, the preexponential factors, υ_{di}, and the desorption activation energies, E_{di}, are assumed to be constant.

The temperature of the catalyst bed is assumed to be uniform and to vary linearly in time with heating rate β;

$$\frac{dT}{dt} = \beta \qquad (6.7)$$

During adsorption the surface sites fill sequentially, with the highest binding energy sites filling first (40). Therefore if the high binding energy sites are denoted as type 2 and the low binding energy sites as type 1, the initial conditions for Equations 6.1, 6.2, and 6.7 are

$$\text{at} \quad t = 0, \quad T = T_0 \tag{6.8}$$

$$\theta_2^{(0)} = \frac{\theta_T^{(0)}}{X_2} \quad \text{and} \quad \theta_1^{(0)} = 0 \quad \text{if} \quad \theta_T^{(0)} < X_2 \tag{6.9a}$$

$$\theta_2^{(0)} = 1.0 \quad \text{and} \quad \theta_1^{(0)} = \frac{\theta_T^{(0)} - X_2}{X_1} \quad \text{if} \quad \theta_T^{(0)} > X_2 \tag{6.9b}$$

where $\theta_T^{(0)}$ is the total initial surface coverage, and $\theta_1^{(0)}$ and $\theta_2^{(0)}$ are the initial coverages on the type 1 and type 2 sites, respectively.

Equations 6.1, 6.2, and 6.7 were solved numerically using a fourth order Runge-Kutta method with variable step size. A printout of the computer program is given in Appendix C. From these results, the net desorption rate

$$R_d = -\left[X_1 \frac{d\theta_1}{dt} + X_2 \frac{d\theta_2}{dt} \right] \tag{6.10}$$

was calculated and plotted as a function of temperature to give the desorption spectrum. Alternatively, one could plot the concentration of the adsorbate in the carrier gas as a function of temperature. These differ only by the factor (N_S/nQ).

Figure 6.2 shows the calculated desorption spectrum from a surface containing equal amounts of two distinct sites as a function of the initial coverage. For these spectra the carrier gas flow rate was 100 cm^3/min (STP) and the heating rate was 1 K/s. The values of the remaining parameters are listed in Table 6.1 and were chosen to be representative of hydrogen desorption from noble metals (40). As seen in Figure 6.2, the spectrum contains only one peak for $\theta_T^{(0)} \leq 0.5$. This peak corresponds to desorption

TABLE 6.1

Parameter Values Used in the Multisite Model

N_S = 3.0 X 10^{-6} moles

m = 2.0

n = 2.0

S_0 = 0.005

σ = 4.0 X 10^8 cm^2/mole (4.0 X 10^4 m^2/mole)

X_1 = 0.5

X_2 = 0.5

υ_{d1} = 1.0 X 10^{13} s^{-1}

υ_{d2} = 1.0 X 10^{13} s^{-1}

E_{d1} = 18.0 kcal/mole

E_{d2} = 23.0 kcal/mole

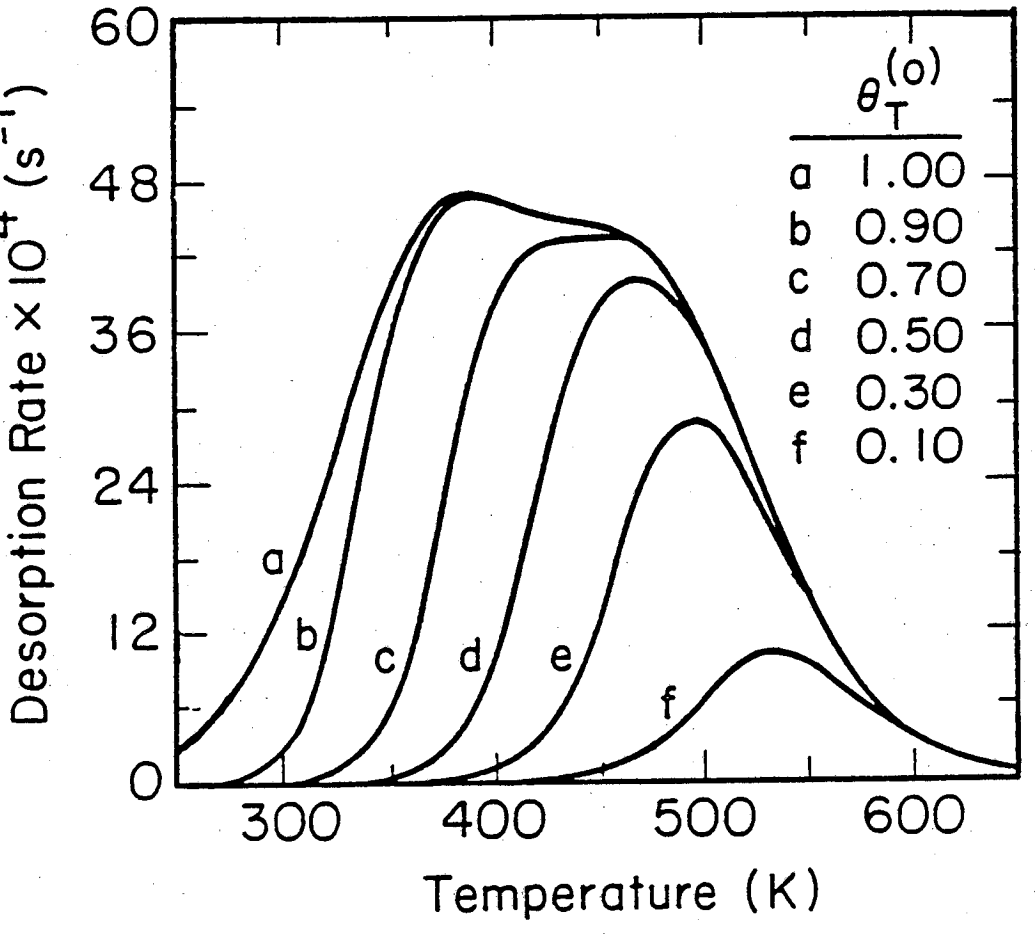

Figure 6.2: Effect of initial coverage on the TPD spectrum simulated by the multisite model. Q_0 = 100 cm^3/min , and β = 1.0 K/s. The rest of the parameter values are listed in Table 6.1.

from the high binding energy adsorption site (type 2). As expected for a second order desorption process, the peak narrows and shifts to lower temperatures as the initial coverage increases (26). Above $\theta_T^{(0)} = 0.5$, the lower binding energy site starts to fill, producing a low temperature desorption peak.

SUBSURFACE DIFFUSION MODEL

The subsurface diffusion model presented here assumes that the surface contains only one adsorption site whose binding energy is coverage independent. These results can be extended to cases where the surface contains multiple adsorption sites by combining this model with the multisite model presented above. In the subsurface diffusion model, the adsorbate is allowed to diffuse between the surface and the layers just beneath the surface during the temperature ramp. The layers just beneath the surface are referred to as the subsurface region. It is important to distinguish between the subsurface region and the bulk since diffusion in the subsurface region may be very different from diffusion in the bulk. Moreover, in most practical catalysts the dispersion is very high so that the small metal crystallites only contain a few subsurface layers, and there may not be any bulk metal present. It is assumed that the subsurface region is homogeneous and that the adsorbate in the subsurface distributes evenly over the entire region. To account for gradients in the adsorbate concentration in the layers near the surface, additional parameters would be required which can not be measured or estimated *a priori*. A continuum model such as Fick's law is not applicable here since we are only considering diffusion in the topmost atomic layers. A schematic picture of the processes occurring during a TPD experiment when both readsorption and subsurface diffusion are important is shown in Figure 6.3.

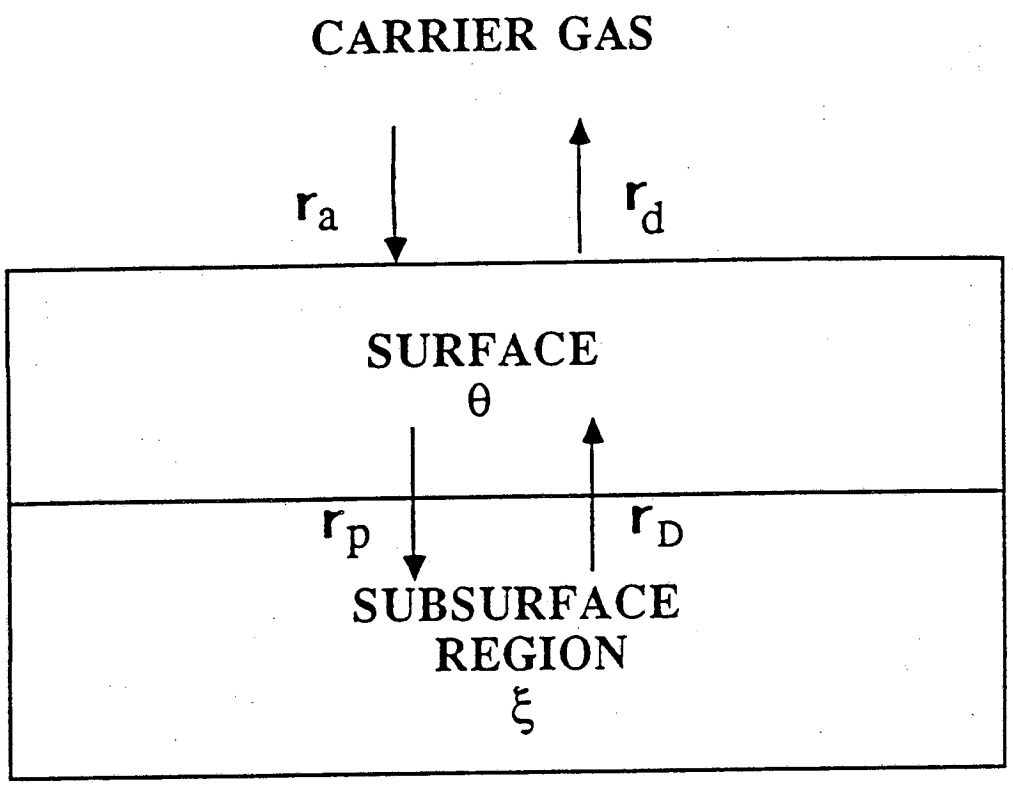

$$r_a = n\, k_a (1 - \theta)^n C_G$$

$$r_d = n\, k_d \theta^n$$

$$r_p = k_p \theta\ (1 - \xi)$$

$$r_D = k_D (1 - \theta)\, \xi$$

Figure 6.3: Schematic diagram of the processes occurring during TPD when both readsorption and subsurface diffusion are important.

Initially, the surface is covered with adsorbate up to some initial coverage θ_0. As the temperature rises, the adsorbate desorbs into the carrier gas stream with rate r_d, from which it either readsorbs with rate r_a, or is swept out of the reactor. During heating, some of the adsorbate also penetrates into the subsurface layers of the catalyst with rate r_p, and then diffuses back to the surface with rate r_D. It is assumed that the rate of penetration into the subsurface region, and the rate of diffusion back to the surface, can be modeled using macroscopic rate equations of the form shown in Figure 6.3. This same assumption was made by Davenport and Dienes (42) in their model which described the kinetics of hydrogen solution in transition metals. Also, it is important to emphasize that we consider only diffusion perpendicular to the surface; the effects of diffusion along the surface or within the subsurface region are not considered.

During a TPD experiment, the surface coverage, θ, decreases with time at a rate equal to the net rate of desorption into the gas phase ($R_d = r_d - r_a$) plus the net rate of diffusion into the subsurface region ($r_p - r_D$). A mass balance on the surface region yields:

$$\frac{d\theta}{dt} = n k_a (1 - \theta)^n C_G - n k_d \theta^n - k_p \theta (1 - \xi) + k_D (1 - \theta) \xi \quad (6.11)$$

The first two terms on the right side of Equation 6.11 are the rates of adsorption and desorption, respectively. The difference between them equals the net rate of desorption, R_d. The third and fourth terms represent the rate of penetration of adsorbate into the subsurface, and the rate of diffusion from the subsurface back to the surface, respectively. The rate of penetration into the subsurface is assumed to be first order in the surface coverage, and first order in the fraction

of subsurface sites which are empty. Similarly, the rate of diffusion from the subsurface to the surface is assumed to be first order in the fraction of filled subsurface sites, ξ, and first order in the fraction of free surface sites. The rate constants for penetration (k_p) and backdiffusion (k_D) are assumed to follow Arrhenius expressions of the form shown in Equation (5.7) with constant preexponential factors and activation energies.

The concentration of the adsorbate in the carrier gas when there is only one adsorption site simplifies to

$$C_G = \frac{\frac{N_S}{Q} k_d \theta^n}{1 + \frac{N_S}{Q} k_a (1 - \theta)^n} \tag{6.12}$$

A mass balance on the subsurface region yields:

$$\frac{d\xi}{dt} = \frac{1}{M}\left[k_p \theta (1 - \xi) - k_D (1 - \theta) \xi\right] \tag{6.13}$$

where M is the ratio of the total number of subsurface sites to surface sites ($M = N_B/N_S$). Equations 6.11 and 6.13 are equivalent to those used by Davenport and Dienes (42) to describe the kinetics of hydrogen solution in transition metals.

In this work, we only consider the case where the adsorbate is not present in the subsurface initially. Therefore, the initial conditions are

$$\text{at} \quad t = 0, \quad T = T_0, \quad \theta = \theta_0, \quad \xi = 0 \tag{6.14}$$

Equations 6.7, 6.11 and 6.13 were solved simultaneously with a fourth order Runge-Kutta method for the parameter values listed in Table 6.2. A printout of the computer program used is given in Appendix D. These values are similar to those used to describe the diffusion of hydrogen in the subsurface of palladium during TPD in Chapter 7. The parameters were modified slightly in this chapter to give better resolution of the peaks.

TABLE 6.2

Parameter Values Used in the Subsurface Diffusion Model

$N_S = 3.0 \times 10^{-6}$ moles

$m = 2.0$

$n = 2.0$

$M = 1.0$

$S_0 = 0.005$

$\sigma = 4.0 \times 10^8$ cm^2/mole (4.0×10^4 m^2/mole)

$\upsilon_d = 1.0 \times 10^{13}$ s^{-1}

$E_d = 19.0$ kcal/mole

$\upsilon_p = 1.0 \times 10^6$ s^{-1}

$E_p = 15.0$ kcal/mole

$\upsilon_D = 1.0 \times 10^6$ s^{-1}

$E_D = 14.0$ kcal/mole

$\xi_0 = 0.0$

The results of the simulation are shown in Figure 6.4. This figure shows that the adsorbate is removed from the surface by both desorption, and

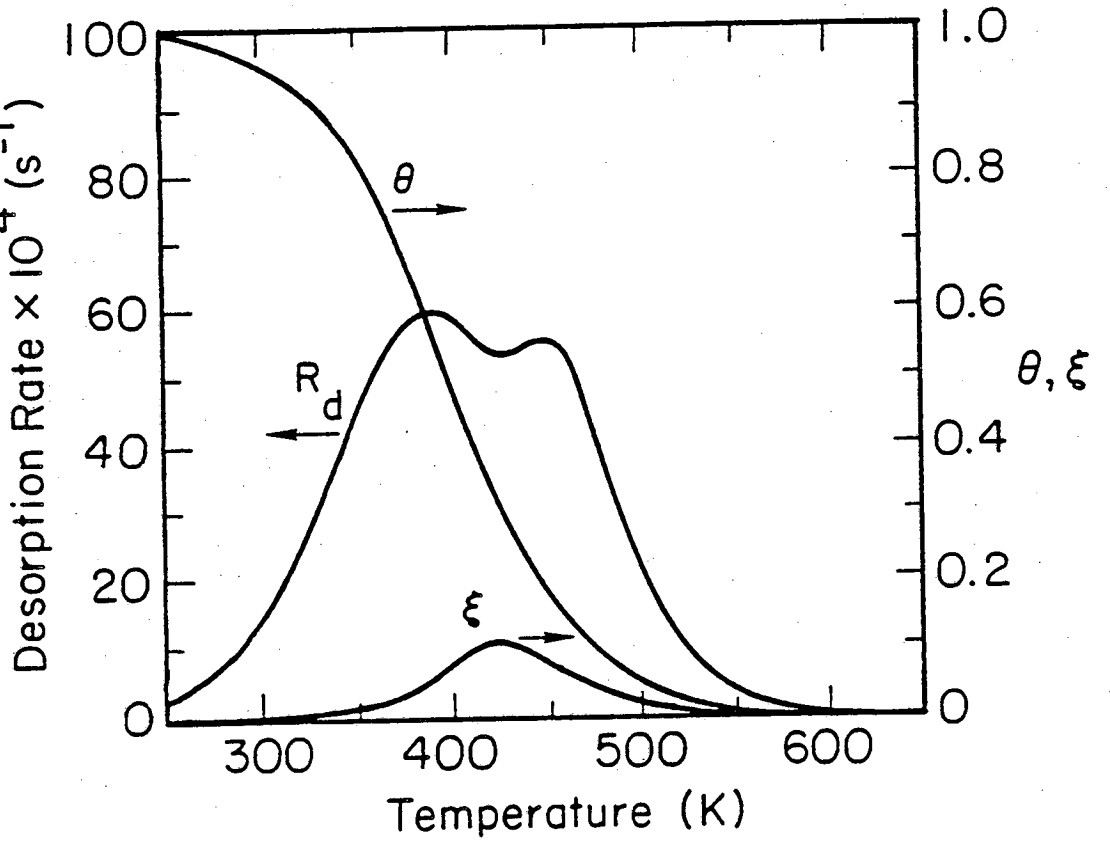

Figure 6.4: Simulated TPD spectrum using the subsurface diffusion model for the parameter values listed in Table 6.2. The changes in the surface and subsurface coverages with temperature also are shown.

penetration into the subsurface region. As the surface adsorbate concentration decreases, R_d goes through a maximum, and then decreases. When the surface coverage becomes sufficiently small, there is a net diffusion of adsorbate from the subsurface region back to the surface, and the desorption spectrum becomes diffusion-limited. As the temperature rises, the diffusion rate increases since diffusion is an activated process, and R_d also increases. Eventually, as the subsurface adsorbate concentration also decreases, R_d goes through another maximum and decreases, producing a second peak which we will refer to as a diffusion peak.

It is important to note that subsurface diffusion does not always lead to an extra peak in a TPD spectrum. In order to observe a diffusion peak, the rate of diffusion between the surface and subsurface must be comparable to the net rate of desorption, R_d. This is illustrated by examining the effect of changing the diffusion preexponential factors. This is shown in Figure 6.5. If diffusion is much slower than the net desorption rate (curve a), then only one peak is observed in the spectrum: the one produced by desorption from the surface. If the diffusion rate is much higher than the net desorption rate (curve d), the desorption never becomes limited by the diffusion process, and we again observe only one peak. This peak occurs at a higher temperature than that in curve (a) because diffusion into the subsurface during the temperature ramp decreases the surface coverage. Since the desorption rate is second order in the surface coverage, the net desorption rate is reduced and the peak shifts to higher temperature.

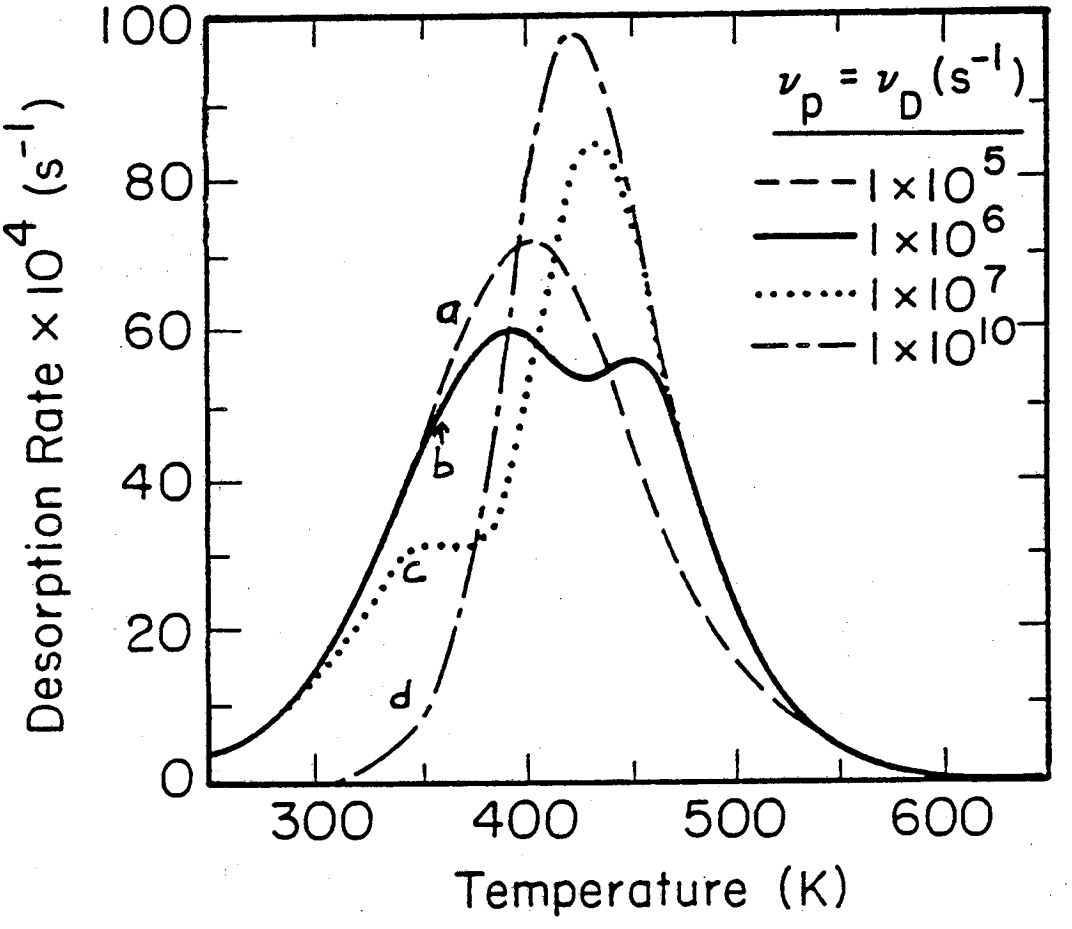

Figure 6.5: Effect on the simulated TPD spectrum of changing the values of the diffusion preexponential factors in the subsurface diffusion model. Q_0 = 100 cm^3/min, θ_0 = 1.0, ξ_0 = 0.0, and β = 1.0 K/s.

COMPARISON OF THE MULTISITE AND SUBSURFACE DIFFUSION MODELS

Thus far we have shown that both the multisite model and the subsurface diffusion model can simulate two peaks in a TPD spectrum. In this section we present a method by which one can distinguish between the two models experimentally.

There are four variables which may be adjusted in a TPD experiment: the initial coverage, the carrier gas flow rate, the heating rate, and the number of surface sites, which is determined by the amount of catalyst placed in the reactor. From Equations 6.3 and 6.12, we know that the number of surface sites and the carrier gas flow rate can be combined into one variable, the ratio N_S/Q. This leaves us with only three variables (θ_0, N_S/Q, and β) which can be varied independently. By comparing the changes in the spectrum predicted by each model as these parameters are varied, we can determine for which variables the two models predict different behavior. We can then use this result to distinguish between the two models.

Figure 6.6 shows the effect of initial coverage on the TPD spectrum simulated by the subsurface diffusion model. Since the desorption rate is second order in the surface coverage and the diffusion rate is first order, the desorption rate decreases with coverage more rapidly than the diffusion rate. Therefore, at low coverages, the diffusion rate is much higher than the desorption rate and the spectrum never becomes diffusion-limited. As a result, only one peak is observed in the spectrum. At higher initial coverages, the desorption rate becomes comparable to the diffusion rate, and two peaks become resolved. If we compare Figure 6.6 with the results from the multisite model in Figure 6.2, we see that the two models predicts similar changes in the

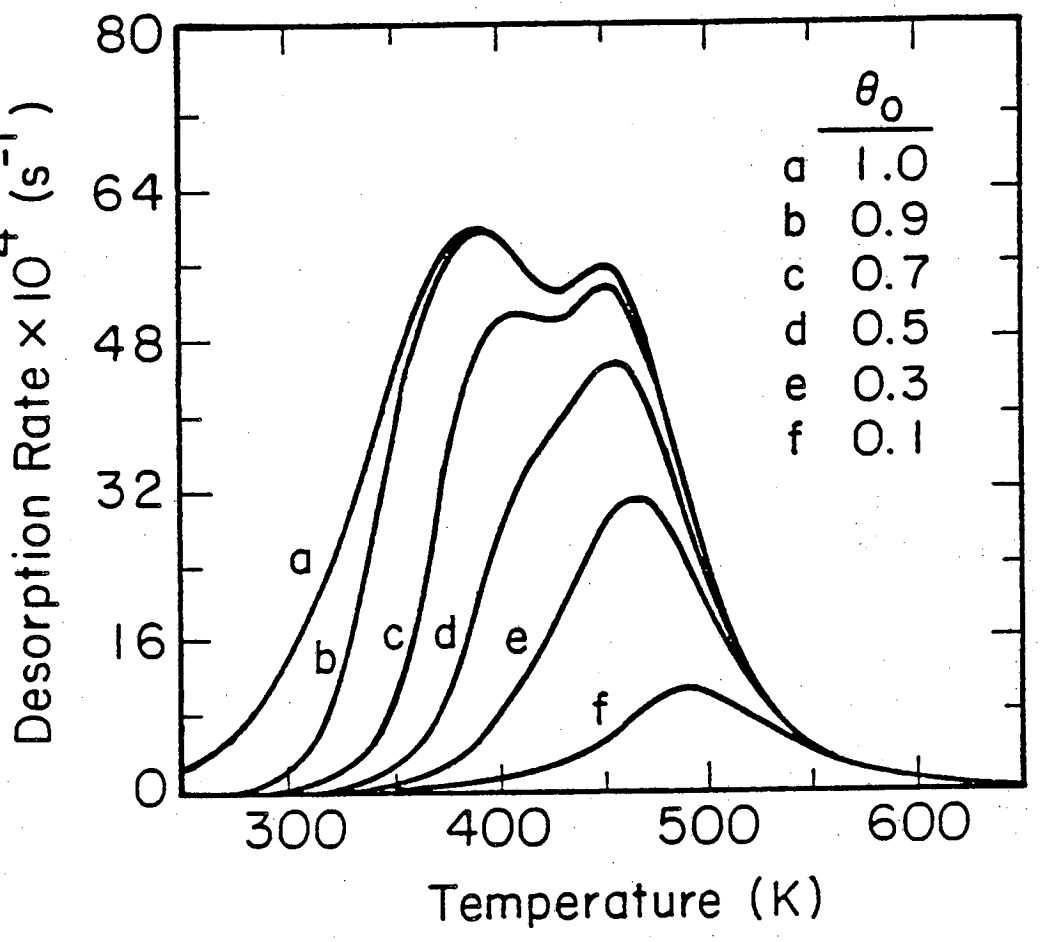

Figure 6.6: Effect of initial surface coverage on the TPD spectrum simulated by the subsurface diffusion model. Q_0 = 100 cm^3/min, ξ_0 = 0.0, and β = 1.0 K/s.

spectrum as the initial coverage is varied. Therefore, varying the initial coverage will not help to distinguish between the two models.

The next experimental parameter which we can change is the ratio N_S/Q. This is accomplished most easily by varying the carrier gas flow rate, Q_0. Figure 6.7 shows how the two models predict the spectrum should change as the flow rate is varied. According to the multisite model (Figure 6.7a), the peaks should shift to lower temperatures and the resolution between the two peaks should improve slightly as the flow rate increases. The reason for this is that an increase in the flow rate causes a decrease in the gas phase adsorbate concentration (see Equation 6.3), and this decreases the rate of readsorption. This, in turn, causes an increase in the net desorption rate and a shift in the peaks to lower temperatures. Figure 6.7a also shows that if the two peaks are produced by two distinct adsorption sites, the relative sizes of the two peaks do not change significantly as the flow rate is varied. This is in sharp contrast to what is predicted by the subsurface diffusion model (Figure 6.7b). While an increase in the flow rate causes an increase in the net desorption rate from the surface, the flow rate does not directly affect the diffusion rate. Therefore as the flow rate increases, the desorption rate increases relative to the diffusion rate and less adsorbate diffuses into the subsurface region during heating. This causes a substantial decrease in the size of the diffusion peak relative to the desorption peak. Thus, the two models predict very different behavior as the flow rate is varied. Therefore, by varying the carrier gas flow rate, we can distinguish between the multisite model and the subsurface diffusion model.

A distinction between the two models also can be made from the effect of heating rate on the spectrum as shown in Figure 6.8. Figure 6.8a shows the changes in the spectrum predicted by the multisite model as the heating rate is varied. As the heating rate increases, the peaks shift to higher temperatures,

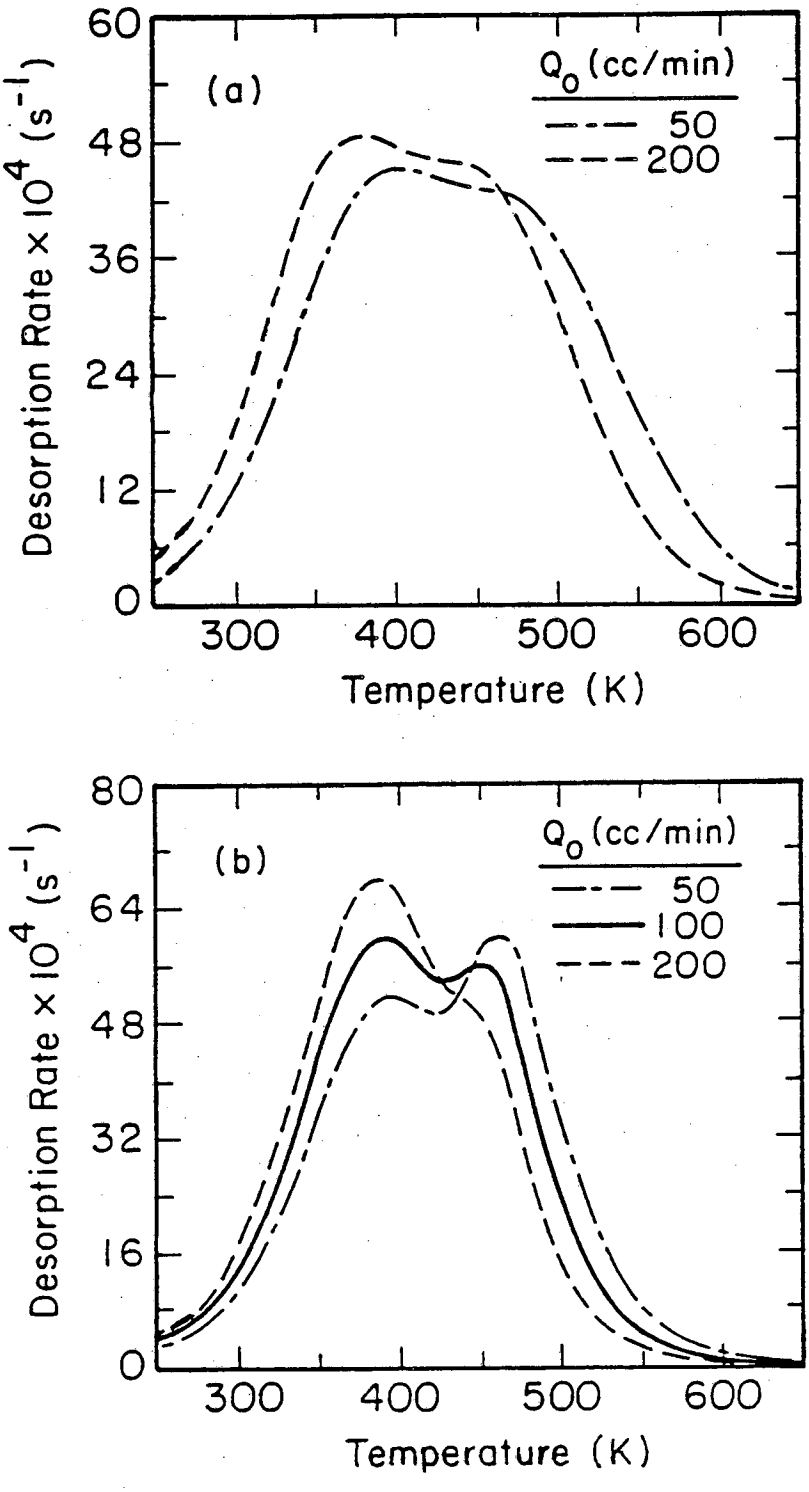

Figure 6.7: Effect of carrier gas flow rate on the TPD spectra simulated by the (a) multisite and (b) subsurface diffusion models. θ_0 = 1.0 and β = 1.0 K/s.

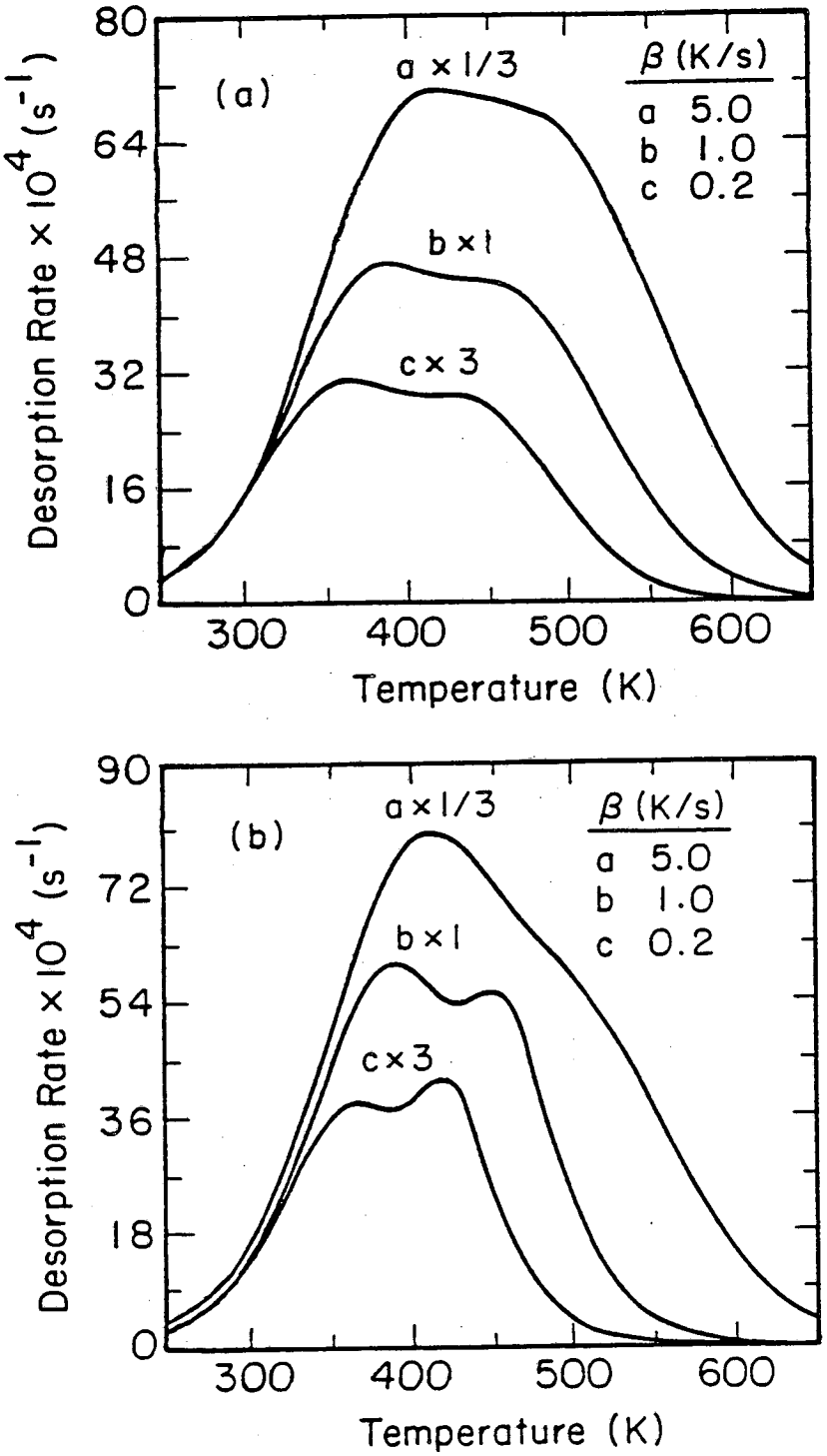

Figure 6.8: Effect of heating rate on the TPD spectra simulated by the (a) multisite and (b) subsurface diffusion models. θ_0 = 1.0 and Q_0 = 100 cm^3/min.

but the relative sizes of the two peaks do not change significantly. However, in the subsurface diffusion model the relative sizes of the peaks can change substantially as the heating rate is varied. When E_D is much greater than E_d, the diffusion peak increases in size relative to the desorption peak as the heating rate increases. Conversely, when E_D is much less than E_d, Figure 6.8b shows that the diffusion peak decreases in size relative to the desorption peak as the heating rate increases.

Thus, by studying the effect of carrier gas flow rate and heating rate on the spectrum, we can distinguish between the multisite model and the subsurface diffusion model experimentally. However, it is important to note that while multiple peaks in TPD spectra are most commonly assigned to multiple adsorption states, there are other models which can account for multiple peaks in a spectrum. Therefore, it is important to be able to distinguish between the subsurface diffusion model and these other models as well. As mentioned earlier, in certain instances, lateral interactions between adsorbate molecules can produce additional peaks in a TPD spectrum. Also if the catalyst has a bimodal pore size distribution, this also could produce two peaks in a spectrum. However, we would expect that in both cases, an increase in the carrier gas flow rate would result in improved resolution of the two peaks without any significant change in the relative peak heights, as was the case in the multisite model. Thus, it should be possible to distinguish between the subsurface diffusion model and the other models by measuring the effect of flow rate on the spectrum.

We also should note that the subsurface diffusion model could also be used to describe spillover of adsorbate from a metal surface onto a support during heating, and then diffusion back to the metal surface when it becomes depleted by the desorption process. As a result, it is not possible to distinguish

between spillover and subsurface diffusion based on the flow rate and heating rate dependence of the spectrum. Therefore, in cases where spillover may occur, additional experiments are required to distinguish between these possibilities. This is discussed in detail in Chapter 7, where we show that subsurface diffusion of hydrogen in palladium produces a high temperature peak in the TPD spectrum of hydrogen on a 9 % Pd/SiO_2 catalyst.

DETERMINATION OF RATE PARAMETERS FROM TPD SPECTRA

As mentioned in Chapter 2, a major advantage of TPD over chemisorption studies is that it can be used to determine the heat of adsorption on each of the individual adsorption sites instead of obtaining an average over the entire surface. In this section we show how the heat of adsorption is usually measured, and note some precautions which must be taken when deriving quantitative information from TPD spectra. We also show that when a diffusion peak is present in the spectrum, TPD can be used to estimate the activation energy for diffusion from the subsurface to the surface.

In the absence of mass transfer limitations, and assuming equilibrium readsorption, the heat of adsorption, ΔH, on each type of site can be determined from the expression (26)

$$\ln\left[\frac{\beta}{T_p^2}\right] = -\frac{\Delta H}{RT_p} + \ln\left[\frac{R\,n\,Q\,A\,\theta_p^{n-1}}{N_S\,\Delta H\,(1-\theta_p)^{n+1}}\right] \qquad (6.15)$$

where T_p is the peak temperature, θ_p is the coverage at the peak temperature, and A is the ratio of the desorption preexponential factor to the adsorption rate

constant. If the adsorption is not activated, ΔH is equal to the activation energy for desorption, E_d. Since our modeling studies show that θ_p does not vary significantly with heating rate, E_d for each site can be determined simply from the slope of a plot of $\ln (\beta/T_p^2)$ vs. $1/T_p$ for each peak. However, when this method is applied to spectra containing multiple peaks, care must be taken in determining the desorption activation energies.

Figure 6.8a shows the effect of heating rate on the TPD spectrum from a surface containing two sites. As the heating rate increases, the peaks shift to higher temperatures as expected from Equation 6.15, and the overlap between the peaks increases. The overlap causes the low temperature peak to be shifted upward in temperature, and the high temperature peak to be shifted downward in temperature. Since the overlap between the peaks increases at higher heating rates, the low temperature peak is shifted upward in temperature more than it would have been in the absence of the high temperature peak. Conversely, the high temperature peak is not shifted as much with temperature as it would be if the low temperature peak were not present. This is shown more clearly in Figure 6.9.

In Figure 6.9, the net desorption rates from the individual sites are plotted as well as R_d from the entire surface. Figures 6.9a and b show that the overlap of the two peaks causes the low temperature peak to be shifted upward in temperature by 14 K when β = 0.2 K/s, and by 27 K when β = 5.0 K/s. The increased overlap at higher heating rates causes the shift in the low temperature peak with heating rate to be overestimated by 13 K. Therefore, when E_d is calculated from the shift in the peak temperature with heating rate, it is underestimated. From the spectra shown in Figure 6.8a, we calculate E_{d1} = 16 kcal/mole which is 11% lower than the value of 18 kcal/mole input to the model.

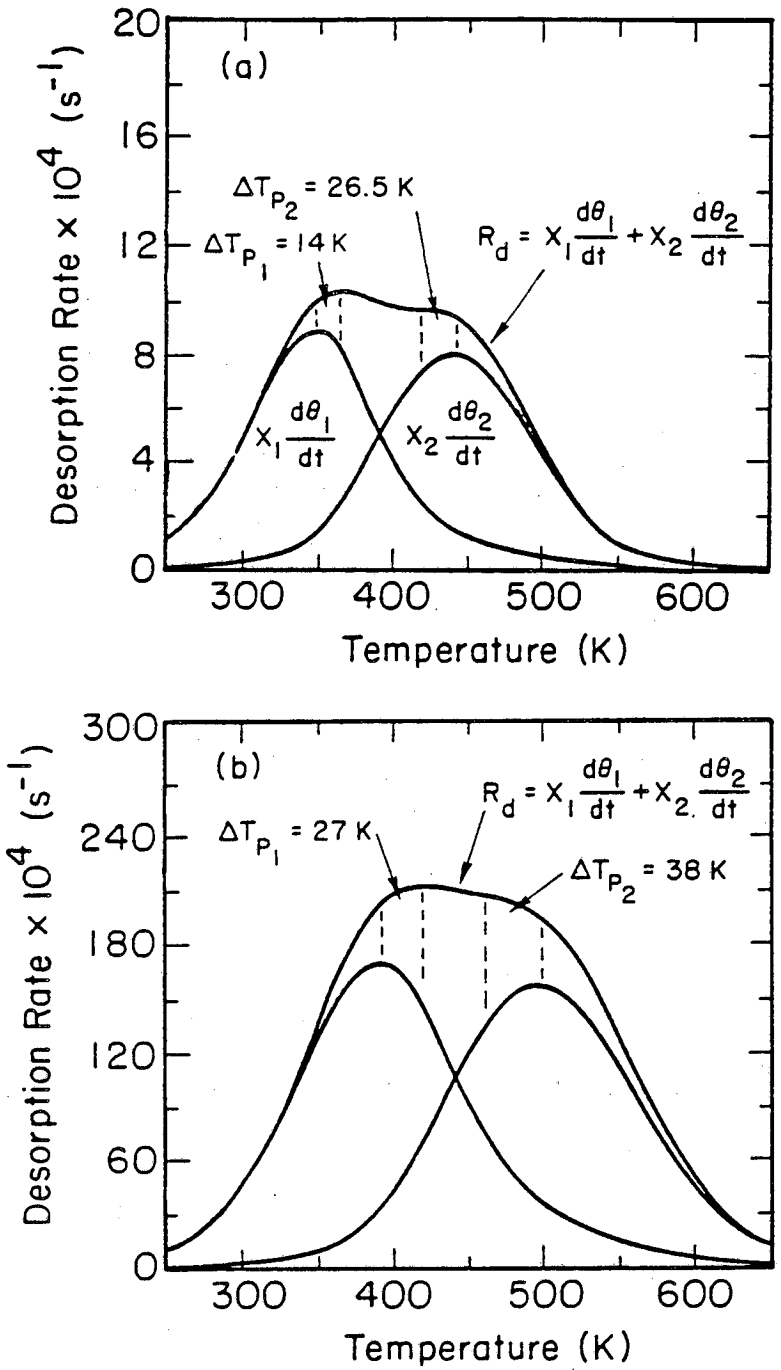

Figure 6.9: TPD spectra simulated by the multisite model at heating rates of (a) 0.2 K/s and (b) 5.0 K/s. The net desorption rates from the individual sites, as well as the net desorption rate from the *entire* surface are shown. Also shown are the shifts in the peak temperatures caused by the overlap between the peaks.

Figures 6.9a and b also show that the high temperature peak is shifted downward in temperature by 26.5 K when β = 0.2 K/s. When β = 5.0 K/s, the high temperature peak is no longer resolved clearly, and appears as a shoulder on the low temperature peak. If the inflection point immediately to the left of the high temperature shoulder is taken as an estimate of the peak temperature, a downward shift of 38 K is obtained. Thus, the shift with peak temperature is underestimated by 11.5 K, causing E_d to be overestimated. From the spectra in Figure 6.8a, we calculate E_{d2} = 26.1 kcal/mole which is 13 % higher than the value of 23 kcal/mole input to the model. The error in measuring the desorption activation energy of the high binding energy site caused by peak overlap can be avoided by performing the heating rate variation experiment at an initial coverage for which only this site is filled.

In cases where a diffusion peak appears in the TPD spectrum, a plot of $\ln (\beta/T_p^2)$ vs. $1/T_p$ can be used to estimate the activation energy for diffusion from the subsurface to the surface. This is because the net desorption rate becomes diffusion-limited. However, since net diffusion of adsorbate from the subsurface to the surface does not occur until the surface is substantially depleted by desorption, the location of the diffusion peak is in part determined by the location of the desorption peak. Therefore, the shift in the diffusion peak temperature with heating rate contains two contributions: the shift due to the activated nature of the diffusion process, and the shift due to the change in the desorption peak temperature. As a result, the measured activation energy will lie between the values for the diffusion activation energy E_D, and the desorption activation energy E_d.

Our modeling studies show that if the relative size of the two peaks and the resolution between them does not change substantially as the heating rate is varied, then the activation energy determined corresponds closely to the

value of E_D. To meet this requirement, a smaller range of heating rates must be used, and this makes it very important to determine the peak temperatures accurately. If the relative sizes of the two peaks or the resolution between them changes substantially, then the measured activation energy may lie closer to the value of E_d. This is the case in Figure 6.8b from which an activation energy of 16.5 kcal/mole is calculated for the diffusion peak. This value is equidistant between the values of E_d = 19 kcal/mole and E_D = 14 kcal/mole. Moreover, it is important to note that mass transfer limitations can cause errors in measuring activation energies from TPD spectra. As discussed by Demmin and Gorte (23), it is often very difficult to eliminate the effects of mass transfer limitations. Thus, care must be taken when estimating E_D from TPD spectra.

SUMMARY

Two models have been presented which can account for two peaks in a TPD spectrum: a multisite model, and a subsurface diffusion model. The multisite model assumes that the two peaks are produced by two distinct types of adsorption sites on the catalyst surface which differ in binding energy. The subsurface diffusion model assumes that the high temperature peak is produced by adsorbate which diffuses into the subsurface of the material during heating and then back to the surface when it becomes depleted by the desorption process. We have shown that it is possible to distinguish between these two models experimentally by measuring the effect of flow rate and heating rate on the spectrum. If the two peaks are produced by two sites, then changing the carrier gas flow rate or heating rate does not affect the relative heights of the two peaks significantly. However, if the high temperature peak is a diffusion peak, then the size of this peak decreases markedly relative to the

desorption peak as the flow rate increases. The relative heights of the diffusion and desorption peaks also can change significantly as the heating rate is varied.

We also have shown that significant errors can be made in determining desorption activation energies from the individual sites from the shifts in peak temperatures with heating rate. The decrease in resolution of the peaks as the heating rate increases can cause the activation energy for desorption from the low binding energy sites to be underestimated, and the activation energy for the high binding energy sites to be overestimated. The activation energy for desorption from the high energy sites can be determined accurately by working at initial coverages where only these sites are filled.

Finally, we have shown that if a diffusion peak is present in the spectrum, the shift in its peak temperature with heating rate can be used to estimate the activation energy for diffusion from the subsurface to the surface.

Chapter 7: Penetration of Hydrogen into Subsurface Sites of a Pd/SiO_2 Catalyst During TPD

There is growing evidence that hydrogen can penetrate into subsurface sites during adsorption and desorption of hydrogen on Group VIII metals. Since the absorption of hydrogen in sites just below the surface could affect the binding energy and reactivity of adsorbates on the surface, this could have important implications in catalysis. However, the studies which have investigated this phenomenon have been performed under ultra-high vacuum conditions on either single crystals (13-19, 43-49) or on bulk polycrystalline materials (50-54). In most practical catalysts, the metals are highly dispersed on a support, and the properties of the small metal crystallites (usually less than 10 nm in size) may be very different from the properties of single crystals or of bulk metals. Therefore it is not clear that the results obtained on metals under ultra-high vacuum conditions can be extended to supported metal catalysts. In this chapter, we use the results of Chapter 6 to show that hydrogen penetrates into subsurface sites of a Pd/SiO_2 catalyst during TPD at atmospheric pressure. These results strongly suggest that hydrogen may be absorbed in subsurface sites of palladium under typical catalytic reaction conditions.

There is considerable evidence for the formation of subsurface hydrogen in palladium single crystals under ultra-high vacuum conditions. For example, Ertl and coworkers (13-15) concluded from LEED intensity-voltage curves and TPD data, that the topmost layers of both Pd(100) (13) and Pd(111) (14,15) expand slightly upon absorption of hydrogen at 300 K. They also found that the concentration of hydrogen in the layers near the surface was considerably higher than the equilibrium bulk concentration predicted by Sieverts' law (55). More recently, several investigators (16-19) reported the

existence of subsurface absorption sites for hydrogen on Pd(110). These sites are separated by distinct activation barriers from species which are adsorbed on the surface or dissolved in the Pd bulk (17). Selective population of these sites occurs by thermal activation from a specific type of chemisorption site which is associated with a substrate reconstruction at high hydrogen surface coverage (18). Based on structural arguments, it was suggested that the subsurface sites correspond to the octahedral interstitials between the topmost and second atomic layers. This would explain why exactly one monolayer of hydrogen can be accomodated subsurface by thermal cycling (19). Thus, there is considerable evidence for the presence of subsurface absorption sites for hydrogen in Pd single crystals, particularly for Pd(110).

The goal of this study was to determine whether subsurface absorption sites for hydrogen exist in a supported palladium catalyst under conditions which more closely resemble catalytic reaction conditions. To probe the subsurface absorption sites under non UHV conditions, we used temperature-programmed desorption (TPD). In Chapters 5 and 6, we showed that if an adsorbate penetrates into the subsurface region of a material during heating, and then moves back to the surface when it becomes depleted by the desorption process, this can produce a high temperature peak in a TPD spectrum. Moreover, in Chapter 6 we showed that a distinction can be made between a high temperature peak produced by subsurface diffusion and a peak produced by desorption from a high binding energy adsorption site, by measuring the effect of flow rate and heating rate on the spectrum. Based on these studies, we postulated that if subsurface absorption sites exist in a supported palladium catalyst, then diffusion of hydrogen between the surface and subsurface sites might produce a high temperature peak in the TPD spectrum of hydrogen on this catalyst.

Thus the effect of flow rate and heating rate on the TPD spectrum of hydrogen on a supported Pd catalyst, can be used to aid in determining whether or not diffusion of hydrogen between surface and subsurface absorption sites produces a high temperature peak in the spectrum. If a diffusion peak is found, then this would demonstrate that subsurface absorption sites for hydrogen can exist in supported Pd catalysts as well as in single crystals.

EXPERIMENTAL

For both the hydrogen and deuterium TPD experiments, 53 mg of the 9 wt % Pd/SiO_2 catalyst were placed in the reactor. This corresponded to a total of 4.0×10^{-6} moles of surface Pd atoms in the hydrogen experiments (dispersion = 9 %), and 6.7×10^{-6} moles of surface sites in the deuterium experiments (dispersion = 15 %). The catalyst was evacuated at room temperature for one hour and subsequently reduced in 100 cc/min (STP) hydrogen at 473 K for 1 hour. Following reduction, the sample was evacuated for 15 minutes at 673 K to remove all the hydrogen from the palladium, and then cooled to 290 K in helium. Hydrogen was adsorbed at 290 K by pulsing known quantities of hydrogen into a helium carrier gas which flowed over the catalyst. By monitoring the amount of hydrogen in the reactor effluent with the mass spectrometer, the amount of hydrogen that adsorbed in each pulse could be determined quantitatively. Following hydrogen adsorption, the reactor was flushed with helium for 10 minutes to remove residual gas phase hydrogen prior to taking a TPD spectrum. In the hydrogen desorption experiments, helium was used as the carrier gas, whereas argon was used in the deuterium experiments.

EXPERIMENTAL RESULTS

The TPD spectrum of hydrogen on the 9 % Pd/SiO_2 catalyst is shown in Figure 7.1. In this experiment, the helium flow rate was 100 cc/min (STP), the heating rate was 0.5 K/s, and the initial hydrogen coverage was $\theta_0 = 1.15$. Monolayer coverage ($\theta_0 = 1.00$) is defined as the coverage at which one hydrogen atom is adsorbed per surface palladium atom, based on the measured 9 % dispersion. As seen in Figure 7.1, the TPD spectrum for $\theta_0 = 1.15$ contains 4 overlapping peaks designated α, β_1, β_2, and β_3. The low temperature α peak is only present for $\theta_0 > 1.00$, and corresponds to reversibly bound hydrogen which can be removed by a 30 minute evacuation at 290 K.

The effect of carrier gas flow rate on the TPD spectrum is shown in Figure 7.2 for $\theta_0 = 1.15$ and a heating rate of 0.5 K/s. As Q increases from 50 to 200 cc/min (STP), the α, β_1 and β_2 peaks all shift to lower temperatures, and the resolution between them improves slightly. Also, there is no significant change in the relative heights of these peaks as the flow rate increases. This result is consistent with what is predicted by the multisite model discussed in Chapter 6, and suggests that the α, β_1, and β_2 peaks are produced by desorption from three distinct adsorption sites with different binding energies. However, the high temperature β_3 peak decreases in size relative to the other three peaks as the flow rate increases. This effect can be seen more clearly at lower initial coverages where the α and β_1 sites are not filled.

Figure 7.3a shows the flow rate dependence of the TPD spectrum for an initial coverage of $\theta_0 = 0.36$ and a heating rate of 0.2 K/s. The lower heating rate was used to improve the resolution between the peaks. At this initial coverage, only the β_2 and β_3 peaks appear in the spectrum. As seen in Figure 7.3a, for Q = 50 cc/min (STP) the β_3 peak is larger than the β_2 peak. As the flow

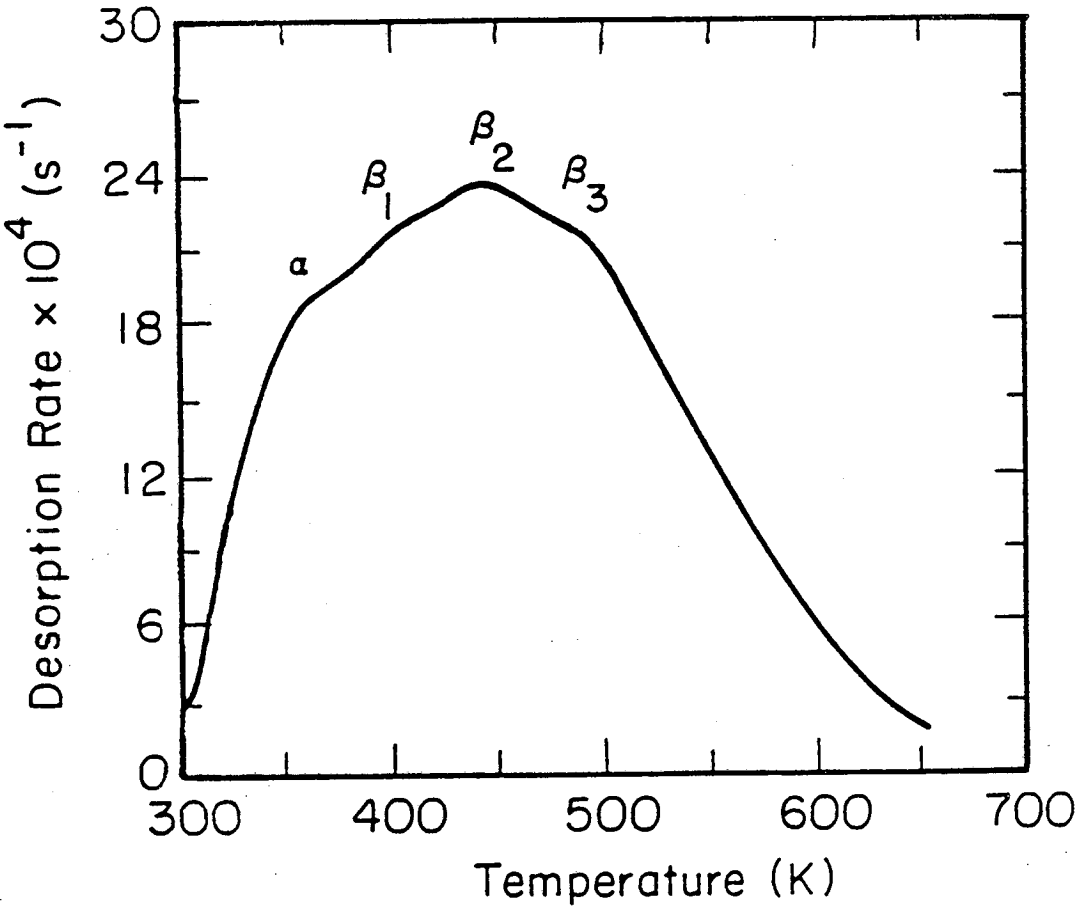

Figure 7.1: TPD spectrum of hydrogen on the Pd/SiO_2 (dispersion = 9 %) catalyst for θ_0 = 1.15, Q = 100 cc/min (STP), and β = 0.5 K/s.

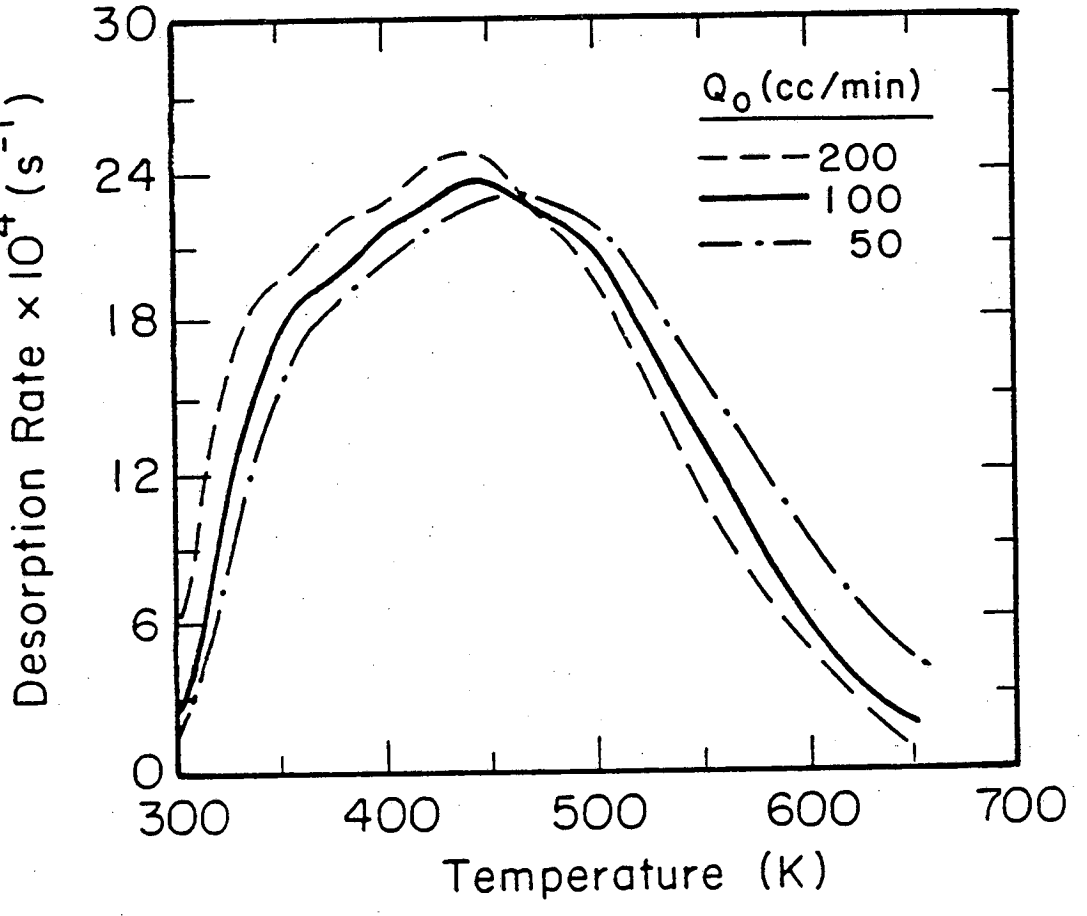

Figure 7.2: Effect of helium flow rate on the TPD spectrum of hydrogen on the Pd/SiO_2 catalyst (dispersion = 9 %) for θ_0 = 1.15, and β = 0.5 K/s.

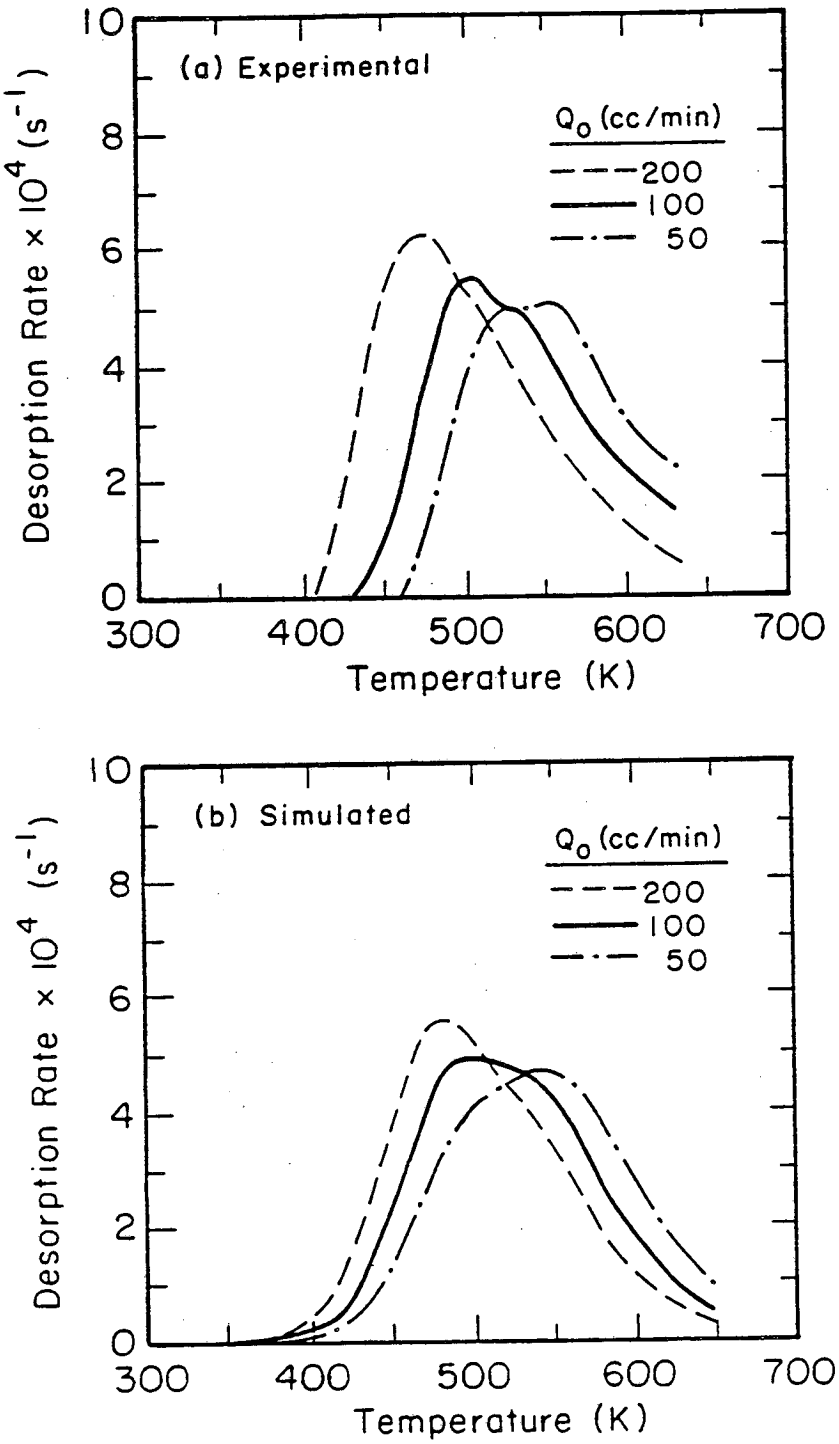

Figure 7.3: Effect of carrier gas flow rate on the (a) experimental and the (b) simulated TPD spectra of hydrogen on the Pd/SiO_2 catalyst (dispersion = 9 %) for $\theta_0 = 0.36$ and $\beta = 0.2$ K/s.

rate increases, the size of the β_3 peak decreases relative to the β_2 peak until at Q = 200 cc/min (STP) the β_3 peak can barely be resolved as a shoulder on the β_2 peak. This result is completely contradictory to what is predicted by the multisite model as shown in Figure 6.7a, and clearly shows that the β_3 peak is not produced by desorption from a high binding energy adsorption site on the catalyst surface.

Additional evidence against assigning the β_3 peak to a high binding energy adsorption site is obtained from the effect of heating rate on the TPD spectrum. This is shown in Figure 7.4a for θ_0 = 0.36 and Q = 100 cc/min (STP). As discussed in Chapter 6, if the β_3 peak is produced by desorption from a high binding energy adsorption site, then the size of this peak should not change significantly relative to the size of the β_2 peak as the heating rate is varied. However, as shown in Figure 7.4a, the β_3 peak decreases in size relative to the β_2 peak as the heating rate increases. Thus, the β_3 peak cannot be assigned to desorption from a high binding energy adorption site.

The results presented in Figures 7.3a and 7.4a are consistent with the predictions of the subsurface diffusion model shown in Figures 6.7b and 6.8b. This strongly suggests that the β_3 peak is produced by hydrogen which penetrates into the subsurface region during the temperature ramp, and then diffuses back to the surface when it becomes depleted by the desorption process. We should emphasize that the subsurface hydrogen must be restricted to the topmost atomic layers of the palladium crystallites since according to Sieverts' law (55), the amount of hydrogen which can dissolve in the bulk is negligible under our experimental conditions.

The results presented above also suggest that the β_1 and β_2 peaks are produced by hydrogen desorption from two distinct adsorption sites with different binding energies on the catalyst surface. These different sites

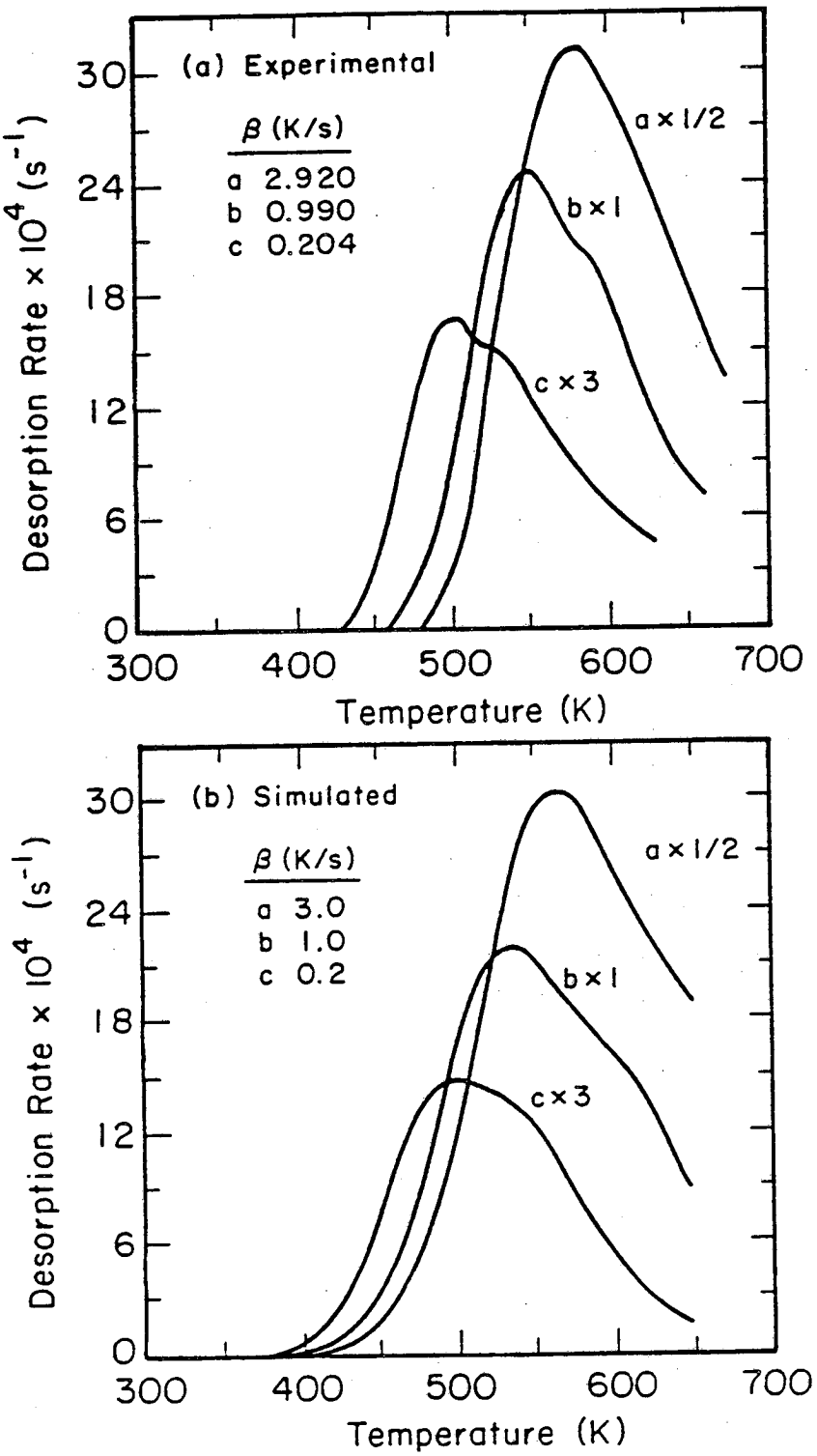

Figure 7.4: Effect of heating rate on the (a) experimental and (b) simulated TPD spectra of hydrogen on the Pd/SiO_2 catalyst (dispersion = 9 %) for $\theta_0 = 0.36$ and Q = 100 cc/min (STP).

probably represent different crystal planes which are exposed by the small metal crystallites. The relative abundance of the β_1 and β_2 sites can be estimated from the initial coverage at which the β_1 peak first appears in the TPD spectrum. Figures 7.5a and b show the TPD spectra of hydrogen and deuterium, respectively, on this catalyst as a function of the initial coverage. In both cases, the β_1 peak is present only for $\theta_0 > 0.75$. Therefore, we estimate that 25 % of the surface is composed of β_1 - type sites, and 75 % is composed of β_2 - type sites. Assignment of the α peak is not clear at this time.

It should be noted that subsurface diffusion is not the only mechanism which could be responsible for the β_3 peak. Another possibility is hydrogen spillover onto the silica support. If dissociatively adsorbed hydrogen were to diffuse onto the support at low temperatures, and subsequently diffuse back to the palladium crystallites at higher temperatures when sites are freed by desorption, this could produce a high temperature peak in the TPD spectrum. However, the spillover hypothesis was rejected for the reasons discussed below.

Following reduction in hydrogen at 473 K, the catalyst was heated in helium to 873 K, and a large hydrogen desorption peak was observed between 750 and 800 K. This peak was accompanied by a water desorption peak, and we attribute both to desorption from the silica support. Removal of this hydrogen peak had no effect on either the hydrogen uptake at 290 K, or the hydrogen TPD spectra. If spillover were responsible for the β_3 peak, then the presence or absence of pre-adsorbed hydrogen on the support should have affected the size of this peak. However, no such effect was observed.

Additional evidence against assigning the β_3 peak to hydrogen spillover can be obtained from a deuterium TPD spectrum. If the catalyst is reduced in deuterium between 473 and 573 K and subsequently heated in helium to

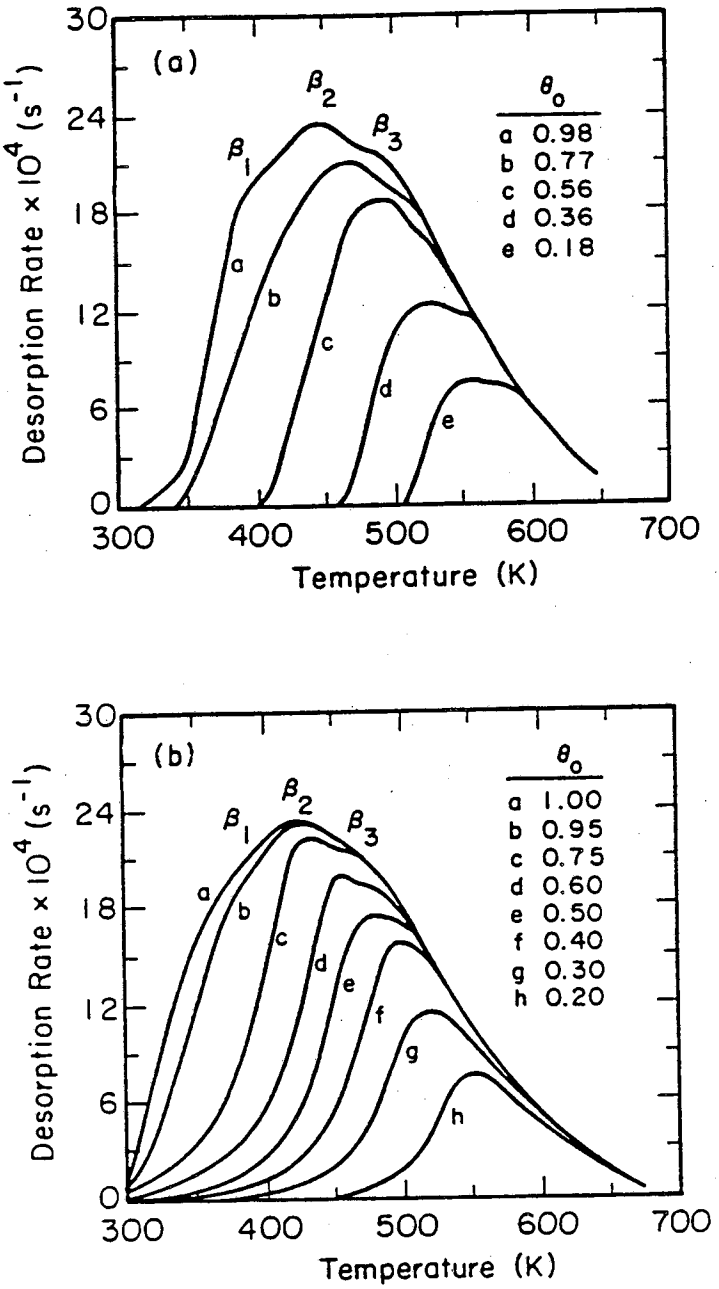

Figure 7.5: Effect of initial coverage on the TPD spectra of (a) hydrogen and (b) deuterium on the Pd/SiO_2 catalyst for β = 0.5 K/s. In the hydrogen spectra, the catalyst dispersion was 9 %, and the helium flow rate was 100 cc/min (STP). In the deuterium spectra, the dispersion was 15 %, and the argon flow rate was 50 cc/min.

873 K, no deuterium desorbs above 700 K. However hydrogen desorbs between 750 and 800 K. This suggests that deuterium spillover does not occur to a significant extent at least up to 573 K. Nevertheless, the β_3 peak is present in the TPD spectrum of deuterium on this catalyst as shown in Figure 7.6. This figure shows the TPD spectrum of deuterium as a function of the argon carrier gas flow rate for $\theta_0 = 1.00$. As was the case for hydrogen, the β_3 peak in the deuterium spectrum decreases in size relative to the other peaks as the flow rate increases, and this is consistent with the subsurface diffusion model. Since the temperature of the β_3 peak is below 573 K, this peak cannot be produced by hydrogen spillover onto the support.

One final possible explanation for the β_3 peak is that it results from lateral interactions between the adsorbate atoms on the surface (induced heterogeneity). If such interactions produce a nonlinear dependence of the desorption activation energy on coverage, they can produce an extra peak in a TPD spectrum (27,28). However, this type of mechanism requires E_d to increase with decreasing coverage. Therefore, the activation energy measured for the β_3 peak would have to be greater than E_d for the β_2 peak for this model to apply. This was not the case as shown below. The flow rate dependence of the TPD spectrum also is inconsistent with this type of model. Therefore, we assign the β_3 peak to hydrogen which penetrates into subsurface absorption sites during heating and then diffuses back to the surface when it becomes depleted by the desorption process. Since desorption in the β_3 peak is limited by diffusion from the subsurface to the surface, we refer to this peak as a diffusion peak.

In Chapter 6, we mentioned that when a diffusion peak appears in a TPD spectrum, it is possible to estimate the activation energy for diffusion from the subsurface to the surface using the heating rate variation method. This

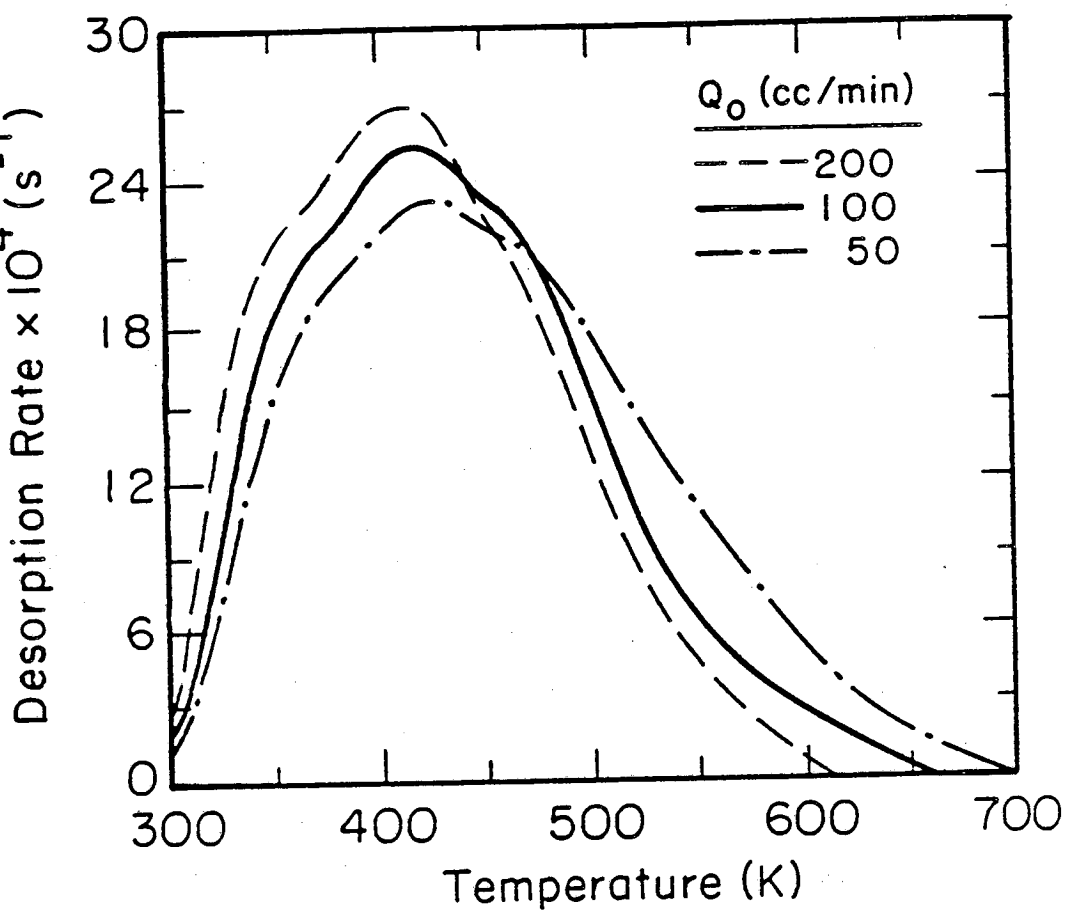

Figure 7.6: Effect of argon flow rate on the TPD spectrum of deuterium on the Pd/SiO_2 catalyst (dispersion = 15%) for θ_0 = 1.00, and β = 0.5 K/s.

method is commonly used to measure heats of adsorption. In the heating rate variation method, the heat of adsorption, ΔH, on each type of site is determined from a plot of ln (β/T_p^2) vs. $(1/T_p)$, where β is the heating rate, and T_p is the peak temperature (see Chapter 6). For each type of site, the plot should give a straight line with a slope = $-\Delta H/R$ where R is the gas constant. If adsorption is not an activated process, then ΔH is equal to the activation energy for desorption, E_d. In the case of a diffusion peak, the slope of the plot is approximately equal to $-E_D/R$, where E_D is the activation energy for diffusion from the subsurface to the surface. As discussed in Chapter 6, this estimate is accurate as long as the range of heating rates investigated is small enough that the relative sizes of the desorption and diffusion peaks do not change significantly.

The heating rate variation experiments were performed using an intitial coverage of $\theta_0 = 0.36$ and a flow rate of 100 cc/min (STP). At this initial coverage the α and β_1 sites are not filled so that errors in determining peak temperatures caused by overlap with these peaks are eliminated. The activation energy for desorption from the β_2 sites was measured using a heating rate range of 0.2 - 3.0 K/s, and was found to be $E_d = 20 \pm 2$ kcal/mole. The $\pm$ 2 kcal/mole uncertainty reflects the $\pm$ 3 K uncertainty in determining the peak temperatures. This uncertainty does not include any possible errors caused by the overlap of this peak with the β_3 peak. The value of E_d is in reasonable agreement with results obtained on single crystals. Conrad, Ertl, and Latta (14) measured activation energies for desorption of hydrogen from Pd(110) and Pd(111) single crystals of 24.4 and 20.8 kcal/mole, respectively. For Pd(100), Behm, et.al. (13) measured $E_d = 24.5$ kcal/mole.

The activation energy for diffusion from the subsurface to the surface was estimated from the shift in the temperature of the β_3 peak with heating rate.

For this measurement, a heating rate range of only 0.2 - 1.0 K/s was used since Figure 7.4a shows that the size of the β_3 relative to the β_2 peak does not change substantially over this heating rate range. Therefore, the activation energy obtained should give a reasonable estimate of E_D. Since the β_3 peak appears as only a shoulder on the β_2 peak, the inflection point immediately to the left (low temperature side) of the shoulder was used as an estimate of the peak temperature. As is shown later, this does not lead to significant errors in estimating E_D. Using this technique, we estimated an activation energy for diffusion of hydrogen from subsurface sites to the surface of $E_D = 15 \pm 3$ kcal/mole. The $\pm$ 3 kcal/mole uncertainty reflects the $\pm$ 4 K uncertainty in determining the temperature of the inflection point. While this number can be regarded only as an estimate of E_D, it is clear that the activation barrier for diffusion of hydrogen from subsurface absorption sites to the surface is much larger than the activation energy for diffusion of hydrogen in bulk palladium which is about 5 - 6 kcal/mole (56).

Thus far, our assignment of the β_3 peak has been based on a qualitative interpretation of the hydrogen and deuterium TPD spectra. To further support this assignment, we now show how the subsurface diffusion model, presented in Chapter 6, semi-quantitatively predicts the changes in the spectrum observed experimentally as the carrier gas flow rate, heating rate, and initial coverage are varied. With the model, we also are able to verify that the activation energy measured for the β_3 peak is an accurate estimate of the activation energy for diffusion from the subsurface to the surface.

SIMULATED RESULTS

Equations 6.11 and 6.13 were solved numerically by a fourth order Runge-Kutta method using the parameter values listed in Table 7.1. These calculations assumed that the temperature increased linearly in time with rate β K/s, and that no hydrogen was present in the subsurface region initially. The model parameters were estimated as follows. As mentioned earlier, 53 mg of catalyst were placed in the reactor, giving a total of 4.0×10^{-6} moles of surface sites in the hydrogen experiments. Of these sites, 25 % were of the β_1-type and 75 % were of the β_2-type. Since the subsurface diffusion model assumes the surface is homogeneous, the model is only valid for initial coverages where just the β_2 sites are filled ($\theta_0 < 0.75$). Therefore in the model, we set $N_S = 3.0 \times 10^{-6}$ moles and converted the initial surface coverage to the coverage of just the β_2 sites by dividing by 0.75. Also, since the net desorption rates, R_d, measured experimentally were based on a total of 4.0×10^{-6} moles of surface sites, the simulated desorption rates had to be multiplied by 75 % to put them on the same basis as the experimental results. The preexponential factor for desorption of hydrogen from palladium, υ_d, was taken as 1.0×10^{13} s^{-1} (26). As mentioned earlier, we measured the activation energy for desorption from the β_2-type sites and found it to be approximately 20 kcal/mole. The actual value used in the model was $E_d = 19.5$ kcal/mole. From the location of the β_2 peak, and the values of υ_d and E_d, the sticking coefficent, S_0, was estimated to be approximately 0.5. This is within the range of values reported for hydrogen on palladium (40). The activation energy for diffusion from the subsurface to the surface was measured to be approximately 15 kcal/mole. The actual value used in the model was 14.5 kcal/mole. Since single crystal studies on Pd(110) (16-19) indicate that only one monolayer of hydrogen can absorb in subsurface

sites, we assumed that M = 1. The preexponential factors for diffusion into (υ_p) and out of (υ_D) the subsurface and the activation energy for penetration into the subsurface (E_p) could not be estimated *a priori*. Therefore, the values of these parameters were chosen to give the best fit of the spectrum shown in Figure 7.3a for θ_0 = 0.36, Q = 100 cc/min (STP), and β = 0.2 K/s. The parameter values listed in Table 7.1 were held fixed while the effects of carrier gas flow rate, heating rate, and initial coverage on the simulated TPD spectrum were investigated. Thus, in the results presented below, there are no adjustable parameters.

TABLE 7.1

Parameter Values Used in the Subsurface Diffusion Model

$N_S = 3 \times 10^{-6}$ moles

$\upsilon_d = 1 \times 10^{13}\ s^{-1}$

E_d = 19.5 kcal/mole

S_0 = 0.5

$\upsilon_p = 1.5 \times 10^{4}\ s^{-1}$

E_p = 16.1 kcal/mole

$\upsilon_D = 1.5 \times 10^{4}\ s^{-1}$

E_D = 14.5 kcal/mole

M = 1

Figure 7.3b shows the effect of carrier gas flow rate on the simulated TPD spectrum for θ_0 = 0.36 and β = 0.2 K/s. Comparison of the simulated spectra in Figure 7.3b with the experimental results in Figure 7.3a shows that the model correctly predicts the changes in the relative heights of the β_3 and β_2 peaks as the flow rate is varied. The only significant difference between the

experimental and simulated results is the better peak resolution in the experimental spectra.

The model also succesfully predicts the effect of heating rate on the TPD spectrum. Figure 7.4b shows the effect of heating rate on the simulated TPD spectrum for $\theta_0 = 0.36$ and Q = 100 cc/min (STP). Comparison of Figures 7.4a and b shows that the model correctly predicts the decrease in size of the β_3 peak relative to the β_2 peak as the heating rate increases. The model also does quite well in predicting the extent to which the peaks shift to higher temperatures as the heating rate increases. This result is especially important since the shift in the peak temperatures with heating rate was used to estimate the activation energies.

If we calculate the desorption activation energy for the β_2 peak from the model results, we obtain a value of 21.5 kcal/mole which is slightly higher than the input value of 19.5 kcal/mole. The reason for the difference is as follows. The location of the β_2 peak is shifted upward in temperature by the overlap with the β_3 peak. As the heating rate increases, the size of the β_3 peak decreases relative to the β_2 peak. As a result, the β_2 peak is not shifted upward in temperature by overlap with the β_3 peak as much at higher heating rates as it is at lower heating rates. This causes the observed shift in temperature of the β_2 peak with heating rate to be smaller than it would have been in the absence of the β_3 peak, which causes the desorption activation energy to be overestimated. We should emphasize, however, that the peaks are resolved much more clearly in the experimental spectra, so that the error in determining E_d should be much smaller.

To verify that the activation energy measured for the β_3 peak corresponds to the activation energy for diffusion from the subsurface to the surface, we calculated E_D from the shift in the temperature of the β_3 peak with

heating rate in the simulated spectra, and compared the value obtained with the value input to the model. As was the case in the experimental spectra, the β_3 peak in the simulated spectra was not clearly resolved so the peak temperature had to be estimated from the inflection point on the low temperature side of the shoulder. For the simulated spectra, this inflection point can be determined exactly. The value of E_D obtained was 15 kcal/mole, which is in excellent agreement with the input value of 14.5 kcal/mole. Thus, the activation energy measured in this manner does correspond to E_D.

As a final test of the subsurface diffusion model, we investigated the effect of initial hydrogen coverage on the experimental and simulated TPD spectra. The results for Q = 100 cc/min (STP) and β = 0.5 K/s are shown in Figures 7.7a (experimental results) and b (simulated results). As seen in these figures, the model also correctly predicts the changes in the spectrum caused by varying the initial coverage. Thus, the predictions of the subsurface diffusion model are consistent with the experimental results.

DISCUSSION

The results presented above clearly show that the β_3 peak in the TPD spectrum of hydrogen on a 9 % Pd/SiO_2 catalyst is not produced by a third adsorption site on the catalyst surface. Instead, the results are consistent with the assignment of the β_3 peak to hydrogen which penetrates into the subsurface region of the palladium crystallites during heating. When the surface becomes depleted by the desorption process, the subsurface hydrogen diffuses back to the surface and desorbs in the high temperature β_3 peak. The assignment of the β_3 peak was made with the aid of a numerical model which correctly predicts the flow rate, heating rate, and initial coverage dependence of

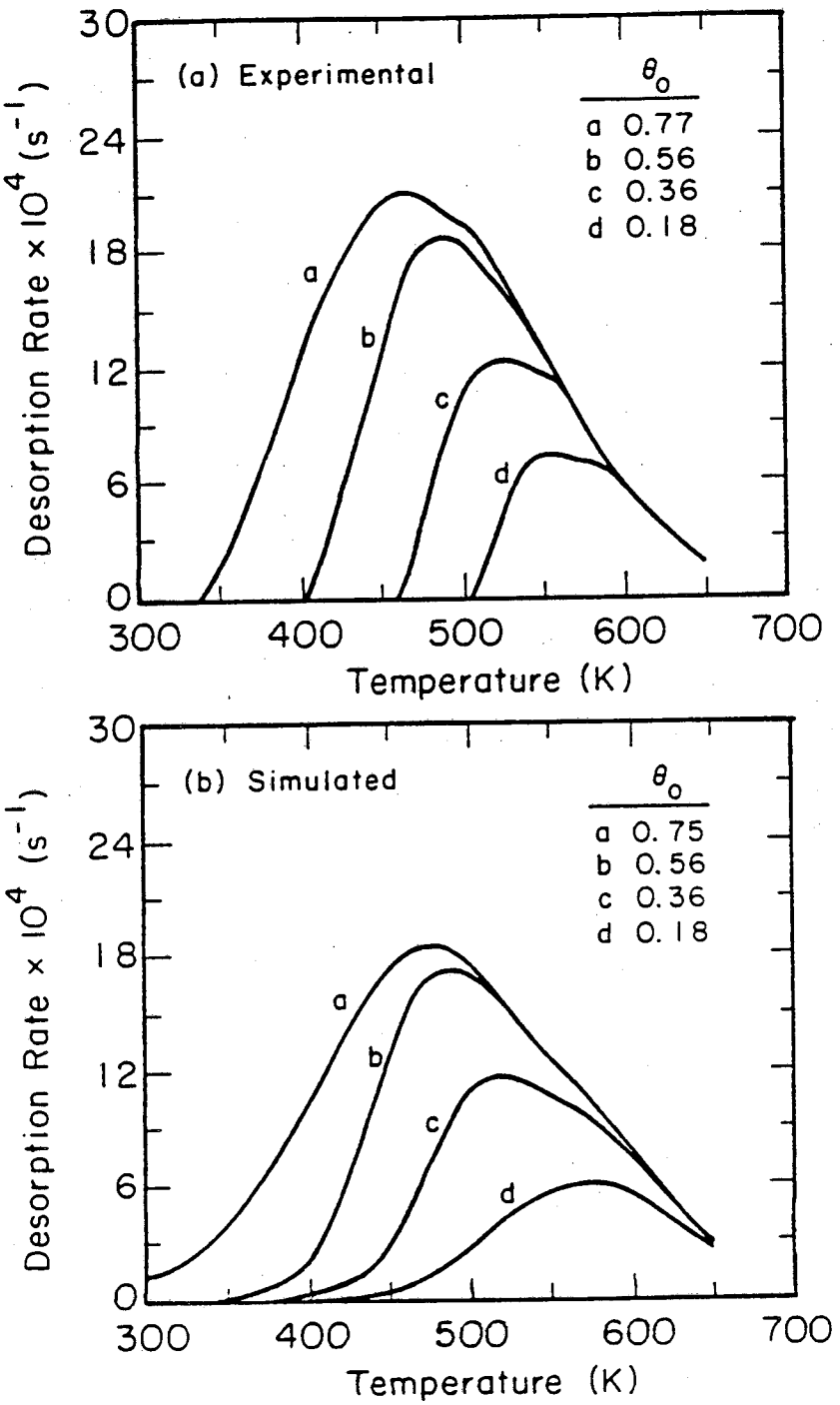

Figure 7.7: Effect of initial coverage on the (a) experimental and (b) simulated TPD spectra of hydrogen on the Pd/SiO_2 catalyst (9 % dispersion) for Q = 100 cc/min (STP) and β = 0.5 K/s.

the TPD spectrum. The only significant difference between the experimental results and the simulated results, was the better resolution between the β_2 and β_3 peaks in the experimental spectra than in the simulated spectra. The reason for this is not clear at this time, but we believe that the better resolution in the experimental spectra may have been caused by a decrease in the sticking coefficient as the subsurface hydrogen concentration increased. A decrease in the sticking coefficient would result in a decrease in the readsorption rate, and therefore an increase in the net rate of desorption. This, in turn, would cause the peaks to become narrower and the resolution to improve. This explanation is consistent with the slightly higher desorption rates observed experimentally.

An important result of this work is that a considerable amount of hydrogen must diffuse into the subsurface region of the palladium crystallites during heating for the β_3 peak to be observed in the TPD spectrum. Since under our experimental conditions, the solubility of hydrogen in bulk palladium is negligible (55), these results provide strong evidence for the presence of subsurface sites for hydrogen absorption in the metal crystallites of the supported palladium catalyst. These results are consistent with the finding of subsurface sites in Pd(110) single crystals (16-19) under ultra-high vacuum conditions. Moreover, since hydrogen diffuses into the subsurface during temperature-programmed desorption, it is likely that it also is present in the palladium subsurface under typical catalytic reaction conditions. This could have important implications in catalysis over this metal.

It is interesting to note that the value of the preexponential factor for hydrogen diffusion from the subsurface back to the surface used in the model is several orders of magnitude lower than the preexponential factor for hydrogen diffusion in bulk palladium. While there is a considerable amount of uncertainty in the value of υ_D since it was obtained merely by fitting one of the experimental

spectra, this extremely low value is difficult to explain. This may suggest that a more detailed microscopic model of hydrogen movement between surface and subsurface sites may be required. The value of the preexponential factor for hydrogen penetration into the subsurface that was used in the model also is extremely low. However, this may only indicate that the value of E_p which is used to fit the spectra is too small.

It is also interesting to note that there are significant differences between the deuterium and hydrogen TPD spectra. Comparison of Figures 7.2 (hydrogen) and 7.6 (deuterium) shows that deuterium desorbs at lower temperatures than hydrogen. This is surprising since the catalyst dispersion, and therefore, the number of sites was higher in the deuterium experiments, which should have shifted the deuterium peaks to higher temperatures. These results suggest that either the sticking coefficient is much lower for deuterium, or that the heat of adsorption is lower for deuterium than for hydrogen. Assuming the sticking coefficients for hydrogen and deuterium are equal, from the locations of the β_1 and β_2 peaks, we estimate a 2 kcal/mole lower heat of adsorption of deuterium on these sites compared to hydrogen. This is consistent with the 1.8 kcal/mole higher dissociation energy for D_2 compared to H_2 (14). Figures 7.2 and 7.6 also show that the β_3 peak is broader in the hydrogen spectra than in the deuterium spectra, and has a more pronounced high temperature tail. This result is consistent with the results reported by Yates, et.al. (46) for desorption of hydrogen isotopes from the Ru(0001) surface, and with the results reported by Greenlief, et.al. (47) for Pt(111). A possible explanation for this is a preferential accomodation of hydrogen in the subsurface absorption sites compared with deuterium (46).

CONCLUSIONS

We have shown that the high temperature β_3 peak in the TPD spectrum of hydrogen on a 9 % Pd/SiO_2 catalyst at atmospheric pressure is not produced by desorption from a high binding energy adsorption site on the catalyst surface. Instead, it is produced by hydrogen which penetrates into subsurface absorption sites in the palladium crystallites during the temperature ramp. When the surface becomes depleted by the desorption process, the subsurface hydrogen diffuses back to the surface and desorbs in the high temperature peak. These results are consistent with the findings of subsurface absorption sites for hydrogen in Pd (110) single crystals under ultra-high vacuum conditions (16 -19).

The activation energy for diffusion of hydrogen from the subsurface to the surface of the palladium crystallites was estimated using the heating rate variation method, a technique commonly used to measure desorption activation energies. The activation energy measured was 15 $\pm$ 3 kcal/mole. This is considerably higher than the activation energy for diffusion of hydrogen in bulk palladium (5 - 6 kcal/mole).

The finding that a significant amount of hydrogen can penetrate into subsurface absorption sites of the palladium crystallites during TPD, strongly suggests that hydrogen also is present in the palladium subsurface under typical catalytic reaction conditions. This could have important implications in catalysis over this metal.

NOMENCLATURE

A	Ratio of the preexponential factor for desorption to the adsorption rate constant (moles/cm^3).
C_G	Gas phase adsorbate concentration (moles/cm^3).
E_d	Activation energy for desorption (kcal/mole).
E_{di}	Activation energy for desorption from site i (kcal/mole).
E_D	Activation energy for diffusion from the subsurface to the surface (kcal/mole).
E_p	Activation energy for penetration of the adsorbate into the subsurface region (kcal/mole).
ΔH	Heat of adsorption (kcal/mole).
k_a	Rate constant for adsorption (cm^3/mole · s).
k_d	Rate constant for desorption (s^{-1}).
k_D	Rate constant for diffusion from the subsurface to the surface (s^{-1}).
k_p	Rate constant for penetration of the adsorbate into the subsurface region (s^{-1}).
m	Molecular weight of the adsorbate.
M	Ratio of the total number of subsurface sites to surface sites ($M = N_B/N_S$).
n	Desorption order.
N_B	Total number of subsurface sites (moles).
N_S	Total number of surface sites (moles).
Q	Temperature-dependent carrier gas flow rate (cm^3/min).
Q_0	Carrier gas flow rate at STP (cm^3/min).
r	Time-dependent ethylene hydrogenation reaction rate (s^{-1}).
r_0	Initial rate of ethylene hydrogenation (s^{-1}).

r_a Readsorption rate (s^{-1}).

r_d Desorption rate (s^{-1}).

r_D Rate of diffusion from the subsurface to the surface (s^{-1}).

r_p Rate of penetration of the adsorbate into the subsurface region (s^{-1}).

R Gas constant.

R_d Net desorption rate ($R_d = r_d - r_a$).

S_0 Sticking coefficient.

t Time (s).

T Temperature (K).

T_p Peak temperature (K).

X_1 Fraction of sites which are type 1.

X_2 Fraction of sites which are type 2.

β Heating rate (K/s).

σ Surface area occupied by one mole of adsorption sites (cm^2/mole).

θ Surface coverage of the adsorbate in the subsurface diffusion model.

θ_o Surface oxygen coverage.

θ_0 Initial surface coverage in the subsurface diffusion model.

θ_1 Fraction of type 1 sites filled in the multisite model.

$\theta_1^{(0)}$ Initial coverage of type 1 sites.

θ_2 Fraction of type 2 sites filled in the multisite model.

$\theta_2^{(0)}$ Initial coverage of type 2 sites.

θ_T Total surface coverage in the multisite model.

$\theta_T^{(0)}$ Initial total surface coverage in the multisite model.

ξ Subsurface coverage of the adsorbate.

υ_d Preexponential factor for desorption (s^{-1}).

υ_{di} Preexponential factor for desorption from site i (s^{-1}).

υ_D Preexponential factor for diffusion from the subsurface to the surface (s^{-1}).

υ_p Preexponential factor for penetration of the adsorbate into the subsurface region (s^{-1}).

REFERENCES

1. Toth, L.E., "Transition Metal Carbides", Academic Press, N.Y. (1971).
2. Muller, J.M. and Gault, F.G., Bull. Soc. Chim. France 2, 416 (1970).
3. Bohm, H., Electrochim. Acta 15, 1273 (1970).
4. Sinfelt, J.H. and Yates, D.J.C., Nature Phys. Sci. 229, 27 (1971).
5. Levy, R.B. and Boudart, M., Science 181, 547 (1973).
6. Leclercq, L., Imura, K., Yoshida, S., Barbee, T., and Boudart, M., in "Preparation of Catalysts II," p. 627 Elsevier, Amsterdam/New York (1979).
7. Boudart, M., Oyama, S.T., and Leclercq, L., in "Proceedings,7'th Intern. Congress on Catalysis, 1980."
8. Kojima, I., Miyazaki, E., Inoue, Y., and Yasumori, I., J. Catal. 73, 128 (1982).
9. Volpe, L., Boudart, M., J. Sol. State Chem. 59, 348 (1985).
10. Storms, E.K., "The Refractory Carbides", Academic Press, N.Y. (1967).
11. Kojima, I., Miyazaki, E., Inoue, Y., and Yasumori, I., J. Catal. 59, 472 (1979).
12. Kojima, I., Miyazaki, E., and Yasumori, I., J. Chem. Soc. Chem. Commun., 573 (1980).
13. Behm, R.J., Christmann, K., and Ertl, G., Surf. Sci. 99, 320 (1980).
14. Conrad, H., Ertl, G., and Latta, E.F., Surf. Sci. 41, 435 (1973).
15. Christmann, K., Ertl, G., and Schober, O., Surf. Sci. 40, 61 (1973).
16. Cattania, M.-G., Penka, V., Behm, R.J., Christmann, K., Ertl, G., Surf. Sci. 126, 382 (1983).
17. Behm, R.J, Penka, V., Cattania, M.-G., Christmann, K., and Ertl, G., J. Chem. Phys. 78 (12), 7486 (1983).
18. Rieder, K.H., Baumberger, M., and Stocker, W., Phys. Rev. Lett. 51, 1799 (1983).

19. Baumberger, M., Stocker, W., and Rieder, K.H., Appl. Phys. A 41, 151 (1986).

20. Cvetanovic, R.J. and Amenomiya, Y., "Application of a Temperature-Programmed Desorption Technique to Catalyst Studies", in Advances in Catalysis, Vol. 17, p. 103, Academic Press, N.Y. (1967).

21. Cvetanovic, R.J. and Amenomiya, Y. , Catal. Rev. 6, 21 (1972).

22. Falconer, J.L., and Schwarz, J.A., Catal. Rev. - Sci. Eng. 25 (2), 141 (1983).

23. Demmin, R.A. and Gorte, R.J., J. Catal. 90, 32 (1984).

24. Tronconi, E. and Forzatti, P., J. Catal. 93, 197 (1985).

25. Gorte, R.J., J. Catal. 75, 164 (1982).

26. Rieck, J.S., and Bell, A.T., J.Catal. 85, 143 (1984).

27. Tokoro, Y., Uchijima, T., and Yoneda, Y., J. Catal. 56, 110 (1979).

28. Yates J.T. Jr., "The Thermal Desorption of Adsorbed Species" in Methods of Experimental Physics, Vol. 22, R.L. Park, Editor, Academic Press (1985).

29. Jones, A. and McNicol, B.D., "Temperature-Programmed Reduction for Solid Materials Characterization", Marcel Dekker, Inc., New York 1986.

30. Keller, S.W., Leary, K.J., Stacy, A.M., and Michaels, J.N., Mat. Lett. in press.

31. Keller, S.W., Leary, K.J., Faltens, T.A., Michaels, J.N., and Stacy, A.M., ACS Symposium Series 351 Ch. 12, in press.

32. Leary, K.J., Zur Loye, H.C., Keller, S.W., Faltens, T.A., Ham, W.K., Michaels, J.N., and Stacy, A.M., Phys. Rev. Lett., in press.

33. Ranhotra, G.S., "Characterization of Molybdenum Carbide Catalysts", M.S. thesis, University of California, Berkeley 1985.

34. Satterfield, C.N., "Heterogeneous Catalysis in Practice", McGraw Hill, New York, 1980.

35. Hicks, R.F., Yen, Q.-J., and Bell, A.T., J.Catal. 89, 498 (1984).

36. Oyama, S.T. and Haller, G.L., in "Catalysis", (G.C. Bond and G. Webb, Eds.), Specialist Periodical Reports, Vol. 5, p. 333, Chem. Soc. London, 1981.

37. Ko, E.I., and Madix, R.J., Surf. Sci. 100, L449 (1980).

38. Niemantsverdriet, J. W., and Van der Kraan, A. M., J. Catal. 72, 385 (1981).

39. Niemantsverdriet, J. W., Van der Kraan, A. M., Van Dijk, W. L., and Van der Baan, H. S., J. Phys. Chem. 84, 3363 (1980).

40. Somorjai, G.A., "Chemistry in Two Dimensions: Surfaces", p. 295, Cornell Univ. Press, Ithaca, N.Y. (1981).

41. Chin, A.A. and Bell, A.T., Phys. Chem. 87, 3482 (1983).

42. Davenport, J.W., Dienes, G.J., and Johnson, R.A., Phys. Rev. B 25 (4), 2165 (1982).

43. Eberhardt, W., Louie, S.G., and Plummer, E.W., Phys. Rev. B 28 (2), 465 (1983).

44. Eberhardt, W., Greuter, F., and Plummer, E.W., Phys. Rev. Lett. 46 (16), 1085 (1981).

45. Greuter, F., Eberhardt, W., DiNardo, J., and Plummer, E.W., J. Vac. Sci. Technol. 18 (2), 433 (1981).

46. Yates, J.T. Jr., Peden, C.H.F., Houston, J.E., and Goodman, D.W., Surf. Sci. 160, 37 (1985).

47. Greenlief, C.M., Akhter, S., and White, J.M, J. Phys. Chem. 90, 4080 (1986).

48. Winkler A., and Rendulic, R.D., Surf. Sci. 118, 19 (1982).

49. Germer, L.H., and MacRae, A.U., J. Chem. Phys. 37 (7), 1382 (1962).

50. Tsuchiya, S., Amenomiya, Y., and Cvetanovic, R.J., J. Catal. 19, 245 (1970).

51. Konvalinka, J.A., and Scholten, J.J.F., J. Catal. 48, 374 (1977).

52. Aldag A.W., and Schmidt, L.D., J. Catal. 22, 260 (1971).

53. Kiskinova, M., Bliznakov, G., and Surnev, L., Surf. Sci. 94, 169 (1980).

54. Konvalinka, J.A., Van Oeffelt, P.H., and Scholten, J.J.F., Appl. Catal. 1, 141 (1981).

55. Wicke, E., Brodowsky, H., and Zuchner, H., "Hydrogen in Palladium and Palladium Alloys" in Hydrogen in Metals, edited by G. Alefeld and J. Volkl (Springer-Verlag, Berlin 1978) Vol. 2, p. 73.

56. Volkl J., and Alefeld, G., "Diffusion of Hydrogen in Metals", in Hydrogen in Metals, edited by G. Alefeld and J. Volkl (Springer-Verlag, Berlin 1978) Vol.1, p. 321.

Appendix A: Computer Program Used to Interface the Mass Spectrometer to the IBM PC

The following is a listing of the computer program which was used to interface the IBM PC to the mass spectrometer using a Metrabyte Model DASH16 interface board. With this program the PC also monitors the gas chromatograph and the temperature of the catalyst bed. The program is written in Basic, and must be compiled before it can be used.

```
1000 '*************************************************************
1010 '
1020 '              CALL NAME:    TPD.BAS
1030 '
1040 '*************************************************************
1050 '
1060 '    This program interfaces the mass spectrometer, the G.C.,
1070 ' and the digital thermometer to the IBM PC. During each
1080 ' scan, the computer reads the temperature from the
1090 ' digital thermometer, the output from the G.C. (if
1100 ' desired), and up to 10 different masses from the mass
1110 ' spectrometer. For each mass, the computer must first set
1120 ' the quadropole voltage for the mass desired, wait for the
1130 ' signal to settle, and then read and signal average the
1140 ' output. Scan rates up to 2 Hz are possible. The maximum
1150 ' number of scans to be done is set by the user, with a
1160 ' maximum of 1000. For temperatures greater than 500 C, the
1170 ' program checks to see if all of the signals have dropped
1180 ' to zero. If the signals for all the masses read zero for
1190 ' 100 scans, the computer automatically stops scanning.
1200 '
1210 '    This program also takes into account the time lag
1220 ' between the reactor and the mass spectrometer, as well as
1230 ' between the reactor and G.C. After the desired number of
1240 ' scans have been completed, the area under the G.C. signal,
1250 ' and the area under the signal vs. time curves for each
1260 ' mass are calculated, and the data are written to data
1270 ' files. The data files consist of 6 byte long records, with
1280 ' the first number in each record a 2 byte integer, and the
1290 ' second, a 4 byte real number; this saves considerable
1300 ' space compared to ASCII data files. For the mass spec and
1310 ' G.C. data files, the raw data is written in the integer
1320 ' section, and the cumulative area under the signal vs time
1330 ' curve is written in the real section. The first record in
1340 ' each file contains the number of data points in the
1350 ' integer section, and the plot mode (0 = dot, 1 = line) in
1360 ' the real section.
1370 '
```

```
1380 '   A control file is also created which consists of 30 byte
1390 ' records divided up into 15 byte sections. The first record
1400 ' contains the date and time of the run. The second contains
1410 ' the number of data files pertaining to that run, and
1420 ' subsequent records list the data files.
1430 '
1440 '************************************************************
1450 '
1460 ' F     define the variable and array sizes
1470 '
1480 ' DIO%(i)     Integer variable which determines which DASH16
1490 '             subroutine is called
1500 ' GC%(i)      GC signal during scan i
1510 ' MASS%(j,i) Mass spectrometer signal for mass j for scan i
1520 ' TEMP%(i)    Temperature during scan i
1530 ' DUMMY%(i)  Dummy variable used in signal averaging
1540 ' QUAD%(i)    Quadrupole setting for mass i
1550 ' AMS(i)      Cumulative area under the mass spec signal for
1560 '             mass i
1570 ' FMS$(i)     Data file name for mass i
1580 ' MMIN%(i)    Minimum value of signal for mass i
1590 ' MMAX%(i)    Maximum value of signal for mass i
1600 '
1610 ' Initialize the dash16.bin routine and set the array sizes
1620 '
1630 CLEAR 60000!  'Set aside 60 kbytes for the program to use
1640 '
1650 DIM DIO%(4), GC%(1001), MASS%(10, 1001),TEMP%(1001)
1660 DIM DUMMY%(201), QUAD%(10), AMS(11), FMS$(11), MMIN%(11)
1670 DIM MMAX%(11)
1680 '
1690 VMS= 5.75     ' volume (cc) between the reactor and mass spec
1700 VGC = 18.25   ' volume (cc) between the reactor and G.C.
1710 '
1720 OPEN "DASH16.ADR" FOR INPUT AS #1
1730 INPUT #1, DIO%(0)
1740 CLOSE #1
1750 DIO%(1) = 2
1760 DIO%(2) = 3
1770 DASH16 = 0
1780 FLAG% = 0
1790 MD% = 0
1800 CALL DASH16 (MD%, DIO%(0), FLAG%)
1810 IF FLAG% <>0 THEN PRINT "installation error":STOP
1830 '
1840 'For documentation of initialization list loadcall.bas
1850 '
1860 '************************************************************
1870 '
1880 'Input the various experimental parameters
1890 '
1900 INPUT "Input the carrier gas flow rate (cc/min) ";FLOW
1910 FLOW = FLOW/60!     'put in cc/s
1920 TMS = VMS/FLOW      'time lag between reactor and mass spec
1930 TGC = VGC/FLOW      'time lag between reactor and G.C.
1940 '
1950 INPUT "How many masses do you want to monitor (0-10) ?  ",M%
1960 FOR J% = 1 TO M%
1970   JK% = J% - 1
1980   PRINT "For mass # ",JK%
1990   INPUT "input the mass to be read ?    ", SET
2000   IF SET < 0 OR SET > 150 THEN PRINT "Out of Range":GOTO 1980
```

```
2010   IF SET < 35 THEN SET = SET - .1   'Determined empirically
2020   IF SET < 10 THEN VOLTS = (SET/30) - (.0009 * SET)
2030   IF SET >= 10 THEN VOLTS = (.033 * SET) - 8.333001E-03
2040   SET = VOLTS * 819!    '819 bits/volt in the D/A
2050   QUAD%(JK%) = SET      'D/A setting for mass jk%
2060 NEXT J%
2070 '
2080 INPUT "Do you want to monitor the G.C. output (y/n) ";A$
2090 IF A$ = "" THEN A$ = "n"
2100 IF A$ = "y" THEN GOTO 2130
2110 IF A$ = "n" THEN GOTO 2180
2120 PRINT "This is not a correct response":GOTO 2080
2130 INPUT "T.C. detector (1) or F.I.D. (2) ";DET%
2140 IF DET% < 0 OR DET% > 2 THEN PRINT "1 or 2 only ":GOTO 2130
2150 IF DET% = 1 THEN CHAN% = 1   'T.C. detector is on channel 1
2160 IF DET% = 2 THEN CHAN% = 3   'F.I.D. is on channel 3
2170 '
2180 INPUT "How many scans (1-1000)?", SCAN%
2190 INPUT "input the scan rate in Hz up to 2 Hz ?  ", RATE
2200 IF RATE > 2 THEN PRINT "too high": GOTO 2190
2210 GCLAG% = TGC * RATE
2220 MSLAG% = TMS * RATE
2230 CLS: LOCATE 12, 30: PRINT "TAKING DATA"
2240 '
2250 '************************************************************
2260 '
2270 'Set the programmable timer interval for the desired frequency
2280 MD% = 17
2290 DIO%(0) = 1000
2300 DIO%(1) = 1000/RATE
2310 CALL DASH16 (MD%, DIO%(0), FLAG%)
2320 IF FLAG% <> 0 THEN PRINT "error in setting timer":STOP
2330 '
2340 '************************************************************
2350 '
2360 TST% = 0
2370 P% = M%
2380 '
2390 'Set up the scan loop
2400 '
2410 IF A$ = "n" THEN FIN% = SCAN% + MSLAG%
2420 IF A$ = "y" THEN FIN% = SCAN% + GCLAG%
2430 FOR J% = 1 TO FIN%
2440   I% = J% - 1
2450 '
2460 '************************************************************
2470 '
2480 'Because IP0/TRIG0 is connected to CTR 0 OUT, it is held low
2490 'and this prevents A/D conversions that are triggered by the
2500 'programmable interval timer. Therefore, IP0/TRIG0 must be
2510 'made high using configuration 0 (pulse on terminal count)
2520 'of counter 0 which will leave IP0/TRIG0 high after it
2530 'decrements through zero.
2540 '
2550  LET BASADR% = &H300
2560  OUT BASADR%+10, 2       'enable 100 kHz clock to counter 0
2570  MD% = 10
2580  DIO%(0) = 0
2590  CALL DASH16 (MD%, DIO%(0), FLAG%)
2600  IF FLAG% <> 0 THEN PRINT "error setting config. 0":STOP
2610  MD% = 11
2620  DIO%(0) = 2             'divisor = 2 to give a 50 kHz pulse
```

```
2630  CALL DASH16 (MD%, DIO%(0), FLAG%)
2640  IF FLAG% <> 0 THEN PRINT "error setting 50 kHz on 0":STOP
2650  '
2660  '************************************************************
2670  '
2680  'Read the temperature from channel 0 whenever the A/D is
2690  'triggered by the programmable interval timer
2700  '
2710   MD% = 1                    'Set up the dash16 to scan channel 0
2720   DIO%(0) = 0
2730   DIO%(1) = 0
2740   CALL DASH16 (MD%, DIO%(0), FLAG%)
2750   IF FLAG% <> 0 THEN PRINT "error in setting channel 0":STOP
2760   MD% = 4           'Read channel 0 and assign value to dummy%
2770   DIO%(0) = 2
2780   DIO%(2) = 1       'triggered by programmable interval timer
2790   DIO%(1) = VARPTR (DUMMY%(0))
2800   CALL DASH16 (MD%, DIO%(0), FLAG%)
2810   IF FLAG% <> 0 THEN PRINT "error in reading channel 0":STOP
2820  '
2830  '************************************************************
2840  '
2850  'Setup counter 0 for 20 kHz
2860  '
2870   MD% = 10           'set timer counter configuration
2880   DIO%(0) = 2        'choose the rate generator configuration
2890   CALL DASH16 (MD%, DIO%(0), FLAG%)
2900   IF FLAG% <> 0 THEN PRINT "error setting ctr0 config.":STOP
2910   MD% =11
2920   DIO%(0) = 5       'divisor = 5 to give a 20000 Hz pulse rate
2930   CALL DASH16 (MD%, DIO%(0), FLAG%)
2940   IF FLAG% <> 0 THEN PRINT "error in loading counter 0":STOP
2950  '
2960  '************************************************************
2970  '
2980  'Now read the temperature 50 times and signal average it
2990  '
3000   IF J% > SCAN% THEN GOTO 3300
3010   MD% = 4
3020   DIO%(0) = 51
3030   DIO%(1) = VARPTR(DUMMY%(0))
3040   DIO%(2) = 0
3050   CALL DASH16 (MD%, DIO%(0), FLAG%)
3060   IF FLAG% <> 0 THEN PRINT "Error in reading channel 0":STOP
3070  '
3080  'Signal average the temperature using integers for speed
3090  '
3100   AVG% = 0
3110   DMM% = 0
3120   DMU% = 0
3130   FOR S% = 1 TO 5
3140     FOR R% = 1 TO 10
3150        DMU% = DMU% + 1
3160        DMM% = DMM% + DUMMY%(DMU%)
3170     NEXT R%
3180     DMM% = DMM%/10
3190     AVG% = AVG% + DMM%
3200     DMM% = 0
3210   NEXT S%
3220   AVG% = AVG%/5
3230   TEMP%(I%) = AVG% * .4885 + 273      '.4885 millivolts/bit
3240   IF I% = 0 THEN TMIN% = TEMP%(0): TMAX% = TEMP%(0):GOTO 3300
3250   IF TEMP%(I%) < TMIN% THEN TMIN% = TEMP%(I%)
```

```
3260  IF TEMP%(I%) > TMAX% THEN TMAX% = TEMP%(I%)
3270  '
3280  '************************************************************
3290  '
3300  IF A$ = "n" THEN GOTO 3740
3310  '
3320  'Now read channel 1 for the T.C. detector, or channel 3 for
3330  'the F.I.D.
3340  '
3350  IF I% = 0 THEN IG% = 0: GOTO 3390
3360  IG% = I% - GCLAG%
3370  IF IG% < 1 THEN GOTO 3740
3380  IF IG% >= SCAN% THEN GOTO 3740
3390  MD% = 1
3400  DIO%(0) = CHAN%
3410  DIO%(1) = CHAN%
3420  CALL DASH16 (MD%, DIO%(0), FLAG%)
3430  IF FLAG% <>0 THEN PRINT "Error in setting channel 1":STOP
3440  MD% = 4
3450  DIO%(0) = 201
3460  DIO%(2) = 0                          'triggered by counter 0
3470  DIO%(1) = VARPTR(DUMMY%(0))
3480  CALL DASH16 (MD%, DIO%(0), FLAG%)
3490  IF FLAG% <>0 THEN PRINT "Error in reading channel 1":STOP
3500  '
3510  'Now signal average the G.C. signal
3520  '
3530  AVG% = 0
3540  DMM% = 0
3550  DMU% = 0
3560  FOR S% = 1 TO 20
3570    FOR R% = 1 TO 10
3580       DMU% = DMU% + 1
3590       DMM% = DMM% + DUMMY%(DMU%)
3600    NEXT R%
3610    DMM% = DMM%/10
3620    AVG% = AVG% + DMM%
3630    DMM% = 0
3640  NEXT S%
3650  AVG% = AVG%/20
3660  GC%(IG%) = AVG%
3670  IF IG% = 0 THEN GMIN%=GC%(IG%): GMAX%=GC%(IG%): GOTO 3740
3680  IF GC%(IG%) < GMIN% THEN GMIN% = GC%(IG%)
3690  IF GC%(IG%) > GMAX% THEN GMAX% = GC%(IG%)
3700  '
3710  '************************************************************
3720  '
3730  'Read each mass from the mass spec which is channel 4
3740  '
3750  IF I% = 0 THEN IM% = 0 : GOTO 3790
3760  IM% = I% - MSLAG%
3770  IF IM% < 1 THEN GOTO 4290
3780  IF IM% >= SCAN% THEN GOTO 4290
3790  FOR K% = 1 TO M%
3800    L%= K% - 1
3810    MD% = 15
3820    DIO%(0) = 0          'Channel 0 is connected to quadropole
3830    DIO%(1) = QUAD%(L%)
3840    CALL DASH16 (MD%, DIO%(0), FLAG%)
3850    IF FLAG% <> 0 THEN PRINT "error in setting D/A":STOP
3860    MD% = 1
3870   DIO%(0) = 4
3880   DIO%(1) = 4
```

```
3890   CALL DASH16 (MD%, DIO%(0), FLAG%)
3900   IF FLAG% <> 0 THEN PRINT "error in setting channel 2":STOP
3910   MD% = 4
3920   DIO%(0) = 201
3930   DIO%(1) = VARPTR(DUMMY%(0))
3940   DIO%(2) = 0                          'triggered by counter 0
3950   CALL DASH16 (MD%, DIO%(0), FLAG%)
3960   IF FLAG% <> 0 THEN PRINT "error in reading channel 4":STOP
3970 '
3980 'Signal avg the mass spec after waiting for quadropole to settle
3990 '
4000   AVG% = 0
4010   DMM% = 0
4020   DMU% = 120
4030   FOR S% = 1 TO 8
4040     FOR R% = 1 TO 10
4050       DMU% = DMU% + 1
4060       DMM% = DMM% + DUMMY%(DMU%)
4070     NEXT R%
4080     DMM% = DMM%/10
4090     AVG% = AVG% + DMM%
4100     DMM% = 0
4110   NEXT S%
4120  AVG% = AVG%/8
4130  MASS%(L%,IM%) = AVG%
4140  IF IM% = 0 THEN MMIN%(L%) = 0: MMAX%(L%) = 0: GOTO 4220
4150 'Subtract off the background and eliminate the noise
4160  MASS%(L%,IM%) = MASS%(L%,IM%) - MASS%(L%,0)
4170  IF ABS(MASS%(L%,IM%)) <= 2 THEN MASS%(L%,IM%) = 0
4180  IF MASS%(L%,IM%) < MMIN%(L%) THEN MMIN%(L%) = MASS%(L%,IM%)
4190  IF MASS%(L%,IM%) > MMAX%(L%) THEN MMAX%(L%) = MASS%(L%,IM%)
4200  IF TEMP%(IM%) < 773 THEN GOTO 4220
4210  IF MASS%(L%,IM%) = 0 THEN P% = P% - 1
4220 NEXT K%
4230 IF M% = 0 THEN GOTO 4280
4240 IF P% = 0 THEN TST% = TST% + 1 ELSE GOTO 4280
4250 IF TST% < 100 THEN GOTO 4280
4260 J% = FIN%
4270 SCAN% = IM% + 1
4280 P% = M%
4290 NEXT J%
4300 CLS
4310 '
4320 '*****************************************************************
4330 '
4340 'Now write the temperature vs. time data to a data file
4350 '
4360 INPUT "input the temp. data file name (drv:name.ext) ";FIL$
4370 LIMIT% = SCAN% - 1
4380 NUM = 1!
4390 OPEN FIL$ AS #1 LEN = 6          'record length = 6 bytes
4400 FIELD #1, 2 AS X$, 4 AS Y$      '2 bytes for temp, 4 for time
4410 LSET X$ = MKI$(LIMIT%): LSET Y$ = MKS$(NUM)
4420 PUT #1,1
4430 FOR J% = 1 TO LIMIT%
4440   H% = J% + 1
4450   TIME = J%/RATE
4460   LSET X$ = MKI$(TEMP%(J%)): LSET Y$ = MKS$(TIME)
4470   PUT #1, H%
4480 NEXT J%
4490 CLOSE #1
4500 '
```

```
4510 '************************************************************
4520 '
4530 'Now calculate the areas under the signal-time curves for
4540 'the G.C. and the mass spec. Then write the data to data
4550 'files on the disk
4560 'The areas are calculated using the trapezoidal rule
4570 '
4580 IF A$ = "n" THEN GOTO 4820
4590 INPUT "G.C. data file name (drive:name.ext)  ";FGC$
4600 OPEN FGC$ AS #1 LEN = 6          'record length is 6 bytes
4610 FIELD #1, 2 AS X$, 4 AS Y$   '2 bytes for signal, 4 for area
4620 NUM = 1
4630 LIMIT% = SCAN% - 1
4640 LSET X$ = MKI$(LIMIT%): LSET Y$ = MKS$(NUM)
4650 PUT #1,1
4660 AGC = GC%(1)/(2! * RATE)
4670 LSET X$ = MKI$(GC%(1)): LSET Y$ = MKS$(AGC)
4680 PUT #1,2
4690 FOR J% = 2 TO LIMIT%
4700   I% = J% - 1
4710   L% = J% + 1
4720   AGC = AGC + ((GC%(J%) + GC%(I%))/2!)/RATE
4730   LSET X$ = MKI$(GC%(J%)): LSET Y$ = MKS$(AGC)
4740   PUT #1, L%
4750 NEXT J%
4760 CLOSE #1
4770 '
4780 '************************************************************
4790 '
4800 'For each mass, calculate the area and write the data to the
4810 'disk
4820 FOR K% = 1 TO M%
4830   L% = K% - 1
4840   PRINT "Input data file name for mass# ";L%;:INPUT;FMS$(K%)
4850   OPEN FMS$(K%) AS #1 LEN = 6
4860   FIELD #1, 2 AS X$,  4 AS Y$
4870   NUM = 1
4880   LIMIT% = SCAN% - 1
4890   LSET X$ = MKI$(LIMIT%):LSET Y$ = MKS$(NUM)
4900   PUT #1,1
4910   AMASS = MASS%(L%,1)/(2! * RATE)
4920   LSET X$ = MKI$(MASS%(L%,1)): LSET Y$ = MKS$(AMASS)
4930   PUT #1, 2
4940   FOR J% = 2 TO LIMIT%
4950     I% = J% - 1
4960     H% = J% + 1
4970     AMASS = AMASS + ((MASS%(L%,J%) + MASS%(L%,I%))/2!)/RATE
4980     LSET X$ = MKI$(MASS%(L%,J%)): LSET Y$ = MKS$(AMASS)
4990     PUT #1, H%
5000   NEXT J%
5010   CLOSE #1
5020   AMS(L%) = AMASS
5030 NEXT K%
5040 '
5050 '************************************************************
5060 '
5070 'Now input the name of the control file which is a file that
5080 'contains the date and time that the run was done in record
5090 '#1, and the number of data files generated by that run in
5100 'record # 2. The names of the data files from that run are
5110 'given in subsequent records
5120 '
5130 PRINT "input the name of the control file ":INPUT; FIL$
```

```
5140 OPEN FIL$ AS #1 LEN = 30
5150 FIELD #1, 15 AS S1$, 15 AS S2$
5160 LSET S1$ = DATE$: LSET S2$ = TIME$
5170 PUT #1, 1
5180 IF A$ = "n" THEN LL% = 3: LIM% = M% + 2
5190 IF A$ = "y" THEN LL% = 4: LIM% = M% + 3
5200 DUM$ = "No. of files"
5210 NOF% = LIM% - 2
5220 IF NOF% = 1 THEN NOF$ = "one": GOTO 5330
5230 IF NOF% = 2 THEN NOF$ = "two": GOTO 5330
5240 IF NOF% = 3 THEN NOF$ = "three": GOTO 5330
5250 IF NOF% = 4 THEN NOF$ = "four": GOTO 5330
5260 IF NOF% = 5 THEN NOF$ = "five": GOTO 5330
5270 IF NOF% = 6 THEN NOF$ = "six": GOTO 5330
5280 IF NOF% = 7 THEN NOF$ = "seven": GOTO 5330
5290 IF NOF% = 8 THEN NOF$ = "eight": GOTO 5330
5300 IF NOF% = 9 THEN NOF$ = "nine": GOTO 5330
5310 IF NOF% = 10 THEN NOF$ = "ten": GOTO 5330
5320 IF NOF% = 11 THEN NOF$ = "eleven": GOTO 5330
5330 LSET S1$ = DUM$: LSET S2$ = NOF$
5340 PUT #1, 2
5350 IF A$ = "n" THEN GOTO 5390
5360 DUM$ = "G.C. data file"
5370 LSET S1$ = DUM$: LSET S2$ = FGC$
5380 PUT #1, 3
5390 KK% = 0
5400 DUM$ = "M.S. data file"
5410 FOR I% = LL% TO LIM%
5420    KK% = KK% + 1
5430    LSET S1$ = DUM$: LSET S2$ = FMS$(KK%)
5440    PUT #1, I%
5450 NEXT I%
5460 CLOSE #1
5470 '
5480 '************************************************************
5490 '
5500 CLS: PRINT "Tmin = "TMIN%" and Tmax = "TMAX%" K "
5510 PRINT "G.C. area = "AGC", gcmin = "GMIN%", gmax = "GMAX%
5520 FOR I% = 1 TO M%
5530    L% = I% - 1
5540 PRINT " Area for MASS#"L%"="AMS(L%)",max="MMAX%(L%)"min="MMIN%(L%)
5550 NEXT I%
5560 END
```

Appendix B: Computer Program for Integrating Equations 5.5 to 5.8

Equations 5.5 to 5.8 were solved numerically using a fourth order Runge-Kutta method. A listing of the Fortran computer program used to perform the integration is shown below. This program is called "O2TPR". The various input parameters are read from a data file which is created by a second program called "O2INP", which is listed directly below the listing of O2TPR.

```
C*****************************************************************
C
C                      PROGRAM NAME: O2TPR
C
C*****************************************************************
C
C This program calculates the TPR spectra of oxygen from the Mo2C
C catalyst, assuming the high temperature peak is produced by
C subsurface diffusion.  It is assumed that the reactor is well-
C mixed and that intraparticle diffusion limitations are
C negligible.
C
C*****************************************************************
C
C DEFINE ALL THE VARIABLES
C
C     Bi      Runge-Kutta parameters
C     BETA    Heating rate (K/s)
C     CTR     Counter
C     CTR2    Counter
C     DELTA   Number of iterations per degree K
C     DES     Desorption rate (1/s)
C     DIF     Rate of diffusion from the subsurface to the surface
C     ED      Desorption activation energy
C     EDF     Activation energy for diffusion from the subsurface
C             to the surface
C     EP      Activation energy for penetration into the subsurface
C     ETA     Fraction of subsurface sites filled
C     H       Step size (1/s)
C     INOF    Number of input files
C     KD      Rate constant for desorption
C     KDF     Rate constant for diffusion from the subsurface to
C             the surface
C     KP      Rate constant for penetration into the subsurface
C     M       Number of subsurface layers
C     NB      Number of subsurface sites for oxygen absorption
C     NOR     Number of records in the output file
C     NS      Number of surface sites for oxygen adsorption
```

```
C     OFILE  Output file name
C     PEN    Rate of penetration into the subsurface (1/s)
C     RD     Desorption rate (1/s)
C     T      Temperature (K)
C     T0     Initial temperature (K)
C     THETA  Fraction of surface sites filled
C     TMAX   Final ramp temperature (K)
C     VD     Desorption preexponential factor (1/s)
C     VDF    Preexponential factor for diffusion from the
C            subsurface to the surface (1/s)
C     VP     Preexponential factor for penetration into the
C            subsurface
C     ZFILE  Input file name
C
      IMPLICIT REAL*8 (A-Z)
      IMPLICIT INTEGER*2 (ILP, INOF, IJ, I, J, DELTA, CTR, CTR2)
      CHARACTER*10 OFILE
      CHARACTER ZFILE(50)*10
      COMMON /RDATA/ VD, VP, VDF, ED, EP, EDF
      COMMON /CONST/ M, NS, NB
C*****************************************************************
C
C   Read in the parameter values from input data files created by
C   the program O2INP
C
      WRITE (*,5)
 5    FORMAT (' INPUT THE NUMBER OF INPUT FILES?   ')
      READ (*,10) INOF
 10   FORMAT (I2)
 20   DO 30 I=1,INOF
           WRITE (*,25) I
 25        FORMAT (' INPUT THE NAME OF INPUT FILE #',I2,' ?   ')
           READ (*,27) ZFILE(I)
 27        FORMAT (A10)
 30   CONTINUE
 35   DO 40 ILP=1,INOF
           OPEN (3,FILE=ZFILE(ILP),STATUS='OLD')
           READ (3,45) VD, ED, EP, VP, EDF
 45        FORMAT (1X,F13.6,1X,F4.1,1X,F4.1,1X,F13.6,1X,F4.1)
           READ (3,50) VDF, M, BETA, TMAX
 50        FORMAT (1X,F13.6,1X,F5.2,1X,F5.2,1X,F5.1)
           READ (3,55) H, THETA, ETA, OFILE
 55        FORMAT (1X,F5.3,1X,F6.4,1X,F7.5,1X,A10)
           CLOSE (3)
C*****************************************************************
C
C   SET THE VALUES OF ALL THE PARAMETERS
C
      T0 = 3.0D2
      T = T0
      NS = 4.0D-6
      NB = NS
      VD = VD * 1.0D6
      ED = ED * 1.0D3
      VP = VP * 1.0D6
      VDF = VDF * 1.0D6
      EP = EP * 1.0D3
      EDF = EDF * 1.0D3
      NOR = TMAX - T0 + 1
      DELTA = 1.0/(BETA * H)
      CTR = 0.0
      CTR2 = 0.0
      RD = 0.0D0
```

```
      KD = RD
      KP = KD
      KDF = KP
      B1 = KP
      B2 = B1
      B3 = B2
      B4 = B3
      L1 = B4
      L2 = L1
      L3 = L2
      L4 = L3
C*****************************************************************
C
C   OUTPUT ALL THE PARAMETER VALUES AND SET UP THE OUTPUT TABLE
C
      WRITE (*,80)
      WRITE (*,80)
      WRITE (*,80)
 80   FORMAT (' ')
      WRITE (*,316) BETA
 316  FORMAT (' BETA = ', F4.1, ' K/S')
      WRITE (*,317) TMAX
 317  FORMAT (' TMAX = ', F5.1, ' K')
      NNS = NS * 1.0D6
      NNB = NB * 1.0D6
      WRITE (*,321) NNS
 321  FORMAT (' NS = ', F5.2, ' uMOLES')
      WRITE (*,326) NNB
 326  FORMAT (' NB = ', F5.2, ' uMOLES/LAYER')
      WRITE (*,333) VD
 333  FORMAT (' VD = ', E10.3)
      WRITE (*,336) ED
 336  FORMAT (' ED = ', F6.0,' CAL/MOLE')
      WRITE (*,339) M
 339  FORMAT (' M = ', F5.2)
      WRITE (*,341) VP
 341  FORMAT (' VP = ', E10.3)
      WRITE (*,346) EP
 346  FORMAT (' EP = ', F6.0,' CAL/MOLE')
      WRITE (*,351) VDF
 351  FORMAT (' VDF = ', E10.3)
      WRITE (*,356) EDF
 356  FORMAT (' EDIFF = ', F6.0, 'CAL/MOLE')
      WRITE (*,361) H
 361  FORMAT (' STEP SIZE = ', F5.3, ' S')
      WRITE (*,80)
      WRITE (*,80)
      WRITE (*,371) OFILE
 371  FORMAT (' THE DATA FILE NAME IS ', A10)
      WRITE (*,80)
      WRITE (*,80)
      WRITE (*,80)
      WRITE (*,85)
 85   FORMAT ('  T(K)       Rd (1/S)       THETA       ETA')
      WRITE (*,80)
      WRITE (*,90) T, RD, THETA, ETA
 90   FORMAT (1X,F5.1,5X,E10.4,5X,F6.4,5X,E10.4)
C
C  Write the data to the output data file
C
      OPEN (4,FILE=OFILE)
      WRITE (4,92) NOR
```

```
 92   FORMAT (F5.0)
      WRITE (4,94) T, RD, THETA, ETA
 94   FORMAT (1X, F5.1, 5X, F9.7, 5X, F9.7, 5X, F9.7)
C*****************************************************************
C
C   DO THE NUMERICAL INTEGRATION BY 4'TH ORDER RUNGE-KUTTA
C
 96   DO 725 IJ = 1,1000
 100  DO 200 J=1,1000
           TP = T
           XN = THETA
           YN = ETA
           CALL RC (TP, KD, KP, KDF)
           CALL KNI (KD, KP, KDF, XN, YN, B1)
           CALL LNI (KP. KDF, XN, YN, L1)
           TP = T + BETA * H/2.0
           XN = THETA + H*B1/2.0
           YN = ETA + H*L1/2.0
           CALL RC (TP, KD, KP, KDF)
           CALL KNI (KD, KP, KDF, XN, YN, B2)
           CALL LNI (KP, KDF, XN, YN, L2)
           XN = THETA + H*B2/2.0
           YN = ETA + H*L2/2.0
           CALL KNI (KD, KP, KDF, XN, YN, B3)
           CALL LNI (KP, KDF, XN, YN, L3)
           TP = T + BETA * H
           XN = THETA + H*B3
           YN = ETA + H*L3
           CALL RC (TP, KD, KP, KDF)
           CALL KNI (KD, KP, KDF, XN, YN, B4)
           CALL LNI (KP, KDF, XN, YN, L4)
           T = TP
           THETA = THETA + (H/6.0)*(B1 + 2.0*(B2 + B3) + B4)
           ETA = ETA + (H/6.0)*(L1 + 2.0*(L2 + L3) + L4)
           IF (THETA .GT. 1.0) GOTO 726
           IF (ETA .GT. 1.0) GOTO 726
           RD = KD*THETA
           CTR = CTR + 1
           IF (CTR .LT. DELTA) GOTO 150
           CTR = 0
           RDF = RD
           THETAF = THETA
           ETAF = ETA
           IF (RDF .LT. 0.0000001) RDF = 0.0
           IF (THETAF .LT. 0.0000001) THETAF = 0.0
           IF (ETAF .LT. 0.0000001) ETAF = 0.0
C
C  Write the output to the output file every 1 K
C
           WRITE (4,94) T, RDF, THETAF, ETAF
           CTR2 = CTR2 + 1
           IF (CTR2 .LT. 5) GOTO 150
           CTR2 = 0
C
C  Write the output to the screen every 5 K
C
           WRITE (*,90) T, RD, THETA, ETA
 150       IF (T .GE. TMAX) GOTO 726
 200  CONTINUE
 725  CONTINUE
 726  CLOSE (4)
 40   CONTINUE
```

```
      STOP
      END
C*****************************************************************
C
C    SUBROUTINE FOR CALCULATING THE RATE CONSTANTS
C
      SUBROUTINE RC (TP, KD, KP, KDF)
      IMPLICIT REAL*8 (A-Z)
      COMMON /RDATA/ VD, VP, VDF, ED, EP, EDF
      KD = VD * DEXP(ED/(-2.0D0*TP))
      KP = VP * DEXP(EP/(-2.0D0*TP))
      KDF = VDF * DEXP(EDF/(-2.0D0*TP))
      RETURN
      END
C*****************************************************************
C
C    SUBROUTINE TO CALCULATE THE Kni = Bi
C
      SUBROUTINE KNI (KD, KP, KDF, XN, YN, B)
      IMPLICIT REAL*8 (A-Z)
      COMMON /CONST/ M, NS, NB
      DES = KD * XN
      PEN = KP * XN * (1.0D0 - YN)
      DIF = KDF * (1.0D0 - XN) * YN
      B = DIF - DES - PEN
      RETURN
      END
C*****************************************************************
C
C    SUBROUTINE TO CALCULATE Lni
C
      SUBROUTINE LNI (KP, KDF, XN, YN, L)
      IMPLICIT REAL*8 (A-Z)
      COMMON /CONST/ M, NS, NB
      PEN = KP * XN * (1.0 - YN)
      DIF = KDF * (1.0 - XN) * YN
      L = (NS/(M*NB)) * (PEN - DIF)
      RETURN
      END
C*****************************************************************
```

```
C*****************************************************************
C
C                      PROGRAM NAME: O2INP
C
C*****************************************************************
C
C This program creates the input data files to be used by the
C program O2TPR
C
C*****************************************************************
C
      IMPLICIT REAL*8 (A-Z)
      IMPLICIT INTEGER*2 (J)
      CHARACTER*10 ZFILE, OFILE
C
      WRITE (*,2)
 2    FORMAT (' INPUT THE NAME OF THIS FILE?   ')
      READ (*,3) ZFILE
 3    FORMAT (A10)
      WRITE (*,4)
C
C  The desorption preexponential factor, and the diffusion
C  preexponential factors are multiplied by 1 X 10^6
C  in the program O2TPR
C
 4    FORMAT (' INPUT VD/1000000 ?   ')
      READ (*,5) VD
 5    FORMAT (F13.6)
      WRITE (*,8)
 8    FORMAT (' INPUT ED (KCAL/MOLE)?   ')
      READ (*,9) ED
 9    FORMAT (F4.1)
      WRITE (*,10)
 10   FORMAT (' INPUT EP (KCAL/MOLE)?   ')
      READ (*,11) EP
 11   FORMAT (F4.1)
      WRITE (*,12)
 12   FORMAT (' INPUT VP/1000000 ?   ')
      READ (*,13) VP
 13   FORMAT (F13.6)
      WRITE (*,20)
 20   FORMAT (' INPUT EDIFF (KCAL/MOLE)?   ')
      READ (*,21) EDF
 21   FORMAT (F4.1)
      WRITE (*,22)
 22   FORMAT (' INPUT VDF/1000000 ?   ')
      READ (*,23) VDF
 23   FORMAT (F13.6)
      WRITE (*,27)
 27   FORMAT (' INPUT THE NUMBER OF LAYERS (M)?   ')
      READ (*,29) M
 29   FORMAT (F5.2)
      WRITE (*,40)
 40   FORMAT (' INPUT THE HEATING RATE (K/S)?   ')
      READ (*,45) BETA
 45   FORMAT (F5.2)
      WRITE (*,47)
 47   FORMAT (' INPUT TMAX (K)?   ')
      READ (*,48) TMAX
 48   FORMAT (F5.1)
      WRITE (*,50)
 50   FORMAT (' INPUT THE STEP SIZE (S)?   ')
```

```
      READ (*,55) H
55    FORMAT (F5.3)
      WRITE (*,60)
60    FORMAT (' INPUT THE INITIAL SURFACE COVERAGE (THETA)?   ')
      READ (*,65) THETA
65    FORMAT (F6.4)
      WRITE (*,70)
70    FORMAT (' INPUT THE INITIAL SUBSURFACE COVERAGE (ETA)?   ')
      READ (*,75) ETA
75    FORMAT (F7.5)
      WRITE (*,105)
105   FORMAT (' INPUT THE OUTPUT DATA FILE NAME (NAME.DAT)?   ')
      READ (*,107) OFILE
107   FORMAT (A10)
      OPEN (4,FILE=ZFILE)
      WRITE (4,200) VD, ED, EP, VP, EDF
200   FORMAT  (1X, F13.6, 1X, F4.1, 1X, F4.1, 1X, F13.6, 1X, F4.1)
      WRITE (4,210) VDF, M, BETA, TMAX
210   FORMAT (1X, F13.6, 1X, F5.2, 1X, F5.2, 1X, F5.1)
      WRITE (4,220) H, THETA, ETA, OFILE
220   FORMAT (1X, F5.3, 1X, F6.4, 1X, F7.5, 1X, A10,' ')
      CLOSE (4)
      END
```

Appendix C: Computer Program for Integrating Equations 6.1, 6.2 and 6.7

Equations 6.1, 6.2, and 6.7 were solved numerically using a fourth order Runge-Kutta method with variable step size. The temperatures at which the step size was adjusted were determined by trial and error for each set of parameters. A listing of the computer program used to perform the integration is listed below. Because of the large number of iterations required, this Fortran program, which is called "MSTPD" is run on the U.C. Berkeley CMS system. The various input parameters are read from an input data file identified at run time as #3. This data file is created using a program called "MSINP", which also is listed below.

```
C*****************************************************************
C                      PROGRAM NAME: MSTPD
C*****************************************************************
C
C This program calculates TPD spectra for a catalyst containing
C up to three disinct adsorption sites with different binding
C energies.  In this model, it is assumed that the reactor is
C well-mixed, and that intraparticle diffusion limitations are
C negligible.
C
C*****************************************************************
C
C DEFINE ALL THE VARIABLES
C
C   A       The temperature-independent portion of the adsorption
C           rate constant
C   AJ      The order of the desorption process (real #)
C   ALPHA0  The ratio of the number of sites to the carrier gas
C           flow rate (STP) in units of umoles*s/cc
C   BCTR    Counter
C   BDELTA  The number of steps per degree K
C   BETA    The heating rate in K/s
C   EDi     The desorption activation energies (kcal/mole)
C   GC      The gas phase adsorbate concentration (mol/cc)
C   H       The step size (s)
C   J       The order of the desorption process (integer)
C   KA      The adsorption rate constant
C   KDi     The desorption rate constants for each site (1/s)
C   KNi     Runge-Kutta paramters
```

```
C   LNi     Runge-Kutta parameters
C   M       The molecular weight of the gas phase species
C   MNi     Runge-Kutta parameters
C   NOR     Number of records in the output file
C   OFILE   The output file name
C   RD      The net desorption rate from the entire surface
C   S       The sticking coefficient
C   T       Temperature (K)
C   THETAi  The initial coverages for each adsorption site
C   TMAX    The final ramp temperature (K)
C   VD      The desorption preexponential factor (1/s)
C   Xi      The relative abundance of each type of adsorption site
C
      IMPLICIT REAL*8(A,B,E-H,K-Z)
      IMPLICIT INTEGER*2(I,J,C,D)
      CHARACTER*20 OFILE
      CHARACTER ZFILE(50)*20
      COMMON /RDATA/ A, VD, ED1, ED2, ED3, ALPHA0
      COMMON /CONST/ H,AJ,M,ALPHA,X1,X2,X3,KD1,KD2,KD3,KA
C
C*****************************************************************
C
C Read J, M, Xi, EDi, THETAi, ALPHA0, BETA, TMAX, S, and OFILE
C from the input file identified as number 3:
C
            READ (3,52) J, M, X1, X2, X3, ED1, ED2, ED3
 52         FORMAT (1X, I1, 1X, F6.2, 3(1X,F5.3), 3(1X,F5.1))
            READ (3,54) THETA1, THETA2, THETA3, ALPHA0, BETA
 54         FORMAT (3(1X,F7.5), 1X, F8.5, 1X, F5.2)
            READ (3,56) TMAX, S, OFILE
 56         FORMAT (1X, F5.1, 1X, F7.5, 1X, A20)
C
C*****************************************************************
C
C    SET THE VALUES OF ALL THE PARAMETERS
C
      AJ = J
      H = 0.01/BETA
      T = 2.5D2
      ALPHA0 = ALPHA0*1.0D-6
      ALPHA = (ALPHA0)*(273.0/T)
      A = 1.454D12 * S/(M**0.5)
      IF (J .EQ. 1) VD = 1.0D15
      IF (J .EQ. 2) VD = 1.0D13
      ED1 = ED1 * 1.0D3
      ED2 = ED2 * 1.0D3
      ED3 = ED3 * 1.0D3
      KD1 = 0.0
      KD2 = KD1
      KD3 = KD2
      KA = KD3
      GC = KA
      KN1 = GC
      KN2 = KN1
      KN3 = KN2
      KN4 = KN3
      LN1 = KN4
      LN2 = LN1
      LN3 = LN2
      LN4 = LN3
      MN1 = LN1
      MN2 = MN1
```

```
      MN3 = MN2
      MN4 = MN3
      RD = MN4
      BDELTA = 1.0000/(BETA*H)
      BCTR = 0.0
      NOR = TMAX - T + 1
C*****************************************************************
C
C Write the number of records and the initial conditions to the
C output data file
C
      OPEN (4,FILE=OFILE)
      WRITE (4,272) NOR
 272  FORMAT (F5.0)
      WRITE (4,275) T, RD, THETA1, THETA2
 275  FORMAT (1X, F5.1, 5X, F9.7, 2(5X, F6.4))
C*****************************************************************
C
C     DO THE NUMERICAL INTEGRATION BY 4'TH ORDER RUNGE-KUTTA
C
      DO 725 IJ = 1, 1000
      DO 300 I=1, 10000
           TP = T
           XN = THETA1
           YN = THETA2
           ZN = THETA3
           CALL RC (TP)
           CALL CG (XN, YN, ZN, GC)
           CALL KNI (XN, YN, ZN, GC, KN1, LN1, MN1)
           TP = T + BETA * H/2.0
           XN = THETA1 + H*KN1/2.0
           YN = THETA2 + H*LN1/2.0
           ZN = THETA3 + H*MN1/2.0
           CALL RC (TP)
           CALL CG (XN, YN, ZN, GC)
           CALL KNI (XN, YN, ZN, GC, KN2, LN2, MN2)
           XN = THETA1 + H*KN2/2.0
           YN = THETA2 + H*LN2/2.0
           ZN = THETA3 + H*MN2/2.0
           CALL CG (XN, YN, ZN, GC)
           CALL KNI (XN, YN, ZN, GC, KN3, LN3, MN3)
           TP = T + BETA * H
           XN = THETA1 + H*KN3
           YN = THETA2 + H*LN3
           ZN = THETA3 + H*MN3
           CALL RC (TP)
           CALL CG (XN, YN, ZN, GC)
           CALL KNI (XN, YN, ZN, GC, KN4, LN4, MN4)
           T = TP
           THETD1 = (H/6.0) * (KN1 + 2.0*(KN2 + KN3) + KN4)
           THETD2 = (H/6.0) * (LN1 + 2.0*(LN2 + LN3) + LN4)
           THETD3 = (H/6.0) * (MN1 + 2.0*(MN2 + MN3) + MN4)
           THETA1 = THETD1 + THETA1
           THETA2 = THETD2 + THETA2
           THETA3 = THETD3 + THETA3
           RD = -1.0D0 * (X1*THETD1 + X2*THETD2 + X3*THETD3)/H
           BCTR = BCTR + 1.0
           IF (RD .LT. .0000001) RD = 0.0
           IF (BCTR .LT. BDELTA) GOTO 290
           BCTR = 0
C
C    Write the data to the output file every 1 K
```

```
C
            WRITE (4,275) T, RD, THETA1, THETA2
 290        CONTINUE
C
C   Adjust the step size by trial and error
            IF (T .GE. 320.0) H = 0.005/BETA
            IF (T .GE. 340.0) H = 0.002/BETA
            IF (T .GE. 360.0) H = 0.001/BETA
            IF (T .GE. 380.0) H = 0.0005/BETA
            IF (T .GE. 400.0) H = 0.0002/BETA
            IF (T .GE. 420.0) H = 0.0001/BETA
            IF (T .GE. 440.0) H = 0.00005/BETA
            IF (T .GE. 460.0) H = 0.00002/BETA
            IF (T .GE. 490.0) H = 0.00001/BETA
            BDELTA = 1.0/(BETA * H)
            IF (T .GE. TMAX) GOTO 726
            IF (THETA2 .GT. 1.0) GOTO 726
            IF (THETA3 .GT. 1.0) GOTO 726
 300   CONTINUE
 725   CONTINUE
 726   CLOSE (4)
 40    CONTINUE
       STOP
       END
C*****************************************************************
C
C      SUBROUTINE TO CALCULATE RATE CONSTANTS
C
       SUBROUTINE RC (TP)
       IMPLICIT REAL*8 (A,B,E-H,K-Z)
       IMPLICIT INTEGER*2(I,J,C,D)
       COMMON /RDATA/ A, VD, ED1, ED2, ED3, ALPHA0
       COMMON /CONST/ H,AJ,M,ALPHA,X1,X2,X3,KD1,KD2,KD3,KA
       E = 2.718281828
       KD1 = VD * (E**(ED1/(-2.0D0*TP)))
       KD2 = VD * (E**(ED2/(-2.0D0*TP)))
       KD3 = VD * (E**(ED3/(-2.0D0*TP)))
       KA = A * (TP**0.5)
       ALPHA = ALPHA0 * (273.0/TP)
       RETURN
       END
C*****************************************************************
C
C      SUBROUTINE TO CALCULATE THE GAS PHASE CONCENTRATION
C
       SUBROUTINE CG (XN, YN, ZN, GC)
       IMPLICIT REAL*8 (A,B,E-H,K-Z)
       IMPLICIT INTEGER*2(I,J,C,D)
       COMMON /CONST/ H,AJ,M,ALPHA,X1,X2,X3,KD1,KD2,KD3,KA
       J = AJ
       GC=(ALPHA)*(X1*KD1*(XN**J)+X2*KD2*(YN**J)+X3*KD3*(ZN**J))
       MM=KA*(X1*((1.0-XN)**J)+X2*((1.0-YN)**J)+X3*((1.0-ZN)**J))
       GC = GC/(1.0 + ALPHA*MM)
       RETURN
       END
C*****************************************************************
C
C      SUBROUTINE TO CALCULATE THE KNi, LNi, MNi
C
       SUBROUTINE KNI (XN, YN, ZN, GC, KN, LN, MN)
       IMPLICIT REAL*8 (A,B,E-H,K-Z)
       IMPLICIT INTEGER*2(I,J,C,D)
```

```
      COMMON /CONST/ H,AJ,M,ALPHA,X1,X2,X3,KD1,KD2,KD3,KA
      J = AJ
      RADS1 = J*KA*GC*((1.0-XN)**J)
      RADS2 = J*KA*GC*((1.0-YN)**J)
      RADS3 = J*KA*GC*((1.0-ZN)**J)
      RDES1 = J*KD1*(XN**J)
      RDES2 = J*KD2*(YN**J)
      RDES3 = J*KD3*(ZN**J)
      KN = RADS1 - RDES1
      LN = RADS2 - RDES2
      MN = RADS3 - RDES3
      IF (X1 .EQ. 0.0) KN = 0.0
      IF (X2 .EQ. 0.0) LN = 0.0
      IF (X3 .EQ. 0.0) MN = 0.0
      RETURN
      END
C*****************************************************************
C*****************************************************************
C
C                      PROGRAM NAME: MSINP
C
C*****************************************************************
C
C This program prompts creates the input data file used by the
C program MSTPD
C
C*****************************************************************
C
      IMPLICIT REAL*8(A-I,K-Z)
      IMPLICIT INTEGER*2 (J)
      CHARACTER*20 ZFILE, OFILE
C
      WRITE (*,2)
 2    FORMAT (' INPUT THE NAME OF THIS FILE?   ')
      READ (*,3) ZFILE
 3    FORMAT (A10)
 4    WRITE (*,5)
 5    FORMAT (' INPUT THE DESORPTION ORDER (1 OR 2)?   ')
      READ (*,10) J
 10   FORMAT (I1)
      IF (J .EQ. 1) GOTO 15
      IF (J .EQ. 2) GOTO 15
      WRITE (*,12)
 12   FORMAT (' INPUT EITHER 1 OR 2')
      GOTO 4
 15   WRITE (*,20)
 20   FORMAT (' INPUT THE MOL WT OF THE GAS PHASE SPECIES?   ')
      READ (*,25) M
 25   FORMAT (F6.2)
      WRITE (*,30)
 30   FORMAT (' INPUT THE FRACTION OF SITES THAT ARE TYPE 1?   ')
      READ (*,35) X1
 35   FORMAT (F5.3)
      WRITE (*,40)
 40   FORMAT (' INPUT THE FRACTION OF SITES THAT ARE TYPE 2?   ')
      READ (*,35) X2
```

```
      WRITE (*,45)
45    FORMAT (' INPUT THE FRACTION OF SITES THAT ARE TYPE 3?   ')
      READ (*,35) X3
      WRITE (*,60)
60    FORMAT (' INPUT ED1 (KCAL/MOLE)?   ')
      READ (*,65) ED1
65    FORMAT (F5.1)
      WRITE (*,70)
70    FORMAT (' INPUT ED2 (KCAL/MOLE)?   ')
      READ (*,65) ED2
      WRITE (*,80)
80    FORMAT (' INPUT ED3 (KCAL/MOLE)?   ')
      READ (*,65) ED3
      WRITE (*,90)
90    FORMAT (' INPUT THETA1?   ')
      READ (*,93) THETA1
93    FORMAT (F7.5)
      WRITE (*,95)
95    FORMAT (' INPUT THETA2?   ')
      READ (*,93) THETA2
      WRITE (*,94)
94    FORMAT (' INPUT THETA3?   ')
      READ (*,93) THETA3
      WRITE (*,105)
105   FORMAT (' INPUT ALPHA0 (UMOLES*S/CC)? ')
      READ (*,110) ALPHA0
110   FORMAT (F8.5)
      WRITE (*,120)
120   FORMAT (' INPUT THE HEATING RATE (K/S)?   ')
      READ (*,125) BETA
125   FORMAT (F5.2)
      WRITE (*,130)
130   FORMAT (' INPUT TMAX (K)?   ')
      READ (*,65) TMAX
      WRITE (*,135)
135   FORMAT (' INPUT THE STICKING COEFFICIENT?   ')
      READ (*,136) S
136   FORMAT (F7.5)
      WRITE (*,145)
145   FORMAT (' INPUT THE OUTPUT DATA FILE NAME (NAME.DAT)?   ')
      READ (*,150) OFILE
150   FORMAT (A20)
      WRITE (3,200) J, M, X1, X2, X3, ED1, ED2, ED3
200   FORMAT (1X, I1, 1X, F6.2, 3(1X,F5.3), 3(1X,F5.1))
      WRITE (3,210) THETA1, THETA2, THETA3, ALPHA0, BETA
210   FORMAT (3(1X,F7.5), 1X, F8.5, 1X, F5.2)
      WRITE (3,220) TMAX, S, OFILE
220   FORMAT (1X, F5.1, 1X, F7.5, 1X, A20,' ')
      END
```

Appendix D: Computer Program for Integrating Equations 6.7, 6.11, and 6.13

Equations 6.7, 6.11, and 6.13 were solved numerically using a fourth order Runge-Kutta method. A listing of the Fortran computer program used to perform the integration is shown below. This program is called "H2TPD"

```
C*****************************************************************
C
C                      PROGRAM NAME: H2TPD
C
C*****************************************************************
C
C This program simulates a two-peak hydrogen TPD spectrum using
C the subsurface diffusion model.  In this model, the reactor is
C assumed to be well-mixed and intraparticle diffusion
C limitations are assumed to be negligible.
C
C*****************************************************************
C
C DEFINE ALL THE VARIABLES
C
C     BETA   Heating Rate (K/s)
C     Bi     Runge-Kutta parameters
C     CTR    Counter
C     CTR2   Counter
C     DELTA  Number of iterations per degree K
C     DES    Net desorption rate (1/s)
C     DIF    Rate of diffusion from the subsurface to the surface
C            (1/s)
C     ED     Desorption activation energy (kcal/mole)
C     EDF    Activation energy for diffusion from the subsurface
C            to the surface (kcal/mole)
C     EP     Activation energy for penetration into the
C            subsurface region (kcal/mole)
C     ETA    Fraction of subsurface sites filled
C     GAMMA  (Ns*273/Q0) * the temperature independent portion of
C            the adsorption rate constant. KA = GAMMA * T**0.5/T
C            where the 1/T arises from the temperature dependence
C            of the carrier gas flow rate.
C     H      Step size (s)
C     INUM   Number of records in the output data file
C     KA     Adsorption rate constant (1/s)
C     KD     Desorption rate constant (1/s)
C     KDF    Rate constant for diffusion from the subsurface to
C            the surface (1/s)
C     KP     Rate constant for penetration into the subsurface
C            region (1/s)
C     Li     Runge-Kutta parameters
C     M      Number of subsurface layers
```

```
C     N       Desorption order
C     PEN     Rate of penetration into the subsurface region (1/s)
C     Q       Temperature-dependent carrier gas flow rate
C     Q0      Carrier gas flow rate (STP)
C     RD      Net rate of desorption from the surface (1/s)
C     T       Temperature (K)
C     T0      Initial temperature (K)
C     THETA   Fraction of surface sites occupied
C     TMAX    Final ramp temperature (K)
C     VD      Preexponential factor for desorption (1/s)
C     VDF     Preexponential factor for diffusion from the
C             subsurface to the surface (1/s)
C     VP      Preexponential factor for penetration into the
C             subsurface region (1/s)
C     ZFILE   Output data file name
C
C
      IMPLICIT REAL*8 (A-Z)
      IMPLICIT INTEGER*2 (I, INUM, J, DELTA, CTR, CTR2)
      CHARACTER*10 ZFILE
      COMMON /RDATA/ GAMMA, VD, VP, VDF, ED, EP, EDF
      COMMON /CONST/ M, N, NSB
C*****************************************************************
C
C   Input the various parameters from the screen, noting that the
C   preexponential factors for diffusion will be multiplied by
C   10^6 later on
C
      WRITE (*,3)
 3    FORMAT (' INPUT ED (KCAL/MOLE)?   ')
      READ (*,5) ED
 5    FORMAT (F4.1)
      WRITE (*,10)
 10   FORMAT (' INPUT EP (KCAL/MOLE)?   ')
      READ (*,5) EP
      WRITE (*,12)
 12   FORMAT (' INPUT VP/1000000 ?   ')
      READ (*,13) VP
 13   FORMAT (F11.6)
      WRITE (*,20)
 20   FORMAT (' INPUT EDIFF (KCAL/MOLE)?   ')
      READ (*,5) EDF
      WRITE (*,22)
 22   FORMAT (' INPUT VDF/1000000 ?   ')
      READ (*,13) VDF
      WRITE (*,27)
 27   FORMAT (' INPUT THE NUMBER OF LAYERS (M)?   ')
      READ (*,5) M
      WRITE (*,30)
 30   FORMAT (' INPUT THE VALUE OF GAMMA = (NS*A*273/Q)?   ')
      READ (*,35) GAMMA
 35   FORMAT (F12.1)
      WRITE (*,40)
 40   FORMAT (' INPUT THE HEATING RATE (K/S)?   ')
      READ (*,5) BETA
      WRITE (*,47)
 47   FORMAT (' INPUT TMAX (K)?   ')
      READ (*,48) TMAX
 48   FORMAT (F5.1)
      WRITE (*,50)
 50   FORMAT (' INPUT THE STEP SIZE (S)?   ')
      READ (*,55) H
 55   FORMAT (F7.5)
```

```
      WRITE (*,60)
 60   FORMAT (' INPUT THE INITIAL SURFACE COVERAGE (THETA)?   ')
      READ (*,65) THETA
 65   FORMAT (F6.4)
      WRITE (*,70)
 70   FORMAT (' INPUT THE INITIAL SUBSURFACE COVERAGE (ETA)?   ')
      READ (*,75) ETA
 75   FORMAT (F7.5)
      WRITE (*,105)
 105  FORMAT (' INPUT THE DATA FILE NAME (NAME.DAT)?   ')
      READ (*,107) ZFILE
 107  FORMAT (A10)
      OPEN (4,FILE=ZFILE)
C*****************************************************************
C
C   SET THE VALUES OF ALL THE PARAMETERS
C
      T0 = 2.5D2
      T = T0
      N = 2.0
      VD = 1.0D13
      ED = ED * 1.0D3
      VP = VP * 1.0D6
      VDF = VDF * 1.0D6
      EP = EP * 1.0D3
      EDF = EDF * 1.0D3
C
      DELTA = 1/(BETA * H) + 0.1
      CTR = 0
      CTR2 = 0
      RD = 0.0D0
      KA = RD
      KD = KA
      KP = KD
      KDF = KP
      B1 = KP
      B2 = B1
      B3 = B2
      B4 = B3
      L1 = B4
      L2 = L1
      L3 = L2
      L4 = L3
C*****************************************************************
C
C   OUTPUT ALL THE PARAMETER VALUES AND SET UP THE OUTPUT TABLE
C
      WRITE (*,80)
      WRITE (*,80)
      WRITE (*,80)
 80   FORMAT (' ')
      WRITE (*,316) BETA
 316  FORMAT (' BETA = ', F4.1, ' K/S')
      WRITE (*,317) TMAX
 317  FORMAT (' TMAX = ', F5.1, ' K')
      WRITE (*,331) GAMMA
 331  FORMAT (' GAMMA = ', F12.1)
      WRITE (*,333) VD
 333  FORMAT (' VD = ', E10.3)
      WRITE (*,336) ED
 336  FORMAT (' ED = ', F6.0,' CAL/MOLE')
      WRITE (*,339) M
 339  FORMAT (' M = ', F5.1)
      WRITE (*,341) VP
```

```
 341  FORMAT (' VP = ', E10.3)
      WRITE (*,346) EP
 346  FORMAT (' EP = ', F6.0,' CAL/MOLE')
      WRITE (*,351) VDF
 351  FORMAT (' VDF = ', E10.3)
      WRITE (*,356) EDF
 356  FORMAT (' EDIFF = ', F6.0, 'CAL/MOLE')
      WRITE (*,361) H
 361  FORMAT (' STEP SIZE = ', F7.5, ' S')
      WRITE (*,80)
      WRITE (*,80)
      WRITE (*,371) ZFILE
 371  FORMAT (' THE DATA FILE NAME IS ', A10)
      WRITE (*,80)
      WRITE (*,80)
      WRITE (*,80)
      WRITE (*,85)
 85   FORMAT ('  T(K)       Rd (1/S)       THETA       ETA')
      WRITE (*,80)
      WRITE (*,90) T, RD, THETA, ETA
 90   FORMAT (1X, F5.1, 5X, E10.4, 5X, F6.4, 5X, E10.4)
      INUM = TMAX - T0 + 1
      WRITE (4,92) INUM
 92   FORMAT (1X, I4)
      THETAF = THETA
      ETAF = ETA
      IF (THETAF .LT. 0.0000001) THETAF = 0.0
      IF (ETAF .LT. 0.0000001) ETAF = 0.0
      WRITE (4,96) T, RD, THETAF, ETAF
 96   FORMAT (1X, F5.1, 5X, F10.7, 5X, F8.6, 5X, F9.7)
C*****************************************************************
C
C   DO THE NUMERICAL INTEGRATION BY 4'TH ORDER RUNGE-KUTTA
C
 98   DO 600 I=1,10000
 100  DO 200 J=1,10000
           TP = T
           XN = THETA
           YN = ETA
           CALL RC (TP, KA, KD, KP, KDF)
           CALL KNI (KA, KD, KP, KDF, XN, YN, B1)
           CALL LNI (KP, KDF, XN, YN, L1)
           TP = T + BETA * H/2.0
           XN = THETA + H*B1/2.0
           YN = ETA + H*L1/2.0
           CALL RC (TP, KA, KD, KP, KDF)
           CALL KNI (KA, KD, KP, KDF, XN, YN, B2)
           CALL LNI (KP, KDF, XN, YN, L2)
           XN = THETA + H*B2/2.0
           YN = ETA + H*L2/2.0
           CALL KNI (KA, KD, KP, KDF, XN, YN, B3)
           CALL LNI (KP, KDF, XN, YN, L3)
           TP = T + BETA * H
           XN = THETA + H*B3
           YN = ETA + H*L3
           CALL RC (TP, KA, KD, KP, KDF)
           CALL KNI (KA, KD, KP, KDF, XN, YN, B4)
           CALL LNI (KP, KDF, XN, YN, L4)
           T = TP
           THETA = THETA + (H/6.0)*(B1 + 2.0*(B2 + B3) + B4)
           ETA = ETA + (H/6.0)*(L1 + 2.0*(L2 + L3) + L4)
           RD = N*KD*(THETA**N)/(1.0 + KA*((1.0D0 - THETA)**N))
           CTR = CTR + 1
```

```
            RDF = RD
            THETAF = THETA
            ETAF = ETA
            IF (RDF .LT. 0.0000001) RDF = 0.0
            IF (THETAF .LT. 0.0000001) THETAF = 0.0
            IF (ETAF .LT. 0.0000001) ETAF = 0.0
C
C  Write T, RD, THETA, ETA to the output file every 1 K
C
            IF (CTR .LT. DELTA) GOTO 150
            WRITE (4,96) T, RDF, THETAF, ETAF
            CTR = 0
            CTR2 = CTR2 + 1
C
C  Write T, RD, THETA, ETA to the screen every 10 K
C
            IF (CTR2 .LT. 10) GOTO 150
            CTR2 = 0
            WRITE (*,90) T, RD, THETA, ETA
 150        IF (T .GE. TMAX) GOTO 601
 200  CONTINUE
 600  CONTINUE
 601  CLOSE (4)
      STOP
      END
C*********************************************************************
C
C   SUBROUTINE FOR CALCULATING THE RATE CONSTANTS
C
      SUBROUTINE RC (TP, KA, KD, KP, KDF)
      IMPLICIT REAL*8 (A-Z)
      COMMON /RDATA/ GAMMA, VD, VP, VDF, ED, EP, EDF
      KA = GAMMA * (TP**(-0.5))
      KD = VD * DEXP(ED/(-1.987*TP))
      KP = VP * DEXP(EP/(-1.987*TP))
      KDF = VDF * DEXP(EDF/(-1.987*TP))
      RETURN
      END
C*********************************************************************
C
C   SUBROUTINE TO CALCULATE THE Kni = Bi
C
      SUBROUTINE KNI (KA, KD, KP, KDF, XN, YN, B, GC)
      IMPLICIT REAL*8 (A-Z)
      COMMON /CONST/ M, N, NSB
      DES = -1.0*N*KD*(XN**N)/(1.0 + KA*((1.0-XN)**N))
      PEN = KP * XN * (1.0D0 - YN)
      DIF = KDF * (1.0D0 - XN) * YN
      B = DES - PEN + DIF
      RETURN
      END
C*********************************************************************
C
C   SUBROUTINE TO CALCULATE Lni
C
      SUBROUTINE LNI (KP, KDF, XN, YN, L)
      IMPLICIT REAL*8 (A-Z)
      COMMON /CONST/ M, N, NSB
      PEN = KP * XN * (1.0 - YN)
      DIF = KDF * (1.0 - XN) * YN
      L = (1.0/M) * (PEN - DIF)
      RETURN
      END
C*********************************************************************
```

LAWRENCE BERKELEY LABORATORY
TECHNICAL INFORMATION DEPARTMENT
UNIVERSITY OF CALIFORNIA
BERKELEY, CALIFORNIA 94720